The PHILOSOPHICAL MAGAZINE

FIRST PUBLISHED IN 1798

L. 42 SEVENTH SERIES No. 328 May, 1951

A Journal of Theoretical Experimental and Applied Physics

PRICE 12s. 0d.
Annual Subscription £6 0s. 0d. payable in advance.

AND PUBLISHED BY TAYLOR & FRANCIS LTD., RED LION COURT, FLEET ST., LONDON, E.C.4.

Early Scientific Publications

DIARY OF ROBERT HOOKE, M.A., M.D., F.R.S.
1672-1680

Edited by **H. W. ROBINSON** and **W. ADAMS**
Recommended for publication by the Royal Society, London

25/-
net

"This vivid record of the scientific, artistic and social activities of a remarkable man during remarkable years has too long remained in obscurity."—Extract from foreword by Sir Frederick Gowland Hopkins, O.M., President of the Royal Society.

MATHEMATICAL WORK OF JOHN WALLIS, D.D., F.R.S.

By **J. F. SCOTT, Ph.D., B.A.**

12/6
net

"His work will be indispensable to those interested in the early history of The Royal Society. I commend to all students of the Seventeenth Century, whether scientific or humane, this learned and lucid book."—Extract from foreword by Prof. E. N. da C. Andrade, D.Sc., Ph.D., F.R.S.
Recommended for publication by University of London

CORRESPONDENCE AND PAPERS OF EDMOND HALLEY

Arranged and Edited by **EUGENE FAIRFI**

21/-
net

First published on behalf of The Hist Society by Oxford University Press. No Taylor & Francis, Ltd.

MEMOIRS OF SIR ISAAC NEWTON'S LIFE

5/-
net

By **WILLIAM STUKELEY, M.D., F**
From an Original Manuscrip
Now in the possession of the Royal So

HEVELIUS, FLAMSTEED AND HALLEY

12/6
net

Three Contemporary Astronomers and their M
By **EUGENE FAIRFIELD MAC**
Published by arrangement with The Hist Society

Established over 150 years

TAYLOR & FRANCIS
RED LION COURT, FLEET ST., LO
PRINTERS & PUBLISHERS OF SCIENTI

L. *Hyperfine Structure in Paramagnetic Salts and Nuclear Alignment.*

By B. Bleaney, F.R.S.,
Clarendon Laboratory, Oxford *.

[Received February 14, 1951.]

Abstract.

Abragam and Pryce (1951) have shown that the hyperfine structure in paramagnetic salts can be interpreted using a simple Hamiltonian involving components of the electron and nuclear spins. On the basis of this Hamiltonian, general formulæ are given for the allowed transitions in strong magnetic fields, assuming that the paramagnetic ions have axial symmetry and that interactions with the electric quadrupole moment of the nucleus are small compared with those involving the magnetic dipole moment.

As far as possible, general formulæ are also given for the energy levels in zero magnetic field, and the allowed transitions are indicated. The use of hyperfine structure in paramagnetic salts for the production of nuclear alignment is discussed, with some quantitative data.

§1. Introduction.

In a general survey of the theory of paramagnetic resonance and hyperfine structure, Abragam and Pryce (1951) have shown that it is possible to represent the behaviour of the energy levels by the following Hamiltonian, if the anisotropy has axial symmetry about the z-axis:

$$\mathscr{H}=\beta\{g_{\parallel}H_zS_z+g_{\perp}(H_xS_x+H_yS_y)\}+D\{S_z^2-\tfrac{1}{3}S\{S+1)\}$$
$$+AS_zI_z+B(S_xI_x+S_yI_y)+Q\{I_z^2-\tfrac{1}{3}I(I+1)\}-\gamma\beta_N\mathbf{H}.\mathbf{I}, \quad . \quad (1)$$

β=Bohr magneton,

β_N=Nuclear magneton.

Here the effective electron spin S is defined by setting the multiplicity of the electronic energy levels equal to $2S+1$, and I is the nuclear spin. g is a tensor, with principal values $g_{\parallel}$ and $g_{\perp}$. The term in D represents the presence of initial splittings of the electronic levels due to second order effects of the crystalline electric field. The terms in A, B correspond to the interaction between the nuclear magnetic moment and the magnetic field of the unfilled electron shell. The term in Q† is due to the interaction of the nuclear electric quadrupole moment with the gradient of the electric field at the nucleus, while the last term takes account of the direct effect of the external magnetic field on the nuclear magnetic moment.

* Communicated by the Author.

† Unfortunately this nomenclature differs from that customary where Q is used for the actual quadrupole moment of the nucleus. The relation between them is that Q (this paper)$=3eQ\,\partial^2V/\partial z^2/4I(2I-1)$ (usual nomenclature).

This Hamiltonian is very convenient for the interpretation of paramagnetic resonance spectra, since it involves only the electronic and nuclear spins, together with a set of parameters representing the strength of the various interactions. These can be regarded as a set of unknowns to be determined experimentally by a comparison of the observed spectrum with that calculated from the Hamiltonian given above. This spectrum is normally relatively simple, but the anisotropy introduces a complicated variation with the direction of the external magnetic field. The computed variation has already been compared with experiments in a number of specific cases and good agreement found.

The purpose of this paper is threefold. First, to give general formulæ for the allowed transitions in strong magnetic field, using perturbation theory carried to the second order. This is only possible with two limitations : (*a*) the axial symmetry presumed in equation (1) ; (*b*) the magnitude of the quadrupole parameter Q must be small compared with A, B. Second, to give, as far as possible, formulæ for the energy levels in zero magnetic field, together with the allowed transitions. These transitions are important because they can give more accurate values of the parameters (in particular, the quadrupole parameter Q) than the strong field case. The energy levels of zero fields are important also because of their effects in experiments on adiabatic demagnetization. Third, to consider the use of hyperfine structure in producing alignment of the nuclear spin, as suggested by Gorter (1948) and Bleaney (1951 a).

§ 2. The Strong Field Spectrum.

In strong fields it is convenient to choose the axes so that elements in S_x, S_y do not occur in the major term $g\beta\,H.S$ in the Hamiltonian. When g is anisotropic this is equivalent to taking the axis about which the spin precesses as the new z-axis. Then, if the external field is applied at an angle θ to the axis of crystalline symmetry, the usual rules for rotation of the axes may be applied to the Hamiltonian if allowance is made for the non-commuting properties of the spin components. We will consider first the fine structure which arises in the absence of nuclear spin from the presence of a crystalline splitting of the electronic levels.

2.1. *The Fine Structure.*

In strong fields the allowed transitions are of the type $\Delta M=\pm 1$. For the transition $M\rightarrow M-1$, we have

$$h\nu=g\beta H+D(M-\tfrac{1}{2})\left\{3\frac{g_\parallel^2}{g^2}\cos^2\theta-1\right\}$$
$$-\left(\frac{Dg_\parallel g_\perp\cos\theta\sin\theta}{g^2}\right)^2\left(\frac{1}{2g\beta H_0}\right)\{4S(S+1)-24M(M-1)-9\}$$
$$+\left(\frac{Dg_\perp^2\sin^2\theta}{g^2}\right)^2\left(\frac{1}{8g\beta H_0}\right)\{2S(S+1)-6M(M-1)-3\}, \quad . \quad . \quad . \quad (2)$$

where
$$g^2=g_\parallel^2\cos^2\theta+g_\perp^2\sin^2\theta. \quad . \quad . \quad . \quad . \quad . \quad . \quad . \quad (3)$$

The physical basis of (3) can be seen from fig. 1. The magnetic field H has components $H\cos\theta$ and $H\sin\theta$ respectively along and normal to the symmetry axis. The components of the magnetic moment are therefore proportional to $g_{\|}H\cos\theta$ and $g_{\perp}H\sin\theta$, and g is proportional to the length of the vector making an angle ϕ with the z-axis which is formed by compounding these two. This vector is parallel to the resultant magnetic moment of the electrons, but is not parallel to H. This is responsible for the factors $(g_{\|}/g)$ and $(g_{\perp}/g)$ which appear as coefficients multiplying $\cos\theta$ and $\sin\theta$ respectively everywhere in equation (2); for $\cos\phi=(g_{\|}/g)\cos\theta$: $\sin\phi=(g_{\perp}/g)\sin\theta$.

Fig. 1.

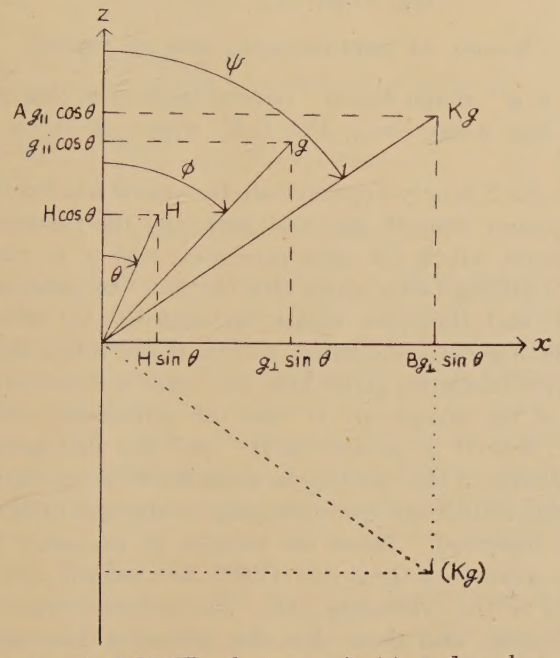

Orientation of magnetic field (H), electron spin (g), and nuclear spin (Kg) when anistropy is present. The figure is drawn for $g_{\perp}>g_{\|}$, and B>A. The dotted vector (Kg) refers to the case where A is negative.

The fine structure results in a splitting into 2S lines, which are equally spaced in the first approximation. The spacing varies with angle, falling to zero where $(g_{\|}/g)\cos\theta=1/\sqrt{(3)}$. This equal spacing is disturbed by the second order terms which vanish in strong fields, or along the axis of symmetry ($\theta=0$). The perturbation denominator in these second order terms is taken as $(g\beta H_0)$, the average spacing of successive levels. The significance of H_0 is that in the absence of the fine structure all the lines would coincide and occur at this field. Writing $h\nu=g\beta H_0$, the formula (2) can be re-arranged in the form

$$H=H_0-\frac{D}{g\beta}(M-\tfrac{1}{2})f_1(\theta)-\left(\frac{D}{g\beta}\right)^2\frac{1}{H_1}f_2(\theta). \quad . \quad . \quad . \quad . \quad (2\,a)$$

This formula shows that when the spectrum is displayed at constant frequency as a function of field, as is normally the case in paramagnetic resonance, its appearance is fundamentally the same (but reversed) as if it were displayed at constant field as a function of frequency. The value of the parameter D can be found from the separations (in field) between the lines.

The intensity of these strong transitions is given by the formula

$$\text{Power absorbed by crystal} = Z\{S(S+1)-M(M-1)\}, \quad . \quad . \quad (4)$$

where

$$Z = \frac{\pi\nu^2(g\beta'H')^2}{4kT}\frac{N}{2S+1}F(\nu, \nu_0, \Delta\nu),$$

N=no. of paramagnetic ions in crystal.

$F(\nu, \nu_0, \Delta\nu)$ is a " shape factor " depending on the line width. At the centre of the line where $\nu=\nu_1$, $F \approx 1/\Delta\nu$, where $\Delta\nu$ is the half-width at half-intensity.

The formula for Z is only approximate because it has been assumed that the radio-frequency field $H' \cos(2\pi\nu t)$ inducing the transitions is normal to the axis about which the spin precesses, and g' is the value of the spectroscopic splitting factor along this normal. In practice H′ is usually normal to H, and therefore makes an angle $(\theta-\phi)$ with the assumed direction. The absolute intensities will therefore differ slightly from (4), but the relative intensities given here and later will be correct. A minor consequence of the anisotropy is that the intensities will not be quite zero if the r.f. field H′ is parallel to H ; and this can occur also through second order effects of the splitting in weak fields, even when g is isotropic.

In finite fields transitions corresponding to changes in M of greater than unity can be observed. These are smaller in intensity than the main transitions by a factor of the order $(D/H)^2$, and vanish only if the external field is parallel to the symmetry axis. The actual intensity formulæ are rather complicated, and show that the intensity does not vary greatly with the angle between the external and r.f. fields. We shall content ourselves with giving the formula for the positions of the lines corresponding to the transition M→M−2 in the strong field quantum numbers. This is

$$\begin{aligned} h\nu = {} & 2g\beta H + 2D(M-1)\left\{3\frac{g_\parallel^2}{g^2}\cos^2\theta - 1\right\} \\ & - \left(\frac{Dg_\parallel g_\perp \cos\theta \sin\theta}{g^2}\right)^2 \left(\frac{2}{g\beta H_0}\right)\{4S(S+1)-24M(M-2)-33\} \\ & + \left(\frac{Dg_\perp^2 \sin^2\theta}{g^2}\right)^2 \left(\frac{1}{2g\beta H_0}\right)\{2S(S+1)-6M(M-2)-9\} \quad . \quad . \quad . \quad (5) \end{aligned}$$

(note that H_0 in the perturbation denominators refers again to the mean field at which the $\Delta M = \pm 1$ transitions occur).

2.2. *The Hyperfine Structure.*

In the presence of hyperfine structure the strong allowed transitions are those in which $\Delta m=0$, where m is the nuclear magnetic quantum number. The position of the transition $(M, m)\rightarrow(M-1, m)$ is found by adding to the right-hand side of equation (2) the quantity

$$\begin{aligned}
&Km+\frac{B^2}{4g\beta H_0}\left(\frac{A^2+K^2}{K^2}\right)\{I(I+1)-m^2\}\\
&\quad+\frac{B^2}{2g\beta H_0}\frac{A}{K}m(2M-1)\\
&\quad+\frac{1}{2g\beta H_0}\left(\frac{A^2-B^2}{K}\right)^2\left(\frac{g_{\|}g_{\perp}}{g^2}\right)^2\sin^2\theta\cos^2\theta\, m^2\\
&\quad+\frac{Q^2\cos^2\theta\sin^2\theta}{2KM(M-1)}\left(\frac{ABg_{\|}g_{\perp}}{K^2g^2}\right)^2 m\{4I(I+1)-8m^2-1\}\\
&\quad-\frac{Q^2\sin^4\theta}{8KM(M-1)}\left(\frac{Bg_{\perp}}{Kg}\right)^4 m\{2I(I+1)-2m^2-1\}, \qquad \ldots\ldots\ (6)
\end{aligned}$$

where

$$K^2g^2=A^2g_{\|}^2\cos^2\theta+B^2g_{\perp}^2\sin^2\theta \qquad \ldots\ldots\ (7)$$

The physical significance of the relation (7), which is due to Pryce (1949), is similar to that of (3). The magnetic moment of the electrons has projections proportional to $g_{\|}\cos\theta$ and $g_{\perp}\sin\theta$ parallel and normal to the symmetry axis respectively. The components of the magnetic field acting on the nucleus are therefore proportional to $Ag_{\|}\cos\theta$ and $Bg_{\perp}\sin\theta$, respectively, and the nucleus is aligned parallel to their resultant (see fig. 1). It may be noted that in deducing these formulæ the axes of quantization of electron and nucleus are taken parallel to their respective magnetic moments. This is responsible for the introduction of factors such as $(Ag_{\|}/Kg)$ multiplying $\cos\theta$, etc.

In the first approximation, the result of the nuclear interaction is to split each electronic transition into $\overline{2I+1}$ equally spaced components, with separation K between successive lines. Each component has the intensity given by (4), divided by $\overline{2I+1}$. Where there is considerable anisotropy the splitting which, measured in field, equals $(K/g\beta)$, may go through a maximum value at an angle to the axis, as in cobalt (Bleaney and Ingram 1951 a); this is due to the different angular variation of K and g. It should be noted that there is no first order effect due to the quadrupole interaction so long as $Q\ll B$. The quadrupole interaction produces a first order shift of the energy levels (see fig. 2), but this is the same for all levels with the same value of m, and does not affect transitions where $\Delta m=0$. This is true for all values of Q if the external magnetic field is parallel to the axis of symmetry, for the quadrupole term then contains only diagonal elements. If H is at an angle with this axis the quadrupole interaction will break down the ordinary selection rule when $Q\approx K$, because of the competition between the magnetic and electrostatic

interactions which are each trying to align the nucleus along its own preferred axis. Perturbation theory can then only be applied if $Q \ll K$, that is, $Q \ll A, B$. This is reflected in the fact that K appears in the denominator in the second order terms in Q^2, which do not therefore vanish in strong fields. The remaining second order terms do.

Fig. 2.

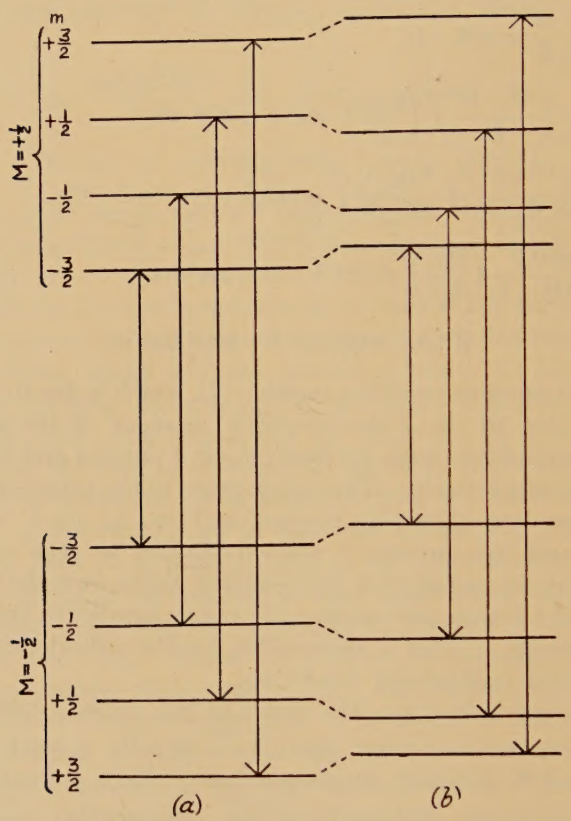

Hyperfine structure and allowed transitions in strong magnetic fields for $S=\frac{1}{2}$, $I=3/2$. (*a*) Magnetic interaction only, (*b*) electric quadrupole interaction added.

It is convenient to consider these two types of second order terms independently. From those which vanish in strong fields, one can separate terms in zero, first and second powers of m. The first of these produces a constant shift of all lines to higher frequencies (lower magnetic fields) which is unimportant except in accurate determinations of the g-value. The second produces a change in the separation of the hyperfine lines, which is different for different electronic transitions. This is important, for it can be used (except when $S=\frac{1}{2}$) to determine the relative signs of

the parameters D, A and B, which cannot be found from any of the first order terms. This point is considered more fully by Bleaney and Ingram (1951 b), with reference to the manganese spectrum. The third terms, in m^2, produce a linear change in the separation of the hyperfine lines within a given electronic transition. For $\theta=0$ or $90°$, the separation increases always towards higher fields, but in intermediate directions it may reverse. For example, in cobalt ammonium sulphate (Bleaney and Ingram 1951 a), where there is great anisotropy, the reversal takes place only $1\frac{1}{2}°$ from the perpendicular direction. Note that none of the terms is really independent of θ, owing to the variation in g and K with angle, unless both g and the hyperfine structure are isotropic.

The second order terms in Q^2 are of importance because they form one method of detecting the presence of a small quadrupole interaction. They contain terms in m, which produce a constant change in the spacing of a group of hyperfine lines, and terms in m^3 which cause the spacing to be greater at the ends of a group than in the middle, when $\theta=90°$. This effect is reversed as θ decreases, owing to the opposite sign of the two terms in Q^2, and both terms become zero at $\theta=0°$. The effects are greatest for the transition $M=\frac{1}{2}\rightarrow-\frac{1}{2}$. If $A>B$, and $g_{\parallel}>g_{\perp}$, the unequal spacing is greatest at some intermediate value of θ between $0°$ and $90°$, but if the inequalities are the other way, it may be greatest at $\theta=90°$. The quadrupole terms may be differentiated from the other second order shifts in two ways: (*a*) they do not vanish in strong fields; (*b*) the separation of successive hyperfine lines is greatest in the middle or at the ends, instead of showing a progressive increase or decrease.

A second method of discovering a small quadrupole interaction depends on the weak lines corresponding to changes of ±1 and ±2 in the nuclear quantum number m, which have intensities of the order of $(Q/K)^2$ compared with the main hyperfine lines. The positions of these lines involve the first power of Q instead of (Q^2/K), and we shall neglect small shifts of the order Q^2/K, and $(A, B)^2/(g\beta H_0)$. In the intensities we shall neglect contributions of the order $(A, B)^2/(g\beta H_0)^2$ which vanish in strong fields, unlike the quadrupole effects. We have then lines $(M, k\pm\frac{1}{2})\rightarrow(M-1, k\mp\frac{1}{2})$,

$$\text{Energy} = Kk\pm\{K(M-\tfrac{1}{2})+Q'k-\gamma'\}, \quad . \quad . \quad . \quad . \quad (8)$$

$$\text{Intensity}=4k^2\{(I+\tfrac{1}{2})^2-k^2\}X, \quad . \quad . \quad . \quad . \quad . \quad . \quad . \quad . \quad (9)$$

where k takes on the values $(I-\frac{1}{2})$, $(I-\frac{3}{2})$, . . ., $-(I-\frac{1}{2})$, and for the lines $(M, m\pm1)\rightarrow(M-1, m\mp1)$

$$\text{Energy} = Km\pm\{K(2M-1)+2Q'm-2\gamma'), \quad . \quad . \quad . \quad . \quad (10)$$

$$\text{Intensity}=\{(I+1)^2-m^2\}\ \{I^2-m^2)Y, \quad . \quad . \quad . \quad . \quad . \quad (11)$$

where m takes on the values $(I-1)$, $(I-2)$, . . ., $-(I-1)$.

In these equations

$$X=\frac{Z}{(2I+1)}\left\{\frac{Q}{2KM(M-1)}\right\}^2\left(\frac{ABg_{\parallel}g_{\perp}}{K^2g^2}\right)^2\cos^2\theta\sin^2\theta, \quad . \quad . \quad . \quad (12a)$$

$$Y=\frac{Z}{(2I+1)}\left\{\frac{Q}{8KM(M-1)}\right\}^2\left(\frac{Bg_{\perp}}{Kg}\right)^4\sin^4\theta, \quad . \quad . \quad . \quad . \quad . \quad . \quad (12b)$$

$$Q'=Q\left(\frac{3A^2g_{\parallel}^2}{K^2g^2}\cos^2\theta-1\right), \quad . \quad . \quad . \quad . \quad . \quad . \quad . \quad . \quad . \quad . \quad (13a)$$

$$\gamma'=\gamma\beta_N H(Ag_{\parallel}\cos^2\theta+Bg_{\perp}\sin^2\theta)/Kg. \quad . \quad . \quad . \quad . \quad . \quad . \quad (13b)$$

Fig. 3.

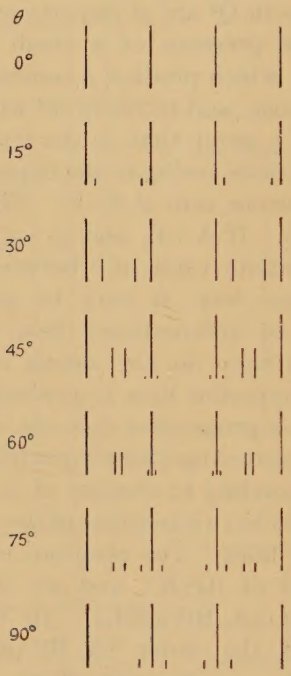

Quadrupole effects in spectrum for $S=\frac{1}{2}$, $I=3/2$, with no anisotropy and $A=B=5Q$.

The significance of these formulæ can best be appreciated by reference to a simple case. Fig. 3 shows the spectrum at various angles for a hypothetical ion where $S=\frac{1}{2}$, $I=3/2$, with no anisotropy ($A=B$ and $g_{\parallel}=g_{\perp}$), and $Q=0{\cdot}2B$. The term $\gamma\beta_N H$ is neglected. As θ increases from zero, four lines corresponding to $\Delta m=\pm 1$ increase in intensity and appear at symmetrical points between the two outer pairs of main lines. They collapse to two lines at $\cos\theta=1\sqrt{(3)}$, then separate out again and disappear. The lines $\Delta m=\pm 2$ are strongest at $\theta=90°$, and are symmetrically disposed about the two inner main lines, coinciding with them at $\cos\theta=1/\sqrt{(3)}$. It will be seen that the spectrum is always symmetrical, and no information can be obtained about the relative signs of Q, A and B.

At fields of the order of 10,000 gauss, the direct effect of the external field on the nucleus is no longer negligible, and important information about the signs of the constants A, B, and Q can be obtained. The term $\gamma\beta_N H$ acts with the quadrupole interaction in increasing the separation of satellite doublets on one side of the spectrum, and against it to decrease the separation on the other side. If A, B, Q and $\gamma\beta_N H$ are all positive, the separation is smaller at the high frequency (low field) end of the spectrum when $\cos\theta < 1/\sqrt{(3)}$, and greater for values of $\cos\theta$ greater than this. (The separation is no longer zero exactly at $\cos\theta = 1/\sqrt{(3)}$ but goes through zero at a smaller angle for the satellites on the high frequency side, and at a greater angle for those on the other side.) If the sign of Q or $\gamma\beta_N H$ is reversed, the asymmetry is also reversed.

When anisotropy is present the nature of the spectrum is not altered in principle, but the angular dependence and relative intensities are changed. The positions of the satellite lines are the same as in fig. 3, if we plot them against the angle ψ between the nucleus and the symmetry axis, for Q′ is simply $Q(3\cos^2\psi - 1)$.

The term γ' in $\gamma\beta_N H$ now contains a multiplying factor which is just the cosine of the angle $(\psi - \theta)$ which the nuclear axis makes with the external field. If A and B are of opposite sign this factor passes through zero, since at some angle the nuclear axis will be perpendicular to the external field, as can be seen from fig. 1.

The considerable intensity of the satellite lines $\Delta m = \pm 1$ at intermediate angles makes these generally the most sensitive method of detecting a small quadrupole interaction, if there is adequate intensity in the observed spectrum. If not, accurate measurement of the line separation, as described previously, is the best, but no information concerning the signs can be obtained.

The question of what nuclear information can be obtained from the relative signs needs careful analysis. The experiments give the relative signs of $(A\gamma)$, $(B\gamma)$ and Q ; but the signs of A, B themselves depend on that of γ, since they involve the product of the nuclear magnetic moment and the field of the electrons. Essentially, therefore, the sign of the latter is compared with Q, which is itself the product of $(\partial^2 V/\partial z^2)$ and the nuclear quadrupole moment. The sign of the nuclear quadrupole moment can therefore be established if crystalline field theory gives the signs of the electronic magnetic field and electric field gradient. The sign of the nuclear magnetic moment cannot be found ; this difference arises because use is made of an external magnetic field.

§ 3. Energy Levels and Susceptibility at Zero Magnetic Field.

3.1. *Levels for* $S = \frac{1}{2}$.

In zero magnetic field, evaluation of the energy levels is somewhat more complicated than in the strong field case because in general we cannot apply perturbation theory. Thus in the case $S = \frac{1}{2}$ the two electronic levels $M = +\frac{1}{2}$ and $M = -\frac{1}{2}$ are degenerate in the absence of hyperfine structure, and the perturbation denominators arising from the

term $B(S_xI_x+S_yI_y)$ in the Hamiltonian would be zero. The energy matrix splits up into a number of doublets in this case, however, so that we can give an explicit formula (14) for the levels by solving the quadratic secular equations

$$W=-\frac{A}{4}+Q\{k^2+\tfrac{1}{4}-\tfrac{1}{3}I(I+1)\}$$
$$\pm\tfrac{1}{2}\sqrt{[\{k(A-2Q)+G\}^2+B^2\{(I+\tfrac{1}{2})^2-k^2\}]}, \quad . \ . \ . \quad (14)$$

where $k=M+m$ takes the values $(I+\frac{1}{2})$, $(I-\frac{1}{2})$, . . ., $-(I+\frac{1}{2})$; with the restriction that only the positive sign is to be taken before the square root when $k=+(I+\frac{1}{2})$, and only the negative sign when $k=-(I+\frac{1}{2})$. Here $G=g_{\|}\beta H$, and the effect of a magnetic field along the symmetry axis has been included, since to do so causes no great complication. The significance of k is that, except for $|k|=I+\frac{1}{2}$, the levels are linear combinations of the states (M, m) and $(M-1, m+1)$. In zero magnetic field they are all doublets, the states k and $-k$ being degenerate, except for the case $k=0$, which gives two singlets of separation $B(I+\frac{1}{2})$. The levels given by $k=\pm(I+\frac{1}{2})$ form a doublet in zero field also, with nuclear magnetic quantum numbers $m=I$ and $-I$ respectively.

The allowed transitions in zero magnetic field are rather complicated when $B\neq 0$, owing to the admixture of wavefunctions in the different levels. A simple case arises when a radio-frequency field is applied parallel to the symmetry axis, which is the axis about which electron and nuclear spin precess. The levels which are found by taking the alternative signs outside the square root in (14) each consist of admixtures of the same states and transitions are allowed between them except in the special cases when either both A and Q are zero, or $B=0$. These transitions, which are all doublets, occur at

$$h\nu=\sqrt{[k^2(A-2Q)^2+B^2\{(I+\tfrac{1}{2})^2-k^2\}]}. \quad . \ . \ . \quad (15)$$

This formula shows that an accurate value of the quadrupole parameter Q may be obtained from the spectrum in zero field in cases where no effect can be observed in the strong field spectrum.

When an r.f. field is applied normal to the symmetry axis the allowed transitions are rather complicated. We shall content ourselves with pointing out that they can arise between any of the levels found by assigning values to k differing by one unit in (14). Here again the frequencies of the transitions may be used to find Q: in particular, a number of transitions fall into doublets where the separation of the components is $2Q(2k-1)$. This splitting gives Q directly, independent of A, B.

3.2. *Levels for* $S>\frac{1}{2}$.

No simple formulæ can be given for this case except when the electronic splitting parameter D is large compared with the hyperfine structure parameters. In the first approximation we have, then, for levels where $M\neq\pm\frac{1}{2}$,

$$W=D\{M^2-\tfrac{1}{3}S(S+1)\}+AMm+Q\{m^2-\tfrac{1}{3}I(I+1)\}. \quad . \ . \quad (16)$$

These are all doublets in this approximation (except when M or $m=0$), the states (M, m) and ($-$M, $-m$) are degenerate.

For $M=\pm\frac{1}{2}$, the formulæ given in the last section still apply, in the first approximation, if the parameter B is replaced by $B(S+\frac{1}{2})$. All the levels will have shifts of the order B^2/D, due to the off-diagonal elements.

The allowed transitions in zero field may be outlined as follows. If the r.f. magnetic field is parallel to the symmetry axis, only transitions internal to the levels $M=\pm\frac{1}{2}$ are allowed, and in the first approximation, these are given by our modified equation (15). When the r.f. field is perpendicular to the symmetry axis, the allowed transitions are of the same type as in strong fields, viz. $\Delta M=\pm 1$, $\Delta m=0$, except where the levels $M=\pm\frac{1}{2}$ are involved. Here again the remarks of §3.1 apply for transitions internal to these levels. Transitions are also allowed between the level (3/2, m) and either of the levels given by $k=(m+\frac{1}{2})$, and between ($-3/2$, m) and either given by $k=(m-\frac{1}{2})$, in (14); these alternative levels are those corresponding to taking the alternative signs before the square root.

These transition rules only apply when $D \gg A, B$. When they are of the same order the spectrum will be much more complicated.

3.3. *Susceptibility at Zero Magnetic Field.*

At high temperatures ($kT \gg A, B, Q, D$) the presence of a hyperfine structure produces almost no effect on the susceptibility of a paramagnetic salt. Bleaney (1950) has pointed out that if the susceptibility is expressed as a power series in $1/T$, the hyperfine structure leaves the term in $1/T$ unaltered, and introduces no term in $1/T^2$, even for a single crystal. The presence of an electronic splitting gives an anisotropic term in $1/T^2$ (equation (4) of Bleaney 1950) which averages to zero for a powder.

At temperatures where kT is of the same order as the splitting parameters A, B, Q, D, the susceptibility varies in a complicated manner and no general formula can be given. One or two special cases are worthy of mention, however, being limiting cases where simple formulæ can be given. These illustrate the general behaviour of the susceptibility.

The cases of $S=\frac{1}{2}$, $B=Q=0$ has been evaluated previously (Bleaney 1951 b) since it approximates closely to several salts of cobalt. Reference to equation (14) shows that when $B=0$ the energy levels show a first order Zeeman effect when a small field is applied along the axis. The magnitude of the Zeeman splitting is the same for all the levels, and the susceptibility therefore follows Curie's law, irrespective of the changing population of the hyperfine doublets. If a small field is applied perpendicular to the axis, only a second order Zeeman effect is produced, and the susceptibility is given by the formula

$$\chi_\perp = \frac{Ng_\perp^2\beta^2}{kA}\left\{\frac{\sum_m \frac{1}{2m}\sinh\frac{mA}{2kT}}{\sum_m \cosh\frac{mA}{2kT}}\right\}, \qquad \ldots\ldots (17)$$

where m takes the positive values I, (I−1), . . . $\frac{1}{2}$ or 0. (In the latter case the terms for which $m=0$ must be weighted by a factor $\frac{1}{2}$ in the summation.) At very low temperatures $\chi_\perp$ passes through a maximum and then falls to a limiting constant value as T→0.

For substances where $S>\frac{1}{2}$, the susceptibility will not differ, in the first approximation, from the case of no nuclear interaction, except for the levels $M=\pm\frac{1}{2}$. If these lie at the bottom (D positive) the remarks of the previous paragraph apply at temperatures where only these levels are occupied, and formula (17) holds if $D \gg A$. If D is negative, these levels lie uppermost, and they will not be populated at temperatures where the deviations due to nuclear interaction would show up. In this case we have simply when $kT \ll D(2S-1)$ (*i. e.* only lowest levels occupied),

$$\chi_{\parallel} = \frac{NS^2 g_{\parallel}^2 \beta^2}{kT},$$

$$\chi_\perp = -\frac{8S^2 g_\perp^2 \beta^2}{(2S-1)D}.$$

Note that $\chi_\perp$ is not really negative because this formula applies only when D is negative.

Paramagnetic ions which do not have Kramers degeneracy in their electronic levels (*i. e.* where S is not half-integral), are not often used in adiabatic demagnetization work, and the levels in zero field are not of great interest. The remarks of this section apply equally to them, however, except when D is positive. The lowest level is then M=0, which has no temperature dependent susceptibility contribution in the first approximation. The hyperfine splitting of this level is also zero, except for second order and quadrupole effects.

§ 4. Nuclear Alignment.

Three methods of producing nuclear alignment at low temperatures by means of hyperfine structure have been proposed. The first of these (Gorter 1948, Rose 1949) utilizes the hyperfine structure due to magnetic interaction in a paramagnetic salt. The method proposed is to demagnetize a paramagnetic salt to a small field, around which the electronic spin will precess. The nuclei are then aligned also parallel to this field by the much more powerful field (10^5–10^6 gauss) of the electrons. The splitting of the nuclear levels produced by this latter field is of the order of 0·01 to 0·1° K., and at such temperatures an appreciable degree of nuclear polarization will be set up.

The second method, due to Pound (1949), utilizes the electric quadrupole interaction to split the nuclear levels. This causes, not a polarization, but only an alignment of the nuclei, since the levels $\pm m$ remain degenerate. This is, however, sufficient for experiments involving radioactive emission, which depends only on even multiples of the angle with the axis of alignment (Spiers 1948, 1949). The latter is, of course, determined by

the crystallographic symmetry, and ideally a substance with one ion in unit cell is required. Since this method does not require the use of paramagnetic salts, it will not be further considered here.

The third method, suggested by Bleaney (1951 a), is similar to that of Gorter in that the magnetic interaction between the nucleus and the electrons of a paramagnetic ion is used, but differs in that no residual magnetic field is applied. As in Pound's method, an alignment, not a polarization, of the nuclei is set up. The nuclei precess about an axis determined by the crystalline field, and again, a substance with one ion in unit cell is required. This method has the advantage over Gorter's that lower temperatures will be reached, since there is no external magnetic field.

At first sight, on the other hand, Gorter's method seems to be simpler in that single crystals are not required, and the method can be used with any paramagnetic salt. Closer examination of the effects of the crystalline electric field shows that this is not the case for small residual magnetic fields and almost the same conditions are required in the two methods. The reason for this is that, in general, a small magnetic field applied normal to the crystalline symmetry axis produces only a second order Zeeman effect, and the spins remain aligned along the crystal axis until fields large enough to overcome the crystalline splitting (if present) or hyperfine splitting are applied. Thus a powder, or a single crystal with many ions in unit cell, such as iron alum, will be unsuitable, and a crystal with only a single ion per unit cell is required, as in the other methods. The magnetic field must then be applied parallel to the axis of this ion. In the following paragraphs some attempt is made to calculate the degree of polarization and of alignment in zero field that can be achieved in limiting cases.

4.1. *Nuclear Alignment and Polarization with* $B=Q=0$.

For both methods the ideal case arises when the energy matrix of the lowest electronic level (assumed a doublet) has vanishing elements off the diagonal. This can occur in two ways : (*a*) if the lowest levels are $M=\pm\frac{1}{2}$, and there is considerable anisotropy so that $A \gg B$; (*b*) if the lowest levels are $M \neq \pm\frac{1}{2}$, in a salt with considerable splitting of the electronic levels in zero magnetic field ($D \gg A$, B). Examples of salts approximating to these two extremes are cobalt fluosilicate and manganese fluosilicate, both of which have only a single ion in unit cell. Then, if the off-diagonal elements are neglected, the lowest energy levels consist simply of a set of $2I+1$ doublets, equally spaced by $A \times |M|$ (*cf.* Bleaney 1951 a, b). Each doublet contains levels in which the electronic spins are opposed and the nuclear magnetic quantum numbers are m and $-m$ respectively. The top and bottom levels have $m=\pm I$, and the intermediate levels are in order of m changing by one unit (see fig. 4 *a*). At a temperature T, the combined population of the two states with a given value of m is proportional to $\cosh(AMm/kT)$.

Fig. 4 *a* has been drawn for the case of $S=\frac{1}{2}$, $I=7/2$, which is appropriate to the stable isotope, cobalt 59. The lowest temperature which could be reached by adiabatic demagnetization of such a cobalt salt is equivalent to $kT=0{\cdot}7A$, and is represented by a vertical line. The populations of the nuclear levels $\pm 7/2 : \pm 5/2 : \pm 3/2 : \pm 1/2$ would then be $1 : 0{\cdot}53 : 0{\cdot}32 : 0{\cdot}21$, showing a considerable preponderance in the states of high m. The radioactive isotope, cobalt 60, is thought to have a spin of approximately 4, and if its magnetic moment is about the same as that of the stable isotope, there would be a similar preponderance.

Fig. 4.

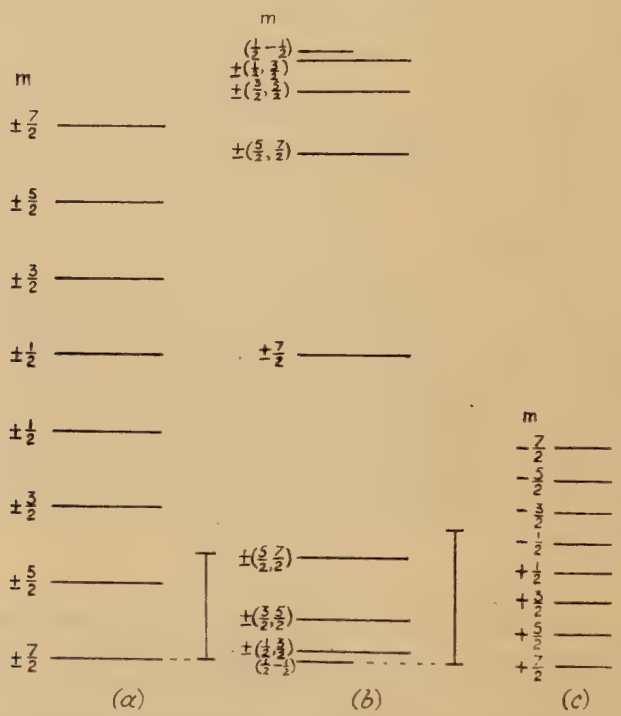

Energy levels in zero magnetic field for $S=\frac{1}{2}$, $I=7/2$, for the extremes (*a*) $B=Q=0$, (*b*) $A=Q=0$.

Cobalt ammonium sulphate approximates to (*a*), and, for comparison, the nuclear levels of a diamagnetic cobalt compound in a field of 100,000 gauss are shown to scale in (*c*). The vertical lines in (*a*) and (*b*) represent kT for the lowest temperatures which could be reached by demagnetization from 1° K.

If a magnetic field is applied parallel to the axis, a first order Zeeman effect splits each doublet by an amount $2g_{\parallel}\beta|M|H$. In each case the two levels originating from the same doublet have opposite signs of m; for the upper doublets the lower component is that with negative m (assuming A positive), but for the lower doublets this is reversed. If it be assumed that the degree of nuclear polarization produced is measured by the ratio

of the total nuclear magnetic moment σ along the axis to the saturation nuclear magnetic moment $\sigma_{sat.}$ (*cf.* Rose 1949), a simple expression for this ratio can be found. It is

$$(\sigma/\sigma_{sat.})=\tanh\frac{|\mathrm{M}|g_{\parallel}\beta\mathrm{H}}{k\mathrm{T}}\,\frac{\sum_m m\sinh\frac{m|\mathrm{M}|\mathrm{A}}{k\mathrm{T}}}{\sum_m\cosh\frac{m|\mathrm{M}|\mathrm{A}}{k\mathrm{T}}}, \quad . \ . \ . \quad (19)$$

where m takes the values I, I-1, . . ., $\frac{1}{2}$ or 0. (In the summation, the terms for which $m=0$ should be weighted by a factor $\frac{1}{2}$.)

As an illustration, we will suppose that a field is applied which would split each doublet by an amount equal to A. In cobalt this would require a field of about 100 gauss, and the temperature would rise so that approximately $k\mathrm{T}=\mathrm{A}$ instead of 0·7A. Then (19) gives $(\sigma/\sigma_{sat.})=0{\cdot}3$ under these conditions. This calculation is, of course, based on the assumption that the cooling of the salt is due entirely to the paramagnetism of the cobalt ions. If the temperature could be lowered, for the same residual field, by the use of another paramagnetic salt in contact with the cobalt salt, the degree of nuclear polarization could be improved.

4.2. *Nuclear Alignment with* A=Q=0.

It is of some interest to examine the other extreme case which can occur for S=$\frac{1}{2}$, namely, when both A and Q are negligible compared with B. The energy levels in this case are given by the equation

$$\mathrm{W}=\pm\mathrm{B}\sqrt{[(\mathrm{I}+\tfrac{1}{2})^2-k^2]},$$

where k takes all values (I+$\frac{1}{2}$), (I$-\frac{1}{2}$), . . ., ($-$I+$\frac{1}{2}$). Each of these levels is a singlet composed of equal admixtures of the nuclear states $m=k\pm\frac{1}{2}$, but (except when $k=0$), the levels $\pm k$ coincide to give doublets. The energy levels for I=7/2 are shown in fig. 4 *b*, the scale being such that B in fig. 4 *b* is assumed equal to A in fig. 4 *a*. The vertical line again represents the value of kT at the lowest temperature which could be reached by adiabatic demagnetization of such a salt. At this temperature the populations of the nuclear states $\pm7/2$: $\pm5/2$: $\pm3/2$: $\pm1/2$ would be 0·34 : 0·62 : 0·86 : 1·0. The predominance lies with the states $\pm\frac{1}{2}$, corresponding to the fact that in this case we have a " plane magnet ", *i. e.* a magnet precessing in the plane normal to the symmetry axis. The nuclear alignment is a good deal less favourable than in the preceding case of B=0 because of the concentration of energy levels near the bottom.

As already pointed out, a small magnetic field applied in any direction produces only a second order Zeeman splitting, so that this is not a favourable case for Gorter's method.

From these extreme cases of B=Q=0 and A=Q=0 it is easy to see what happens in intermediate cases, which are obviously less favourable.

If A is large but B is not entirely negligible and $|M|=\frac{1}{2}$, the energy levels in fig. 4 *a* are displaced by amounts of the order B^2/A, and each level m has admixed with it the state $(m-1)$ or $(m+1)$ to an extent $(B/A)^2$. This is not serious until B becomes comparable with A. The case B=A corresponds to no anisotropy, and the energy levels fall into the usual two groups for $S=\frac{1}{2}$, corresponding to a new quantum number F with values $I+\frac{1}{2}$ and $I-\frac{1}{2}$. The splitting of this doublet (for $I=7/2$) is 4A=4B and each level contains an equal admixture of all the nuclear states m, so that no nuclear alignment in zero field is achieved at any temperature. This corresponds to the fact that with no anisotropy there is no preferred axis of alignment. As the value of B increases further relative to A the situation gradually changes to the extreme case A=0 which has already been considered.

The remarks of this section can be applied when $S>\frac{1}{2}$, if the levels $M=\pm\frac{1}{2}$ are lowest and $D\gg A, B$, if the parameter B is everywhere replaced by $B(S+\frac{1}{2})$. Thus a substance of this kind will approximate to the case of A negligible, even if A=B, when S is large, since the essential criterion is $A\ll B(S+\frac{1}{2})$.

§ 5. Discussion.

From the point of view of entropy, the use of the same paramagnetic salt for cooling and alignment can be summarized as follows. When the salt is magnetized in a very strong field at 1° K., the electronic entropy is completely removed. On demagnetizing to zero field, the entropy remains constant, but is divided between the electron and nuclear spins. In the simple cases considered in §4, each level is a doublet, and in the two levels of every doublet the electron spins are oppositely oriented. Thus at all temperatures the " electronic entropy " will be R log 2 in zero field, with a corresponding decrease in the nuclear entropy, giving a degree of alignment. When a magnetic field is applied, the electronic entropy decreases, and the nuclear entropy increases, until at fields large enough to separate the electronic levels so that their hyperfine patterns do not overlap, the electronic entropy is again zero, and the nuclear entropy $R\log_e(2I+1)$, with no polarization or alignment.

For this reason the discussion of the merits of the Gorter–Rose method has primarily been limited to the case of small magnetic fields. The formulæ given by Rose correspond, however, to the case of an applied field so large that the hyperfine structures of the different electronic levels no longer overlap (*cf.* fig. 2). Rose assumes that only the lower electronic level is occupied, and further, that the temperature is so low that the nuclear levels corresponding to the splitting of this electronic level are not all equally populated. This can only be achieved by the use of a second paramagnetic salt to produce the cooling, but it would be necessary to adopt an experimental arrangement whereby the external magnetic field used to produce the nuclear polarization is not applied to the second paramagnetic salt.

The requirement of a "dilute" paramagnetic salt for these experiments has already been pointed out (Bleaney 1951 a). The reason for this is that the random magnetic fields of neighbouring ions broaden the energy levels, and if these overlap considerably, the alignment will be largely destroyed. The criterion for the degree of dilution required is that the hyperfine structure shall be reasonably well resolved in the paramagnetic resonance spectrum. Thus salts of the iron group will require "dilution" with isomorphous diamagnetic compounds, but in the rare earth group this will probably not be necessary if the ethyl sulphates are used. These have only one ion in unit cell, and hyperfine structure lines can be resolved in the neodymium salt without dilution (Bleaney and Ingram 1949). The use of such dilute salts is also advantageous in cooling, since lower temperatures can be obtained; a disadvantage is that the rate of warming is larger owing to the smaller heat capacity.

§ 6. Conclusion.

In the first section of this paper general formulæ are given for the allowed transitions in the paramagnetic resonance spectrum. These are used to determine the magnitude of the parameters in the Hamiltonian (1). When a hyperfine structure is present, a certain amount of nuclear data may be obtained from the spectrum, the simplest datum being the value of the nuclear spin I from the multiplicity. From the experiments, values of the hyperfine structure constants A and B, and Q, if it is comparable in magnitude with A and B, can be found with fair accuracy. The relative signs of the parameters A, B, Q and D are much more difficult to elucidate from the spectrum, since they can only be found from second order effects. Where a crystalline splitting of the electronic levels is present ($D \neq 0$), second order effects in the overall size of the hyperfine structure in intermediate fields can be used for this purpose. An example of this is manganese (Bleaney and Ingram 1951 b), where, in addition, a subsidiary experiment on the anisotropy of the susceptibility gave the sign of D, and so determined all the signs.

For a salt where $S=\frac{1}{2}$, relative signs can only be found when weak transitions involving changes in the nuclear magnetic quantum number are observable. In strong fields such transitions arise from the electric quadrupole interaction, but, of the salts so far investigated, only those of copper have shown such an effect (Ingram 1949). In other cases the relative signs of A and B can in principle be found from the second order transitions $\Delta m = \pm 1$, which occur in weak fields, using the small displacement of these transitions due to the direct effect of the external field on the nuclear moment. This method is not generally feasible, since this effect is too small to detect except in strong fields, and there the transitions vanish in intensity, if the quadrupole interaction is negligible.

In cases where no weak transitions $\Delta m = \pm 1$ are visible, or no anomalous spacing of the hyperfine structure is detectable, the formulæ given in §2.2

can be used to obtain upper limits for the magnitude of Q. A more sensitive method is observation of the allowed transitions in zero magnetic field, as emphasized in §3. This necessitates covering a wide wavelength range, generally in the decimetre wavelength region, where the sensitivity of the method, using a small single crystal to obtain the greatest accuracy, is rather low. Such experiments are under way in this laboratory.

In this paper the author has not attempted to consider the relation of the parameters D, A, B, and Q to the electronic state of the ion and the crystalline field. The intricate theory required for this purpose has been the subject of a general review by Abragam and Pryce (1951 a). It seems that the theory is now sufficiently accurate to enable quantitative data concerning the nuclear moments to be deduced from the paramagnetic spectra in many cases (see, for example, Elliott and Stevens 1951). Relative values of the moments of different isotopes of the same element can be obtained, of course, directly from the spectra.

Acknowledgment.

The author wishes to acknowledge the many contributions made by Professor M. H. L. Pryce in discussion, particularly in the evaluation of the transitions in strong fields, and the use of the direct effect of the external field on the nucleus to obtain the relative signs of the parameters in the Hamiltonian. He is also indebted to Dr. K. W. H. Stevens for much helpful discussion and criticism.

References

Abragam, A., and Pryce, M. H. L., 1951, *Proc. Roy. Soc.* A, **205,** 135.

Bleaney, B., 1950, *Phys. Rev.*, **78,** 214; 1951 a, *Proc. Phys. Soc.* A, **64,** 315; 1951 b, *Proc. Phys. Soc.* A, **64,** 316.

Bleaney, B., and Ingram, D. J. E., 1949, *Nature, Lond.*, **164,** 116; 1951 a, *Proc. Roy. Soc.* A (in publication); 1951 b, *Proc. Roy. Soc.* A, **205,** 336.

Elliott, R. J., and Stevens, K. W. H., 1951, *Proc. Phys. Soc.* A, **64,** 205.

Ingram, D. J. E., 1949, *Proc. Phys. Soc.* A, **62,** 664.

Gorter, C. J., 1948, *Physica*, **14,** 504.

Pound, R. V., 1949, *Phys. Rev.*, **76,** 1410.

Pryce, M. H. L., 1949, *Nature, Lond.*, **164,** 116.

Rose, M. E., 1949, *Phys. Rev.*, **75,** 213.

Spiers, J. A., 1948, *Nature, Lond.*, **161,** 807; 1949, *Directional Effects in Radioactivity* (Chalk River, Ontario: National Research Council of Canada).

LI. *The Communal Entropy of Dense Systems.*

By J. A. Pople,
Department of Theoretical Chemistry, University of Cambridge*.

[Received February 16, 1951].

Summary.

This paper contains an approximate method of calculating the communal entropy of an assembly of monatomic particles. The method of dealing with dense systems may be regarded as an extension of that used by Lennard-Jones and Devonshire in their theory of liquids and dense gases. The available volume is divided into cells and the communal free energy expressed in terms of a set of parameters related to the probability of two, three or more particles occupying a given cell simultaneously. Application to an assembly of rigid spheres leads to the conclusion that the communal entropy does not become appreciable until the available volume is over five times that of a close-packed assembly. This suggests that, for more accurate intermolecular potentials, the communal entropy is practically zero in the solid and liquid states, but that the extra terms in the free energy may have an appreciable effect on the calculated critical constants and vapour pressures.

§1. Introduction.

According to classical statistical mechanics, the thermodynamic functions of a system of N particles confined to a volume v can be derived from the free energy A given by

$$\exp(-A/kT) = \frac{1}{N!}\left(\frac{2\pi mkT}{h^2}\right)^{3N/2}\int^v \ldots \int^v \exp(-V/kT)\, dv_1 \ldots dv_N, \quad (1.01)$$

where V is the potential energy of any configuration and $\int^v dv_i$ indicates integration of the coordinates of particle i over the whole volume v.

The only exact method of calculating the integral in (1.01) is that of Mayer (1937). However, this only applies to a limited range of densities and is exceedingly difficult to handle mathematically. Of the approximate methods used many (Eyring and Hirschfelder 1937, Lennard-Jones and Devonshire 1937) have been based on a model in which each particle is confined to a cell by its neighbours. Lennard-Jones and Devonshire calculate the field in such a cell on the assumption that the neighbours are in their equilibrium positions. An improved form for the cell field has recently been suggested by Kirkwood (1950).

Although these cell models may give a reasonable picture of molecular environment at high densities, they will become increasingly inaccurate as the cell size increases. At low densities restriction to cells will prevent

* Communicated by Prof. Sir John Lennard-Jones.

collisions occurring and the method gives no second virial coefficient. An attempt to remedy this situation and to extend the cell method to low densities has recently been made by Buehler, Wentorf, Hirschfelder and Curtiss (1951). In addition to the model used by Lennard-Jones and Devonshire, which they call the "empty centre model", they consider another in which the wandering particle moves in the field of particles fixed at the centres of neighbouring cells *and* one fixed at the centre of the cell in question. This is called the "occupied centre model"*. The arithmetic mean of the two free volumes is then used to construct the partition function. This method reduces to that of Lennard-Jones and Devonshire at high densities and gives the correct second virial coefficient at low densities. No theoretical justification is given for this averaging process, however; in the intermediate region the arithmetic mean formula is no more than a convenient method of interpolation.

When the cell method was originally developed, it was pointed out by Hirschfelder, Stevenson and Eyring (1937) and also by Lennard-Jones and Devonshire (1937) that the approximation of placing one particle in each cell, from which all others were excluded, constitutes an artificial restriction on the region of phase space over which integration is to be performed. It can be shown that, in the limit of low density, this corresponds to the omission of a factor e^N in the partition function and leads to an error of k per particle in the calculated entropy. This extra term is usually referred to as the communal entropy; it has been discussed in some detail by Lennard-Jones (1940). The chief purpose of this paper is to examine this term and show how it is connected with the work of Buehler *et al.*

Although we know that the communal entropy increases from zero to k per particle as the volume increases to infinity, no satisfactory theory of the point at which it becomes effective has been advanced. Originally, it was suggested by Hirschfelder, Stevenson and Eyring (1937) that it becomes available at the melting point. This hypothesis has been examined by O. K. Rice (1938) who concludes that it is without sufficient justification and that the communal entropy is unlikely to play a major part in the fusion process. We shall see that the theory of this paper confirms Rice's conclusions.

In this and subsequent work (1944) Rice has discussed the communal entropy of an aggregate of hard spheres in some detail. In the later paper he claims to show that for a gas of hard elastic spheres the communal entropy is fully excited for each direction of space, and amounts in all to 3 R per mole. As these results are at variance with those obtained in this paper, it is well to find the cause of the discrepancy before proceeding further. The difference lies in the meaning attached to the phrase "restriction to a cell". Rice interprets this as meaning that the whole of the molecule must lie within the cell. Although this has a precise meaning in the case of hard elastic spheres, it leads to difficulties when we deal with

* In the published version of their work, Buehler *et al.* have used the terms "soft-centre model" and "hard-centre model".

actual molecules which have no fixed boundaries. Here we shall say that a given particle occupies a certain cell if its centre (or some fixed point of the molecule if it is non-central) lies in that cell.

In this paper we shall discuss the way we should set about calculating the communal entropy and free energy in a general manner. These are expressed in terms of a set of quantities $\omega_2, \omega_3 \ldots$. which are related to the probabilitity of two, three or more particles occupying a given cell simultaneously. It is shown that ω_2 is the most important of these and that a good approximation to the extra terms in the thermodynamic functions can be obtained if we neglect the others. This is followed by a simple model for the calculation of ω_2. With some further approximations, it is found that ω_2 can be expressed in terms of the free volumes of the empty and occupied centre models used by Buehler *et al.* In this way we have obtained a formula for the communal free energy which is, in effect, a theoretical foundation for the use of these models. The most important result of the investigation is the modification of the arithmetic mean formula. If v_{fe} and v_{fo} are the free volumes of the empty and occupied centre models respectively, it is suggested that the true free volume should be calculated from

$$v_f = v_{fe} + \sqrt{(2 v_{fe}\, v_{fo})}. \qquad (1.02)$$

At the end of the paper, this formula is applied to estimate the communal free energy of a system of rigid spheres, using the values of v_{fe} and v_{fo} calculated by Buehler *et al.*

§ 2. A General Method for Calculating the Communal Entropy.

We shall base our work on the recent analysis of the cell method given by Kirkwood (1950), using a similar notation. If we write

$$\mathrm{Z} = \int^{v} \ldots \int^{v} \exp\left(-\mathrm{V}/k\mathrm{T}\right) dv_1 \ldots dv_{\mathrm{N}}, \qquad (2.01)$$

the free energy is given by

$$\frac{\mathrm{A}}{\mathrm{N}k\mathrm{T}} = -\frac{3}{2}\log\frac{2\pi m k\mathrm{T}}{h^2} - \frac{1}{\mathrm{N}}\log \mathrm{Z} + \frac{1}{\mathrm{N}}\log \mathrm{N}! \qquad (2.02)$$

Kirkwood now supposes the volume v to be divided up into a lattice of N equal cells and writes $\mathrm{Z}^{(m_1 \ldots m_{\mathrm{N}})}$ for the restricted phase integral in which the cells are occupied by $m_1 \ldots m_{\mathrm{N}}$ particles respectively. Z/N! can then be divided up as follows :

$$\frac{\mathrm{Z}}{\mathrm{N}!} = \sum_{\substack{m_1 \ldots m_{\mathrm{N}} \\ \Sigma m_i = \mathrm{N}}}^{\mathrm{N}} \frac{1}{\Pi m_s!}\, \mathrm{Z}^{(m_1 \ldots m_{\mathrm{N}})}. \qquad (2.03)$$

The usual cell method is concerned with an approximate evaluation of $\mathrm{Z}^{(1 \ldots 1)}$. If we write

$$\frac{\mathrm{Z}}{\mathrm{N}!} = \sigma^{\mathrm{N}} \mathrm{Z}^{(1 \ldots 1)}, \qquad (2.04)$$

the communal free energy may be defined as $-\mathrm{N}k\mathrm{T}\log\sigma$ and the communal entropy as

$$\mathrm{N}k\left\{\log\sigma+\frac{\mathrm{T}}{\sigma}\left(\frac{\partial\sigma}{\partial\mathrm{T}}\right)_v\right\}.$$

From (2.03) and (2.04) we see that the value of σ will depend on the ratio of the phase integral with multiple occupation $\mathrm{Z}^{(m_1,\cdots m_\mathrm{N})}$ to $\mathrm{Z}^{(1\cdots 1)}$. We shall suppose that this ratio can be expressed as a product of the form

$$\frac{\mathrm{Z}^{(m_1\cdots m_\mathrm{N})}}{\mathrm{Z}^{(1\ldots 1)}}=\prod_{s=1}^{\mathrm{N}}\omega_{m_s}, \qquad \ldots\ldots \quad (2.05)$$

where there is an ω-factor for each type of occupation (vacancy, single occupation, double occupation, etc.). Clearly we must have $\omega_1=1$. Also we may take $\omega_0=1$ without loss of generality, for if $\omega_0\neq 1$ we may replace it by 1 and at the same time replace $\omega_i(i\neq 0)$ by $\omega_0^{i-1}\,\omega_i$ without altering $\Pi\omega_{m_s}$.

The approximation (2.05) is equivalent to assuming that multiply occupied cells do not interfere with one another. It will be accurate at high densities when there are very few multiply-occupied cells and at low densities when the cells are large and effectively independent. It therefore seems reasonable to use it throughout the full range of volume. ω_2 may be described as the ratio in which the restricted phase integral is altered if we remove a particle from a singly occupied cell and move it to another also singly occupied, leaving a doubly occupied cell and a hole. ω_3. ω_4 . . . . . may be defined in similar ways.

We next have to solve the problem of finding σ when we are given the values of the ω's. The full expression,

$$\sigma^\mathrm{N}=\sum_{\substack{m_1\ldots m_\mathrm{N}\\ \Sigma m_i=\mathrm{N}}}^{\mathrm{N}}\prod_{s=1}^{\mathrm{N}}\left(\frac{\omega_{m_s}}{m_s!}\right), \qquad \ldots\ldots \quad (2.06)$$

obtained from (2.03), (2.04) and (2.05) has to be converted into a less unwieldy form.

Suppose that a given partition $m_1\ldots m_\mathrm{N}$ contains $n_i(m_1\ldots m_\mathrm{N})$ cells with i and not more than i particles. Then, since we are dealing with N particles and N cells, we must have

$$\left.\begin{aligned}\sum_{i=0}^{\mathrm{N}} i\,n_i&=\mathrm{N},\\ \sum_{i=0}^{\mathrm{N}} n_i&=\mathrm{N}.\end{aligned}\right\} \qquad \ldots\ldots \quad (2.07)$$

The number of partitions $m_1\ldots m_\mathrm{N}$ with n_0 empty cells, n_1 singly occupied cells, etc., is

$$\frac{\mathrm{N}!}{n_0!\,(\mathrm{N}-n_0)!}\,\frac{(\mathrm{N}-n_0)!}{n_1(\mathrm{N}-n_0-n_1)!}\cdots=\frac{\mathrm{N}!}{n_0!\,n_1!\ldots n_\mathrm{N}!}. \qquad (2.08)$$

Equation (2.06) can therefore be written

$$\sigma^{N}= \underset{n_0 n_1 \ldots n_N}{\Sigma^*} \frac{N!}{n_0!\ n_1! \ldots n_N!} \prod_{s=0}^{N} \left(\frac{\omega_s}{s!}\right)^{n_s}, \quad . \ . \ . \quad (2.09)$$

where Σ^* indicates summation over those values of $n_0, n_1 \ldots n_N$ which satisfy (2.07). As we shall only be concerned with the logarithm of σ we may follow the usual procedure and replace the series in (2.09) by its largest term. We therefore seek the unconditional maximum of

$$G=\log\left\{\frac{N!}{n_0!\ n_1! \ldots n_N!} \prod_{s=0}^{N} \left(\frac{\omega_s}{s!}\right)^{n_s}\right\} + \left(\log\frac{\lambda}{N}\right) \sum_{i=0}^{N} n_i + (\log\mu) \sum_{i=0}^{N} i\, n_i,$$
$$\ldots \quad (2.10)$$

$\log(\lambda/N)$ and $\log\mu$ are Lagrange multipliers taken in this form for convenience in the subsequent analysis.

Using Stirling's formula we find that the maximum term occurs when

$$n_i=N\lambda\mu^i\,\omega_i/i! \qquad (i=0, \ldots N), \quad . \ . \ . \ . \quad (2.11)$$

where the parameters λ and μ are determined from the conditions

$$\left.\begin{aligned} \Sigma n_i &= \sum_{i=0}^{N} N\lambda\mu^i \frac{\omega_i}{i!} &&= N, \\ \Sigma i\, n_i &= \sum_{i=0}^{N} N\lambda\mu^i \frac{\omega_i}{(i-1)!} &&= N. \end{aligned}\right\} \quad . \ . \ . \ . \ . \quad (2.12)$$

If we define

$$f(x)= \sum_{i=0}^{N} (\omega_i/i!)\, x^i, \quad . \ . \ . \ . \ . \ . \quad (2.13)$$

(2.12) may be written

$$\lambda^{-1}=f(\mu)=\mu f'(\mu). \quad . \ . \ . \ . \ . \ . \quad (2.14)$$

Finally we have

$$\sigma=\left[\left\{\frac{N!}{n_0!\ldots n_N!} \prod_{s=0}^{N} \left(\frac{\omega_s}{s!}\right)^{n_s}\right\}_{\max}\right]^{1/N} = \frac{1}{\lambda\mu}=f'(\mu). \quad . \quad (2.15)$$

The complete solution may therefore be written in implicit form

$$\sigma= f(\mu)/\mu=f'(\mu). \quad . \ . \ . \ . \ . \ . \quad (2.16)$$

§ 3. The Contribution of Double Occupation.

If all the ω's except ω_2 vanish, equation (2.16) can be solved explicitly. In this case

$$f(x)=1+x+\tfrac{1}{2}\omega_2 x^2, \quad . \ . \ . \ . \ . \ . \quad (3.01)$$

whence

$$\mu=\sqrt{(2/\omega_2)}, \qquad \sigma=1+\sqrt{(2\omega_2)}. \quad . \ . \ . \ . \quad (3.02)$$

This leads to a free energy

$$\frac{A}{NkT}=-\frac{3}{2}\log\frac{2\pi mkT}{h^2} - \log Z^{(1\ldots1)} - \log\{1+\sqrt{(2\omega_2)}\}. \quad (3.03)$$

This is the solution we get if we replace the limitation of single occupation by a condition which prevents more than two particles occupying a cell simultaneously. We know that ω_2 varies for 0 to 1 as the volume increases, so (3.03) shows at once that at low densities $\log\{1+\sqrt{2}\}$ or 88 per cent of the communal entropy is due to double occupation of cells. It is also possible to get the equation of state from (3.03) by the usual formula

$$\frac{pv}{\mathrm{RT}} = v\frac{\partial}{\partial v}\left(-\frac{\mathrm{A}}{\mathrm{N}k\mathrm{T}}\right). \quad . \quad . \quad . \quad . \quad . \quad . \quad . \quad (3.04)$$

To find ω_2 at low densities we may neglect the effect of particles in other cells and write

$$\omega_2 = \frac{\mathrm{N}^2}{v^2}\int^{\Delta}\int^{\Delta} \exp\left[-\mathrm{E}(r_{12})/k\mathrm{T}\right] dv_1\, dv_2$$

$$= 1 - \frac{\mathrm{N}^2}{v^2}\int^{\Delta} dv_1 \int^{\Delta} \{1-\exp\left[-\mathrm{E}(r_{12})/k\mathrm{T}\right]\} dv_2, \quad . \quad . \quad (3.05)$$

where $\mathrm{E}(r_{12})$ is the intermolecular energy of the pair of particles 1 and 2. As far as terms of order v^{-1} are concerned, we can replace integration over Δ with respect to v_2 by integration to infinity, so that we get

$$\omega_2 = 1 - \frac{4\pi\mathrm{N}}{v}\int_0^{\infty} r^2\{1-\exp\left[-\mathrm{E}(r)/k\mathrm{T}\right]\} dr. \quad . \quad . \quad . \quad (3.06)$$

From (3.03) and (3.06) we now get the equation of state

$$\frac{pv}{\mathrm{RT}} = 1 + \frac{1}{1+1/\sqrt{2}}\frac{2\pi\mathrm{N}}{v}\int_0^{\infty} r^2\{1-\exp\left[-\mathrm{E}(r)/k\mathrm{T}\right]\} dr + \mathrm{O}\left(\frac{1}{v^2}\right). \quad (3.07)$$

From this equation we see that the theory allowing for double occupation gives a second virial coefficient equal to $\sqrt{(2)}/[\sqrt{(2)}+1]$ or 58·6 per cent of the correct value. Thus, even in the limiting case, (3.03) corrects the major part of the deficiency of the original cell method. At higher densities, the value of ω_3, ω_4, etc. will be smaller relative to ω_2 and (3.03) will become even more accurate. It seems very probable that, in the critical region, the terms ω_3, ω_4 . . . will, in fact, be quite unimportant, so we shall not discuss them further.

§ 4. Models for Evaluating ω_2.

The next step in the theory is to set up simple models for the calculation of the multiple occupation factor ω_2. To find this we shall use a modification of the method of Lennard-Jones and Devonshire, in which each particle is treated as moving independently in a cell field $\psi(\mathbf{r})$. We shall make the further approximation of supposing that this field is unaltered when a neighbouring cell becomes vacant or doubly occupied. The errors in the two cases to some extent cancel. ω_2 can then be expressed in terms of the phase intergal for two particles moving in the ordinary cell field $\psi(\mathbf{r})$. If we write

$$\psi_1(\mathbf{r}) = \psi(\mathbf{r}) - \psi(0), \quad . \quad . \quad . \quad . \quad . \quad . \quad (4.01)$$

this expression for ω_2 is, from the definition in § 2.

$$\omega_2 = \frac{\int^{\Delta}\int^{\Delta} \exp\{-[\psi_1(\mathbf{r}_1)+\psi_1(\mathbf{r}_2)+\mathrm{E}(r_{12})]/k\mathrm{T}\}\, dv_1\, dv_2,}{\left\{\int^{\Delta} \exp[-\psi_1(\mathbf{r})/k\mathrm{T}]\, dv\right\}^2} \quad . \quad (4.02)$$

where $\int^{\Delta}$ indicates integration over the cell. Similar formulæ could be given for ω_3, ω_4, etc.

If the integral in the numerator of (4.02) is written as I_2, we have

$$\mathrm{I}_2 = \int^{\Delta} \mathrm{Q}(\mathbf{r}_1) \exp[-\psi(\mathbf{r}_1)/k\mathrm{T}]\, dv_1, \quad . \quad . \quad . \quad (4.03)$$

where

$$\mathrm{Q}(\mathbf{r}_1) = \int^{\Delta} \exp\{-[\psi_1(\mathbf{r}_2)+\mathrm{E}(r_{12})]/k\mathrm{T}\}\, dv_2, \quad . \quad . \quad (4.04)$$

$\mathrm{Q}(\mathbf{r}_1)$ may be described as the free volume of particle 2 in the cell, given that particle 1 is the point $\mathbf{r}_1$.

In the case of a spherically symmetric cell, $\mathrm{Q}(\mathbf{r})$ can be expanded about the origin as follows :

$$\mathrm{Q}(r_1) = \sum_{i=0}^{\infty} \frac{r_1^{2i}}{(2i)!}\left(\frac{\partial^{2i}\mathrm{Q}}{\partial r^{2i}}\right)_0. \quad . \quad . \quad . \quad . \quad . \quad (4.05)$$

The integral I_2 then becomes

$$\mathrm{I}_2 = \sum_{i=0}^{\infty} \left(\frac{\partial^{2i}\mathrm{Q}}{\partial r^{2i}}\right)_0 \frac{1}{(2i)!}\int^{\Delta} r^{2i} \exp[-\psi(r)/k\mathrm{T}]\, dv. \quad . \quad . \quad (4.06)$$

The coefficients $\left(\frac{\partial^{2i}\mathrm{Q}}{\partial r^{2i}}\right)_0$ can be written

$$\left(\frac{\partial^{2i}\mathrm{Q}}{\partial r^{2i}}\right)_0 = \int^{\Delta}\left\{\frac{\partial^{2i}}{\partial r_1^{2i}} \exp[-\mathrm{E}(r_{12})/k\mathrm{T}]\right\}_0 \exp[-\psi_1(r_2)/k\mathrm{T}]\, dv_2, \quad (4.07)$$

leading to

$$(\mathrm{Q})_0 = \int^{\Delta} \exp\{-[\psi_1(r)+\mathrm{E}(r)]/k\mathrm{T}\}\, dv,$$

$$\left(\frac{\partial^2\mathrm{Q}}{\partial r^2}\right)_0 = -\frac{1}{k\mathrm{T}}\int^{\Delta}\left[\frac{2}{3r}\mathrm{E}' + \tfrac{1}{3}\left(\mathrm{E}'' - \frac{\mathrm{E}'^2}{k\mathrm{T}}\right)\right] \exp\{-[\psi_1(r)+\mathrm{E}(r)]/k\mathrm{T}\}\, dv.$$

. . . (4.08)

A simple first approximation would be to neglect all but the first term in (4.05) and write $\mathrm{Q} = (\mathrm{Q})_0$. Examination of equation (4.08) shows that this is just the free volume of the occupied-centre model used by Buehler, Wentorf, Hirschfelder and Curtiss (1951). In their notation v_{fe} is the free volume in an empty cell and v_{fo} is the free volume when there is a particle at the centre*. Thus to this approximation

$$\mathrm{Q} = v_{fo}, \qquad \mathrm{I}_2 = v_{fe}v_{fo}, \qquad \omega_2 = v_{fo}/v_{fe}. \quad . \quad . \quad . \quad (4.09)$$

If we neglect ω_i for $i > 2$ the free energy is given by

$$\frac{\mathrm{A}}{\mathrm{N}k\mathrm{T}} = -\frac{3}{2}\log\frac{2\pi mk\mathrm{T}}{h^2} - \log v_{fe} - \frac{\Phi_0}{\mathrm{N}k\mathrm{T}} - \log\{1+\sqrt{(2v_{f0}/v_{fe})}\}, \quad . \quad . \quad (4.10)$$

* Buehler *et al.* use v_{fs} and v_{fh} in the published version of their paper.

where $(-\Phi_0)$ is the potential energy of the system when each particle is at the centre of its cell.

This formula could be used to calculate the equation of state from the thermodynamic relation

$$p=-\left(\frac{\partial A}{\partial v}\right)_T . \quad . \quad . \quad . \quad . \quad . \quad . \quad . \quad (4.11)$$

In their modification of the original work of Lennard-Jones and Devonshire, Buehler, Wentorf, Hirschfelder and Curtiss use the formula

$$\frac{A}{NkT}=-\frac{3}{2}\log\frac{2\pi mkT}{h^2}-\log v_f-\frac{\Phi_0}{NkT} \quad . \quad . \quad . \quad . \quad . \quad (4.12)$$

where

$$v_f=\tfrac{1}{2}(v_{fe}+v_{f0}) \quad . \quad . \quad . \quad . \quad . \quad . \quad . \quad . \quad (4.13)$$

This formula, however, is only an empirical way of interpolating the equation of state, and does not give the correct entropy changes. From the theory of this paper, it appears that a more satisfactory procedure would be to replace the arithmetic mean formula (4.13) by

$$v_f=v_{fe}+\sqrt{(2v_{fe}\,v_{f0})} \quad . \quad . \quad . \quad . \quad . \quad . \quad . \quad (4.14)$$

Buehler, Wentorf, Hirschfelder and Curtiss (1951) have found v_{fe} and v_{f0} for a gas of rigid spheres. Using their figures we can easily get ω_2 and the communal part of the free energy as functions of the volume. The results are shown below. v_0 is the least volume into which the spheres of diameter r_0 can be packed.

TABLE.

The communal free energy of a gas of rigid spheres.

v/v_0	$v_{fe}/48r_0^3$	$v_{fo}/48r_0^3$	w_2	$-(A/NkT)_{\text{Communal}}$
1·000	—	—	—	—
2·828	·0102	—	—	—
4·887	·0550	·0018	·032	·044
7·761	·1143	·0272	·238	·290
10·0	·1473	·0600	·407	·454
15·0	·2210	·1337	·605	·618
20·0	·2946	·2073	·704	·691

Examination of this table shows that the communal entropy does not become appreciable until the total volume is about five times the volume of the close-packed lattice. It seems probable that the results would be similar if other, more accurate, inter-molecular potentials were used. The general conclusion is, therefore, that the communal entropy is practically zero in the solid and liquid states, but may form an appreciable part of the entropy of evaporation. Cell theories of critical phenomena, such as that of Lennard-Jones and Devonshire, should be corrected to allow for it. In the application of their theory to vapour pressures and boiling points,

Lennard-Jones and Devonshire (1938) included the additional factor e^N in the liquid partition function. At the end of their paper, however, they stated that if this factor was omitted, the calculated vapour pressures would be reduced by a factor of e and the calculated boiling points by about 9 per cent. The present work shows that these corrections should be applied.

The author is indebted to Professor Sir J. Lennard-Jones for the loan of an advance copy of a paper by Buehler, Wentorf, Curtiss and Hirschfelder, sent to him by Professor Hirschfelder.

References.

Beuhler, R. J., Wentorf, R. H., Hirschfelder, J. O., and Curtiss, C. F., 1951, *J. Chem. Phys.*, **19,** 61.

Eyring, H., and Hirschfelder, J. O., 1937, *J. Phys. Chem.* **41,** 249.

Hirschfelder, J. O., Stevenson, D., and Eyring, H., 1937, *J. Chem. Phys.*, **5,** 896.

Kirkwood, J. G., 1950, *J. Chem. Phys.*, **18,** 380.

Lennard-Jones, J. E., 1940, *Proc. Phys. Soc.*, **52,** 729.

Lennard-Jones, J. E., and Devonshire, A. F., 1937, *Proc. Roy. Soc.* A, **163,** 53; 1938, *Ibid.*, **165,** 1.

Mayer, J. E., 1937, *J. Chem. Phys.*, **5,** 67.

Rice, O. K., 1938, *J. Chem. Phys.*, **6,** 476 ; 1944, *Ibid.*, **12,** 1.

LII. *Grain Boundary Diffusion in Metals.*

By A. D. Le Claire,
Atomic Energy Research Establishment, Harwell *.

[Received February 16, 1951.]

Abstract.

By an extension of a recent analysis of the problem of grain boundary diffusion in metals, the expression

$$\frac{D'}{D} = \frac{1}{\delta} \cdot 2\,(\pi D t)^{1/2} \cot^2 \alpha$$

has been derived relating the diffusion coefficients D′ and D for grain boundary and for volume diffusion, δ the effective " width " of the grain boundary and α the angle at time t between a line of constant concentration and the grain boundary at the point where it meets the grain boundary. Some remarks are made on the use of the equation and when it is applied to a recent experimental observation on grain boundary diffusion of copper in nickel, the result is deduced that $D' = 8$ cm.^{2}/day at 1000° C.

A discussion follows on some aspects of the relation of other work on grain boundaries to grain boundary diffusion. Evidence is presented, based on models of the grain boundary, which suggests that the activation energies for grain boundary and for volume diffusion may not differ appreciably.

§ 1. Introduction.

Work on preferential grain boundary diffusion in metals has in the past been hampered by the lack both of a quantitative treatment of the process and of reliable experimental methods for studying it. It is the purpose of this note to extend a recent analysis (Fisher 1950) of the problem in such a way that the simple qualitative method of study reported from this laboratory (Barnes 1950) can be made to yield quantitative results with very little extra work. A discussion is then given of the importance of such quantitative studies insofar as they may give information on the nature of the grain boundaries themselves.

§ 2. Quantitative Methods for Grain Boundary Diffusion Studies.

(a) *Fisher's Analysis.*

Fisher (1950) has recently obtained, with certain assumptions, an expression for the concentration of diffusing material in the neighbourhood of a grain boundary in terms of the time t during which diffusion has been

* Communicated by the Author.

taking place down the grain boundary, the coordinates x, y, (see fig. 1) and the coefficients D′ and D for grain boundary and for volume diffusion respectively.

$$C = \mathrm{Exp}\left(\frac{-y_1\sqrt{(2)}}{(\pi t_1)^{1/4}}\right) . \mathrm{Erfc}\left(\frac{x_1}{2t_1^{1/2}}\right)^{*} \quad . \quad . \quad . \quad . \quad . \quad (1)$$

where $t_1 = \frac{Dt}{\delta^2}$; $x_1 = \frac{x}{\delta}$; $y_1 = \frac{y}{\delta}\left(\frac{D'}{D}\right)$.

The grain boundary commences at the point $x=0$, $y=0$ and δ is its effective " width ".

Fig. 1.

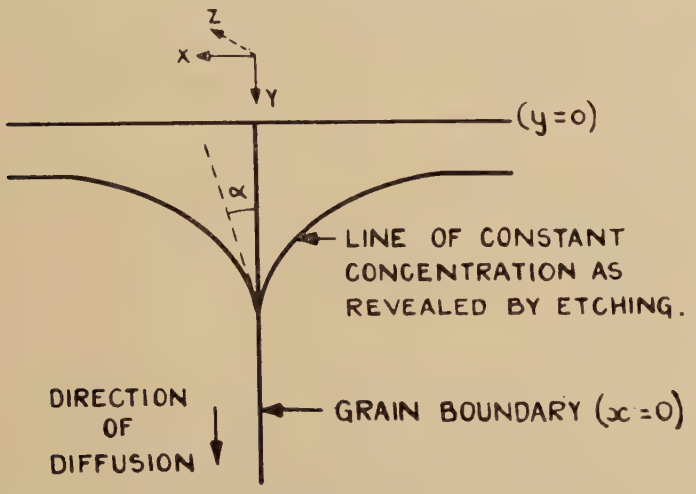

Diffusion down a grain boundary.

As a confirmation of the validity of equation (1), Fisher has successfully applied it to an interpretation of the results of an experiment on the grain boundary diffusion of radioactive silver in polycrystalline silver, by the standard technique of measuring the activity of layers of silver perpendicular to the diffusion direction, machined from the diffusion zone. He obtains with the assumption $\delta = 5\times10^{-8}$, *i. e.* about two atomic spacings,

$$D'/D = 9{\cdot}4\times10^{5}.$$

(b) *Author's Extension.*

More recently a publication from this laboratory (Barnes 1950) has described how the contours of concentration in the neighbourhood of a grain boundary, down which preferential diffusion (in this case of copper in the grain boundaries of nickel) is taking place, can be revealed by etching. It was suggested therein that the angle α between the grain boundary and a

---

* $\mathrm{Erfc}\ x = 1 - \frac{2}{\sqrt{(\pi)}}\int_0^x e^{-t^2}\,dt$,

concentration contour at the point where it meets the grain boundary could be used as a measure of the ratio of the rates of diffusion down the grain boundary and into the grain. This ratio of course is only of secondary importance but by development of equation (1) measurements of the angle α can be used to calculate the ratio of the actual diffusion coefficients for grain boundary and for volume diffusion.

Simple differentiation of equation (1) gives the slope at any point (x, y) of a line of constant concentration c at time t. From this is readily deduced the equation

$$\frac{D'}{D} = \frac{1}{\delta} 2(\pi D t)^{1/2} \cot^2 \alpha. \quad . \quad . \quad . \quad . \quad . \quad . \quad (2)$$

connecting the ratio of D′ and D with the angle α. When this equation is applied to the previously published work on copper–nickel, taking $\alpha = 30°$ (see fig. 1, Barnes 1950) $D \sim 10^{-5}$ cm.^{2}/day and assuming again $\delta = 5 \cdot 10^{-8}$, we find

$$D'/D = 8 \cdot 10^5 \text{ at } 1000°\text{C.},$$

a ratio the order of magnitude of which is the same as that obtained for self diffusion in silver.

Inserting the known value of D into this equation gives

$$D' = 8 \text{ cm.}^2\text{/day.}$$

Fisher's analysis provides the first real attempt to study grain boundary diffusion in metals in a quantitative way and it is suggested that the extension of his relation to give equation (2), together with the experimental method for providing values of α, constitute a simpler and quicker means of obtaining grain boundary diffusion coefficients in metals than a sectioning technique such as used by Fisher. Possibly many micro-photographs showing diffusion in metals may already exist in which a preferential grain boundary penetration is apparent and to which the relation (2) could be usefully applied.

A calculation of D′/D from equation (2) requires some assumption as to the magnitude of δ, the width of the grain boundary. This is usually stated as being a "few atomic diameters", this estimate being based on the assumption of the transitional lattice theory of the grain boundary and the assertion of very short range forces between atoms. A precise evaluation of δ, and so of D′, is not possible at present, but for practical purposes we may use D′δ in place of D′ to characterize grain boundary diffusion rates, for D′δ clearly represents the amount of material diffusing in unit time under unit concentration gradient per unit length of the grain boundary in the "z" direction (fig. 1) and perpendicular to that length. D′δ can be obtained by measurement of only α, D and t, and requires no assumptions about the structure of the grain boundary. The results for copper in nickel give

$$D'\delta/D = 0{\cdot}04 \text{ cms.}$$

There are two points that need bearing in mind in any use of equation (2). The first is to ensure that the grain boundary is normal to the plane in which α is being measured, and that the grain boundary has not migrated during the diffusion anneal. The second point is to remember that the equation (1) is derived on the assumption that D and D′ are independent of concentration, so that the value of D′/D obtained will only be a mean value for the concentration range covered in the experiment. It should be noted that any variation of α with the position of the point on the grain boundary at which it is measured will indicate a variation not of D′/D but of $D'/D^{3/2}$ with concentration. (Such a variation was in fact found in the experiment on copper and nickel.) It can probably be assumed that each value of D′/D corresponds, although probably only roughly when D′/D is strongly dependent on concentration, with the concentration at the point where the corresponding value of α was measured.

§3. Grain Boundary Models and Diffusion.

It is interesting to consider how other work on the properties of grain boundaries might be related to grain boundary diffusion studies.

In view of the difference between D′ and D it is important to know whether it is due to a decrease in the activation energy "Q" for grain boundary diffusion over volume diffusion, or to an increase in the constant term D_0 in the expression usually used to express the temperature dependence of diffusion rates.

$$D=D_0 \exp(-Q/RT). \quad . \quad . \quad . \quad . \quad . \quad . \quad (3)$$

We may perhaps draw some conclusions by considering some of the grain boundary models that have been proposed.

To explain his result that the activation energy for grain boundary slip in several metals is the same as that for their volume diffusion and for the constant rate creep of single crystals, Kê (1949) has suggested the concept of "disordered groups" of atoms as the units responsible for all three processes. These exist in certain concentration in the body of the crystal, but in much higher concentration at the grain boundary which therefore consists of regions of good fit separated by regions of disorder, the "disordered groups". The rearrangement of atoms within a group normally constitutes a diffusion process, but in the presence of a shear stress leads to slip. The equality of the activation energies for the three processes considered by Kê is thus satisfactorily explained. But the same rearrangement of the atoms of a disordered group at the grain boundary will lead to grain boundary diffusion, so that on Kê's model, the activation energies for volume and grain boundary diffusion will also be the same.

A study of the temperature dependence of D′ and comparison with that of D would both settle the relative values of the corresponding activation energies Q′ and Q and provide useful confirmation or otherwise of such grain boundary models as this one of Kê. In such studies one must remember that any impurities which segregate in the grain boundary will most likely

have an effect on Q′ out of all proportion to their total concentration. As an example of the great importance of impurities in grain boundary studies, we may quote Kê (1949) who found that even very small quantities of impurity may completely block grain boundary slip.

Dislocation models of the grain boundary have been proposed in the past (Burgers 1940, Bragg 1940) and recently studied by Read and Shockley (1950), some of whose conclusions have been verified by Aust and Chalmers (1950). On this model the grain boundary is made up of a suitable array of dislocations. With certain assumptions it can be shown that the measured value of $D'\delta/D$ can be explained on the further assumption that $Q' \doteqdot Q$.

Dislocations exist also, of course, within the crystal, and we will suppose that for our present purpose the grain boundary differs from the crystal only in that it contains a much higher concentration of dislocations. Seitz (1950) has suggested that it is dislocations which provide the very high density of vacancies in crystals required to explain certain phenomena, particularly the Kirkendall Effect. We will assume then that the main sources of vacancies are the dislocations, and further, that the density of vacancies in any region is proportional to the density of dislocations. The vacancies provided by the dislocations will then lead to diffusion by the normal vacancy mechanism, so that we can write

$$D = \text{const.}\ \rho \exp(-Q/RT), \quad \ldots\ldots \quad (4)$$

where D is the diffusion coefficient in a region where the density of dislocations is ρ. Q is the activation energy for the diffusion process and does not include the energy of formation of a vacancy, as it does when it is supposed that the vacancies exist in thermal equilibrium with the lattice. In the present case the energy required to form a vacancy, from a dislocation, is negligible. If we suppose first that Q and Q′ are not equal, we can write for $D'\delta/D$, from equation (4),

$$\frac{D'\delta}{D} = \frac{\rho_{gb}}{\rho_e} \frac{\exp(-Q'/RT)}{\exp(-Q/RT)}, \quad \ldots\ldots \quad (5)$$

where ρ_{gb} and ρ_e are the densities of dislocations per unit length of the grain boundary and per unit area of the crystal respectively. We should expect the excess density of dislocations at the grain boundaries to provide an excess density of vacancies for some distance from the grain boundry, so that for diffusion the effective width δ of the grain boundary will be greater than the distance over which the normal lattice structure is disturbed. We avoid having to make an estimate of δ by considering in equation (5) the ratio $D'\delta/D$ instead of D'/D.

With estimates of ρ_{gb} and ρ_e we can calculate the difference between Q′ and Q that would be necessary to account for the measured ratio of $D'\delta/D$. We may take for ρ_e the value of 10^8, an estimate for fully annealed metals based upon the dislocation theory of their strength (see Cottrell 1949). The value of ρ_{gb} will vary considerably with the orientation difference between

the two grains adjoining the grain boundary. As a maximum value of ρ_{gb} we may take $1/2a$ (a=lattice constant), for we should not expect the number of dislocations in the grain boundary to exceed about one every two lattice planes. With $a=3\times10^{8}$ cm. this gives $\rho_{gb}(\text{max.})=1{\cdot}5\times10^{7}$/cm.

A minimum value for ρ_{gb} can be estimated from the expression given by Read and Shockley for the density of dislocations in a grain boundary defined by the angles θ and ϕ (see fig. 2),

$$\rho_{gb}=2\,.\,\frac{\text{Sin}\,\frac{1}{2}\theta}{a}\{\text{Cos}\,\phi+\text{Sin}\,\phi\}.$$

Taking $\phi=0$ (ρ_{gb} is not very sensitive to the value of ϕ) and $\theta\sim2°$ we find $\rho_{gb}\,(\text{min})=1{\cdot}3\times10^{6}$.

Fig. 2.

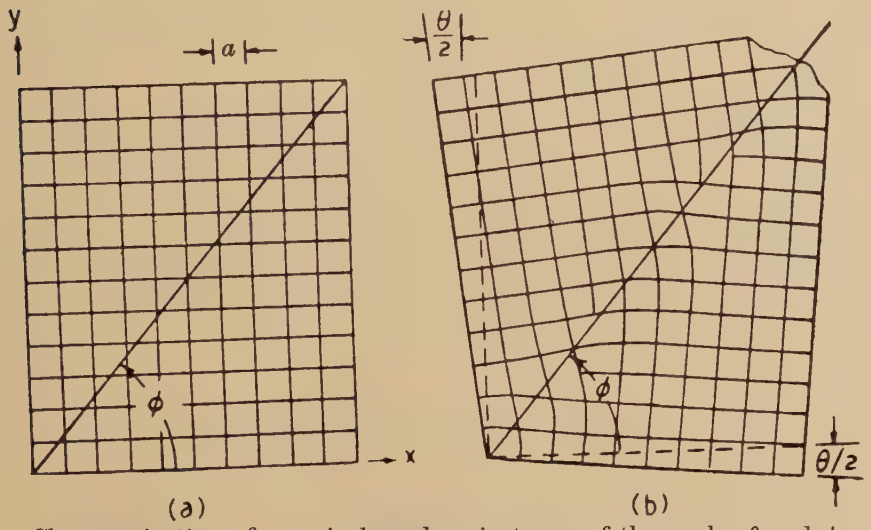

Characterization of a grain boundary in terms of the angles θ and ϕ. (Read and Shockley 1950.)

Inserting these values of ρ_{gb} and of ρ_e into equation (3) and using the value of $D'\delta/D=0{\cdot}04$ (Cu/Ni) we find, when

$$\left.\begin{array}{ll}\rho_{gb}\,(\text{max.})=1{\cdot}5\times10^{7} & Q-Q'=-2{\cdot}7\text{ K.cals/mole,}\\ \rho_{gb}\,(\text{min.})=1{\cdot}3\times10^{6} & Q-Q'=+2{\cdot}2\text{ K.cals/mole.}\end{array}\right\}\text{ for T}=1000°\text{ K.}$$

It is also readily shown that Q and Q′ would be equal if we supposed the grain boundary to have characteristic angles $\theta=6°$, $\phi=0$, which are not unlikely values.

We see then that the measured ratio of $D'\delta$ to D can be well accounted for on the assumption that Q and Q′ are equal, and therefore from equation (3) that the whole of the difference in the diffusion rates for grain boundary and for volume diffusion arises from a difference in the D_0 term in equation (3). But if the activation energies do differ, they will not do so by more than about 2·5 K. cals/mole.

Similar calculations based on Kê's model of the grain boundary are impossible in the absence of estimates of the grain boundary and volume densities of disordered groups.

The experimental results at present available in the literature on the relative values of Q and Q′ are very few and conflicting. Measurements of the diffusion coefficient of molybdenum in tungsten by Van Liempt (1932) and of thorium in tungsten by Fonda *et al.* (Fonda, Young and Walker 1933) show that D_0 increases with decreasing grain size, but that the activation energy is independent of the grain size of the tungsten, indicating the $Q=Q'$. On the other hand (Langmuir 1934) finds that $Q-Q'$ for the diffusion of thorium in tungsten is about 25 K. cals/mole and that D_0 for grain boundary diffusion is less than for volume diffusion. (See Barrer 1941.)

On the other hand, we have seen that theoretical considerations lead us to expect that Q and Q′ might be equal and experimental work to confirm or disprove this would be very interesting.

Another important line of work would be a study of the dependence of D′/D upon the relative orientations of the crystal faces forming the boundary. Any marked dependence would provide further evidence in favour of the " transitional lattice " theory of the grain boundary.

A study of grain boundary diffusion rates is then of importance, not only as a diffusion study but also in investigating other properties of grain boundaries. It is hoped that this new method of investigation, requiring only micrographical techniques, will facilitate such studies.

Acknowledgment.

The author is indebted to the Director, Atomic energy Research Establishment, Harwell, for permission to publish this note.

References.

Aust, K. T., and Chalmers, B., 1950, *Proc. Roy. Soc.* A, **204,** 359.
Barnes, R. S., 1950, *Nature, Lond.*, **166,** 1032.
Barrer, R. M., 1941, *Diffusion in and through solids* (Cambridge : University Press).
Bragg, W. L., 1940, *Proc. Phys. Soc.*, **52,** 54.
Burgers, J. M., 1940, *Proc. Phys. Soc.*, **52,** 23.
Cottrell, A. H., 1949, *Progress in Metal Physics*, Vol. 1, p. 104.
Fisher, J. C., 1950, *General Electric Research Lab. Report* GEPM 18.
Fonda, G., Young, A., and Walker, A., 1933, *Physics*, **4,** 1.
Kê T'ing Sui, 1949, *J. Appl. Phys.*, **20** (3), 274–80.
Langmuir, I., 1934, *J. Franklin Inst.*, **217,** 543.
Read, W. T., and Shockley, W., 1950, *Phys. Rev.*, **78** (3), 275–89.
Seitz, F., 1950, *Phys. Rev.* **79** (6), 1002.
Van Liempt, J. A. M., 1932, *Rec. Trav. Chim. Pays Bas*, **51,** 117.

LIII. *The Rectification and Observation of Signals in the Presence of Noise.*

By R. E. Burgess, B.Sc.,
National Physical Laboratories*.

[Received January 10, 1951.]

Summary.

The rectification of random narrow-band noise in the presence of a C.W. or modulated signal is analysed. The detector considered is of the type providing a rectified voltage which is a function of the instantaneous amplitude of the input wave. The smoothing present in the detector circuit is such that the high-frequency components of the applied wave are removed but the low-frequency variations of its envelope are faithfully transmitted.

The mean (or D.C.) component of the rectified voltage and its r.m.s. fluctuation about that mean (or L.F. noise output) are calculated as a function of the input signal/noise ratio and particular attention is paid to linear and square-law detectors.

The output signal/noise ratio for an amplitude-modulated signal input and for the audible beat reception of a C.W. signal are calculated.

The spectrum of the L.F. noise output from a detector supplied with random noise is shown to be closely similar for linear and square-law detectors.

The discrimination of a weak signal in noise is shown to be not critically dependent upon the law of the detector, and in particular the difference for a linear and a square-law detector is negligible.

The effect of receiver bandwidth, meter time-constant and integration time in improving the discernment of a weak signal is considered.

More Important Symbols.

A=instantaneous amplitude of the wave applied to the detector.
B=bandwidth of input noise.
E=r.m.s. input noise voltage.
$F(\omega)$=input noise spectrum.
$G(\omega_a)$=output noise spectrum.
H=amplitude of heterodyne voltage.
M=r.m.s. improvement due to meter time-constant.
N=number of observations.
Q=detector discrimination.
$R(\tau)$=an autocorrelation coefficient of the input noise.
S=amplitude of C.W. signal.
T=time constant of meter.

---

* Communication from the National Physical Laboratory.

T_0=duration of period of integration.
X, Y=" in phase " and " quadrature " amplitudes of noise voltage.
$f_p(\omega_a)$=normalized component spectra of the L.F. output noise.
m=depth of signal modulation.
n=exponent of detector law.
u=instantaneous rectified voltage.
v=instantaneous input noise voltage.
x=S/$\sqrt{(2)}$E=r.m.s. signal/noise ratio.
y=A/$\sqrt{(2)}$E.
β=2πB=angular bandwidth.
θ=instantaneous meter indication.
τ=time interval in autocorrelation.
ω_a=angular frequency in L.F. output.
ω_0=central angular frequency of input noise.

§1. Introduction.

The calculation of the transmission of signal and noise voltages by a linear amplifier is a familiar and simple process for it is known that the output from an amplifier supplied with a mixture of signal and noise is the sum of the outputs if each were applied separately. However, this principle of superposition cannot be applied when the signal and noise pass through a non-linear circuit such as a rectifier or a limiter.

The rectification of noise and of a mixture of noise and signal is of practical importance in relation to

(i.) its effect on the signal/noise ratio in reception,

(ii.) the measurement of noise,

(iii.) the measurement of a signal in the presence of noise, and

(iv.) the measurement of receiver sensitivity.

The analysis of the rectification of noise presents difficulties which arise partly from the non-linear characteristics of the circuit and partly from the inherent characteristics of the noise which can only be specified statistically. (It should be stated at this stage that only fluctuation noise is considered in the present paper.)

Fränz (1940) considered the case of a detector whose current/voltage characteristic could be represented by a power series. The results of the analysis were not applicable to the case of the discontinuous characteristic of the linear detector nor did they refer to the practical condition in which the detector output follows the envelope of the applied wave rather than the instantaneous voltage.

Fränz (1941) later published an analysis of the rectification of noise by a detector with a discontinuous linear characteristic. In this paper the method of using a singular integral to represent the characteristic was successfully applied to derive the mean rectified voltage, and the spectrum of the low frequency output.

Ragazzini (1942) considered the rectification of a mixture of a modulated signal and noise by an ideal linear detector in which the output voltage accurately follows the envelope of the applied wave. In order to make the analysis tractable it was found necessary to approximate in the evaluation of the components of the envelope and for this reason some of the equations are not exact.

In the present paper it is proposed to analyse by elementary methods the rectification of a mixture of signal and noise by linear and square-law detectors and to compare the results so obtained with those appearing in the papers mentioned above. The practical application of the formulæ to the evaluation of the sensitivity of reception of modulated signals and of C.W. signals using a heterodyning oscillator is also discussed.

It is convenient to draw attention at this point to the significance of the time constant of the detector circuit. Fig. 1 shows a typical

Fig. 1.

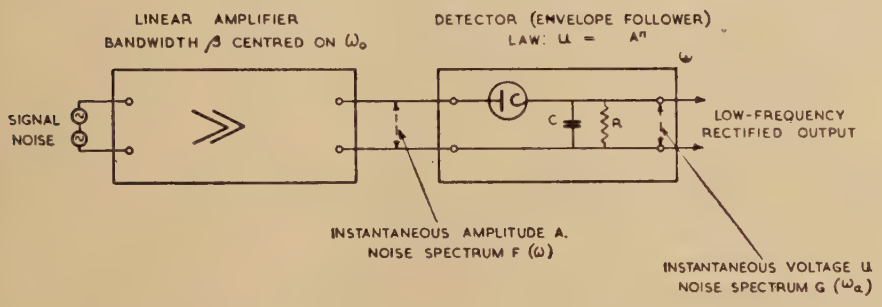

Schematic circuit of a typical receiver.

arrangement of a receiver ; the amplifier having a central frequency ω_0 and bandwidth β passes the signal and noise to a detector having a load circuit RC across which the rectified voltage is developed. There are three possible cases of the time constant RC to be considered :

$$(a)\ \mathrm{RC} \ll \frac{1}{\omega_0}.$$

In this case there is practically no smoothing of the rectified voltage so that the latter consists of the positive half-waves of the applied voltage with the result that a considerable high-frequency component is present in the output and rectification is inefficient. This is the case considered by Fränz, but it does not conform with the usual circuital practice.

$$(b)\ \frac{1}{\omega_0} \ll \mathrm{RC} \ll \frac{1}{\beta}.$$

In this case the high frequency components are filtered from the output and yet the time constant is small enough for the output to follow accurately the envelope of the input voltage. This is the case of practical importance in receiving technique.

(*c*) $\frac{1}{\beta} \ll RC$

In this case the time constant is so large that the fluctuations of the envelope of the applied wave are smoothed out and the output voltage is steady. This case is relevant to the measurement of signal and noise by a diode voltmeter, and will be dealt with in a further paper.

The law of the detector can be defined in terms of the relationship between the detector output voltage u and the instantaneous amplitude A of the input wave. In an ideal detector free from distortion the relation would be linear ; in other cases, either through non-ideal behaviour in the detector or by design the dependence can be non-linear. In particular, for small applied voltages the rectified voltage from a diode detector tends to be proportional to the square of the amplitude while for large applied voltages it tends to equality with the amplitude. (See Appendix IV.). From the point of view of the present analysis there is no essential difference between a linear detector followed by a non-linear aperiodic amplifier and a non-linear detector.

The detector characteristic considered in this paper is assumed to have the general form

$$u = A^n. \quad . \quad . \quad . \quad . \quad . \quad . \quad . \quad . \quad . \quad (1)$$

It has been assumed for simplicity (but with only trivial loss of generality) that the constant of proportionality is unity.

§2. Statistical Properties of a Mixture of a C.W. Signal and Narrow-Band Noise.

Since fluctuation noise arises from a succession of random and independent elementary events it obeys certain statistical distributions which can be conveniently specified in terms of the r.m.s. value E of the noise voltage, defined by

$$E^2 = \operatorname*{Lim}_{T \to \infty} \frac{1}{T} \int_0^T v^2(t) \, . \, dt, \quad . \quad . \quad . \quad . \quad . \quad . \quad . \quad (2)$$

where $v(t)$ is the instantaneous noise voltage.

Since the amplifier supplying the noise is assumed to have a narrow band * β centred on ω_0, the noise at the input to the rectifier can be written

$$v(t) = X(t) \cos \omega_0 t + Y(t) \sin \omega_0 t \quad . \quad . \quad . \quad . \quad . \quad (3)$$

in which X and Y are relatively slowly varying functions of time, and can be regarded as the " in phase " and " quadrature " amplitudes of noise relative to a C.W. signal A cos $\omega_0 t$.

* For the purpose of setting a limit on the term " narrow band " it may be arbitrarily defined as applying to the case in which the bandwidth is not greater than one-fifth of the central frequency This sort of restriction is necessary for the concept of " instantaneous amplitude " to be applicable to the noise wave.

Now v, X and Y have a normal or Gaussian distribution about zero; thus for v,

$$\mathrm{P}(v) \,.\, dv = \frac{1}{\sqrt{(2\pi)} \,.\, \mathrm{E}} \exp\left(-\frac{v^2}{2\mathrm{E}^2}\right) . \, dv. \quad . \quad . \quad . \quad . \quad (4)$$

From this distribution the following averages may be formed:

$$\overline{v^2} = \overline{\mathrm{X}^2} = \overline{\mathrm{Y}^2} = \mathrm{E}^2,$$

$$\overline{\mathrm{XY}} = 0,$$

$$\overline{|v|} = \overline{|\mathrm{X}|} = \overline{|\mathrm{Y}|} = \sqrt{(2/\pi)}\mathrm{E}.$$

The amplitude or envelope of the fluctuation noise voltage is given by the positive value of

$$r = \sqrt{(\mathrm{X}^2 + \mathrm{Y}^2)}$$

and its distribution function is of the Rayleigh type

$$\mathrm{P}(r) \,.\, dr = \frac{r}{\mathrm{E}^2} \exp\left(-\frac{r^2}{2\mathrm{E}^2}\right) . \, dr, \quad . \quad . \quad . \quad . \quad . \quad (5)$$

from which

$$\overline{r^2} = 2\mathrm{E}^2 \text{ and } \bar{r} = \sqrt{(\pi/2)}\mathrm{E}.$$

If now a sinusoidal signal $\mathrm{S} \cos \omega_0 t$ is added to the noise the r.m.s. signal/noise voltage ratio is given by

$$x = \frac{\mathrm{S}}{\sqrt{(2)}\mathrm{E}}$$

or $20 \log_{10} x$ in decibels.

The instantaneous amplitude A of the mixture is given by

$$\mathrm{A} = \sqrt{[(\mathrm{X}+\mathrm{S})^2 + \mathrm{Y}^2]} \quad . \quad . \quad . \quad . \quad . \quad . \quad . \quad . \quad (6)$$

whose distribution is readily shown (Appendix I.) to be given by

$$\mathrm{P}(\mathrm{A}) \,.\, d\mathrm{A} = \frac{\mathrm{A}}{\mathrm{E}^2} \exp\left(-\frac{\mathrm{A}^2 + \mathrm{S}^2}{2\mathrm{E}^2}\right) \mathrm{I}_0\left(\frac{\mathrm{AS}}{\mathrm{E}^2}\right) . \, d\mathrm{A}, \quad . \quad . \quad . \quad (7)$$

I_0 being the modified Bessel Function of the first kind, zero order. If the parameter

$$y = \frac{\mathrm{A}}{\sqrt{(2)}\mathrm{E}}$$

is introduced we may write (7) in the form

$$\mathrm{P}(y) \,.\, dy = 2y \exp(-y^2 - x^2) \,.\, \mathrm{I}_0(2yx) \,.\, dy. \quad . \quad . \quad . \quad (8)$$

For weak signals ($x \ll 1$) the amplitude distribution of the mixture is still of the Rayleigh type

$$\mathrm{P}(y) \,.\, dy = \frac{2y}{1+x^2} \exp\left(-\frac{y^2}{1+x^2}\right) dy, \quad . \quad . \quad . \quad . \quad . \quad (9)$$

which shows that the addition of the weak signal effectively increases the r.m.s. noise voltage from E to $E(1+x^2)^{\frac{1}{2}}$, which is equal to $(E^2+\frac{1}{2}S^2)^{\frac{1}{2}}$ the r.m.s. voltage of the mixture. This property will be found useful later in considering signals below noise level.

In the case of large signals ($x \gg 1$) we have from the asymptotic expansion of I_0

$$P(y) \, . \, dy \sim \sqrt{(y/\pi x)} \exp\left[-(y-x)^2\right] \, . \, dy \quad . \quad . \quad . \quad . \quad (10)$$

which shows that the amplitude distribution of the mixture is centred on the signal amplitude and is approximately Gaussian with r.m.s. fluctuation equal to the r.m.s. noise voltage E.

§3. The Mean Rectified Voltage.

If the voltage output V from the rectifier is related to the amplitude A of the applied voltage by the nth-power law, the d.c. or mean rectified voltage which would be indicated by a voltmeter of long time constant is

$$\bar{u} = \overline{A^n} = \int_0^\infty A^n P(A) \, . \, dA$$

$$= 2(\sqrt{(2)}E)^n \int_0^\infty y^{n+1} \exp\left(-y^2-x^2\right) I_0(2yx) \, . \, du,$$

where, as above, the signal/noise ratio is denoted by x. This integral can be evaluated by a general relation due to Hankel which leads to

$$\bar{u} = \overline{A^n} = (\sqrt{(2)}E)^n \left(\frac{n}{2}\right)! \;\; {}_1F_1\left(-\frac{n}{2}, 1, -x^2\right), \quad . \quad . \quad (11)$$

in which ${}_1F_1$ is the hypergeometric function expressible by the Kummer series

$${}_1F_1\left(-\frac{n}{2}, 1, -x^2\right) = 1 + \frac{(-n/2)}{1}\frac{(-x^2)}{1!} + \frac{(-n/2)(1-n/2)}{1 \cdot 2}\frac{(-x^2)^2}{2!} +$$

(This function is denoted by M in Jahnke–Emde's Tables.)

It is clear that if n is a positive even integer the series terminates and the average of A^n can be simply expressed. Thus for a square law rectifier $n=2$ for which

$$\overline{A^2} = 2E^2(1+x^2), \quad . \quad . \quad . \quad . \quad . \quad . \quad . \quad (12)$$

showing that the mean rectified voltage is accurately proportional to the mean square value of the applied voltage, as in the case of the thermocouple for measurement of coexistent signal and noise. The anode-bend and the diode rectifier approximate to this condition for small input voltages.

The mean square output voltage is obtained in the general case by replacing n by $2n$ in equation (11):

$$\overline{u^2} = \overline{A^{2n}} = (2E^2)^n n! \;\; {}_1F_1(-n, 1, -x^2). \quad . \quad . \quad . \quad (13)$$

A case of practical importance is the linear rectifier ($n=1$) for which

$$\overline{u}=\overline{A}=\sqrt{(\pi/2)}\mathrm{E}\,{}_1\mathrm{F}_1(-\tfrac{1}{2},\,1,\,-x^2). \quad . \quad . \quad . \quad . \quad (14)$$

Fig. 2 shows $\overline{A}/\sqrt{(\pi/2)}\mathrm{E}$ as a function of the signal/noise ratio x. For a small signal/noise ratio ($x \ll 1$) the Kummer series gives

$$\overline{A}=\sqrt{(\pi/2)}\mathrm{E}\left(1+\tfrac{1}{2}x^2-\frac{x^4}{16}+\frac{x^6}{96}\cdots\right)$$

$$=\sqrt{[(\pi/2)\mathrm{E}^2(1+x^2)]}\ \text{approx.} \quad . \quad . \quad . \quad . \quad . \quad . \quad . \quad (15)$$

showing that the linear rectifier tends to give an indication proportional to the r.m.s. value of the mixture of signal and noise when the latter predominates.

Fig 2

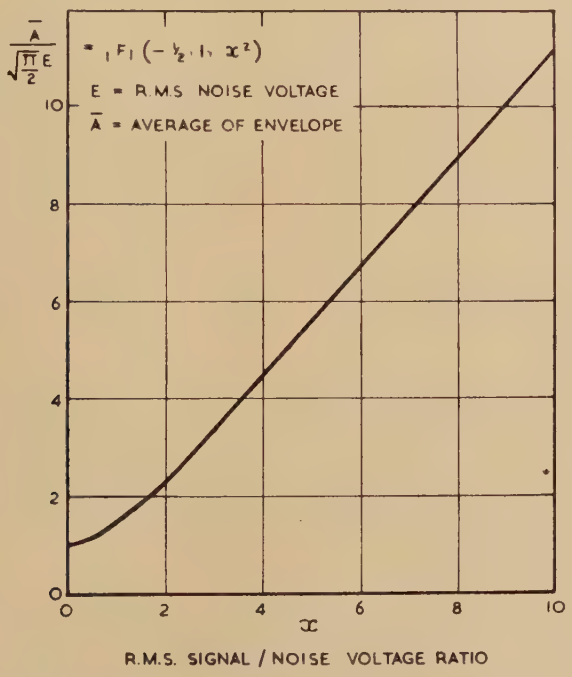

Average amplitude of the envelope of a mixture of signal and noise (as would be indicated by a linear rectifier).

For a large signal/noise ratio ($x \gg 1$) the asymptotic expansion of the hypergeometric function

$${}_1\mathrm{F}_1\left(-\frac{n}{2},\,1,\,-x^2\right)\sim\frac{x^n}{(n/2)\,!}\left(1+\frac{n^2}{4x^2}+\cdots\right) \quad . \quad . \quad (16)$$

gives

$$\overline{A}=\sqrt{(2)}\,\mathrm{E}x\left(1+\frac{1}{4x^2}\right). \quad . \quad . \quad . \quad . \quad . \quad . \quad (17)$$

In the above it has been assumed that the time constant of the rectifier circuit is such that the R.F. or I.F. is removed from the output, but sufficiently small for the envelope to be accurately followed, the long time constant of the meter providing the averaging. In Fränz's analysis (1941) of the linear rectifier, however, it was assumed that no smoothing was present, so that the rectified output consisted of the positive half-waves of the applied voltage. Since the average positive voltage is related to the average amplitude by

$$\bar{v}_+ = \frac{1}{2\pi}\int_0^{\pi} \overline{\mathrm{A}} \sin\theta \,.\, d\theta = \frac{\overline{\mathrm{A}}}{\pi}, \quad \ldots\ldots (18)$$

it is seen that Fränz's rectified output should be $1/\pi$ of the value calculated above, *i. e.*

$$\bar{v}_+ = \frac{\mathrm{E}}{\sqrt{(2)}\pi}\,{}_1\mathrm{F}_1(-\tfrac{1}{2},\, 1,\, -x^2). \quad \ldots\ldots (19)$$

Fränz (1941) obtained the average in the form

$$\bar{v}_+ = \frac{\mathrm{E}}{\sqrt{(2)}\pi}\left[x^2\,{}_1\mathrm{F}_1(\tfrac{1}{2},\, 2,\, -x^2) + \exp\left(-\frac{x^2}{2}\right)\mathrm{I}_0\left(\frac{x^2}{2}\right)\right]. \quad (20)$$

It may be shown that equations (20) and (19) are identical by using Kummer's relation for the Bessel function and the recurrence formulæ for F. For:

$$\left.\begin{aligned} &e^{-\frac{1}{2}x^2}\mathrm{I}_0(\tfrac{1}{2}x^2) = {}_1\mathrm{F}_1(\tfrac{1}{2},\, 1,\, -x^2),\\ &e^{-\frac{1}{2}x^2}[\mathrm{I}_0(\tfrac{1}{2}x^2) + \mathrm{I}_1(\tfrac{1}{2}x^2)] = {}_1\mathrm{F}_1(\tfrac{1}{2},\, 2,\, -x^2),\\ &x^2\,{}_1\mathrm{F}_1(\tfrac{1}{2},\, 2,\, -x^2) + {}_1\mathrm{F}_1(\tfrac{1}{2},\, 1,\, -x^2) = {}_1\mathrm{F}_1(-\tfrac{1}{2},\, 1,\, -x^2). \end{aligned}\right\} \quad \ldots (21)$$

§4. Mean Square Voltage of the Output Noise.

The noise output from a linear rectifier which accurately follows the envelope of the applied voltage can be expressed in terms of the fluctuation of the envelope about its average value. Thus the mean square noise output is given by

$$u_n^2 = \overline{\mathrm{A}}^2 - (\overline{\mathrm{A}})^2 = \mathrm{E}^2\left[2(1+x^2) - \frac{\pi}{2}\mathrm{F}^2\right], \quad \ldots (22)$$

where F denotes the hypergeometric function in equation (14).

If the signal/noise ratio is small ($x \ll 1$) the noise output is

$$u_n^2 = \left(2 - \frac{\pi}{2}\right)\mathrm{E}^2(1+x^2) = 0{\cdot}43(1+x^2)\mathrm{E}^2, \quad \ldots (23)$$

which shows that the mean square noise output is proportional to the total mean square value of the applied signal and noise.

For large signal/noise ratios ($x \gg 1$) the output noise tends to the limit given by

$$u_n^2 = \mathrm{E}^2, \quad \ldots\ldots (24)$$

which shows that in the presence of a large C.W. signal the r.m.s. values of the input and output noise are equal.

To illustrate equation (22) the ratio u_n/E has been plotted as a function of x in fig. 3. It is of interest to compare this evaluation with the approximate analysis by Ragazzini (1942) who finds the simpler but less accurate value

$$u_n^2 = E^2\left[\frac{x^2+\frac{1}{2}}{x^2+1}\right], \quad \ldots\ldots\ldots \quad (25)$$

which gives $\frac{1}{2}E^2$ instead of $0{\cdot}43E^2$ for the output in the absence of a signal, but tends to the same upper limit of E^2 as above. For comparison Ragazzini's equation is plotted as a dashed curve in fig. 3, and it is seen to give a very good approximation to the exact value of $x>1$.

Fig 3

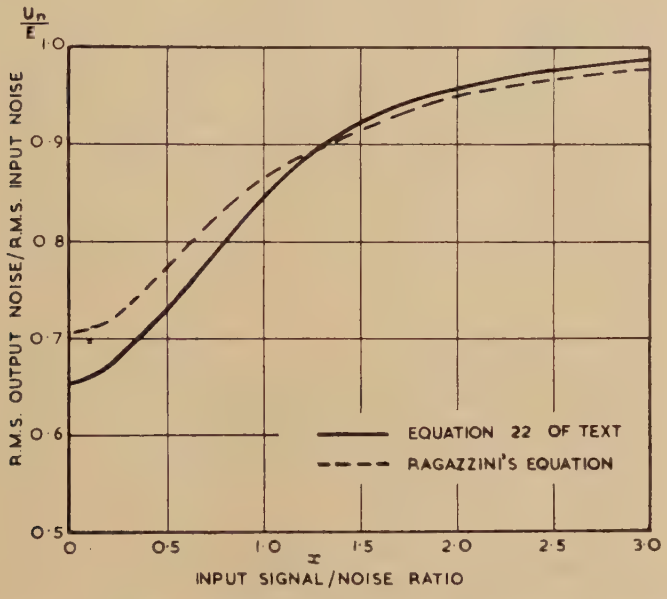

Response of a linear rectifier to a mixture of noise and C.W. signal.

For the linear rectification of noise in the absence of a signal and with no smoothing Fränz (1941) found for the mean square output noise voltage

$$u_n^2 = \frac{E^2}{8\pi}\sum_{r=1}^{\infty} 16^{1-r}\frac{(2r-2)!^2}{r!^2(r-1)!^2}.$$

Now in this series the ratio of the $(r+1)$th term to the rth term is $(r-\frac{1}{2})^2/(r+1)^2$ showing that the series is hypergeometric and is in fact equal to $4[F(-\frac{1}{2}, -\frac{1}{2}, 1, 1)-1]$ which by Gauss's theorem$= 4[(4/\pi)-1]$ (Fränz gave 25/2816 instead of the correct value 25/4096 for the fourth term). Thus Fränz's expression becomes

$$u_n^2 = \frac{1}{\pi^2}\left(2-\frac{\pi}{2}\right)E^2,$$

which is $1/\pi^2$ of the value given by equation (23) for the output from an envelope follower with no signal. This reduction factor occurs since in Fränz's case of no smoothing the noise output arises from fluctuations in the average of the positive voltage ($\bar{v}_+$) which was seen in the last section to be $1/\pi$ times the corresponding average of the envelope $\overline{A}$.

The square law detector can be considered in a manner similar to that used for a linear detector. In this case the mean square noise output is given by

$$\begin{aligned} u_n^2 &= \overline{u^2} - \overline{u}^2 = [\overline{A^4} - (\overline{A^2})^2] \\ &= E^4\left[8\left(1+2x^2+\frac{x^4}{2}\right) - 4(1+x^2)^2\right] \\ &= 4E^4(1+2x^2) = 4E^2(E^2+S^2), \quad \ldots\ldots\ldots \quad (26) \end{aligned}$$

Fig 4

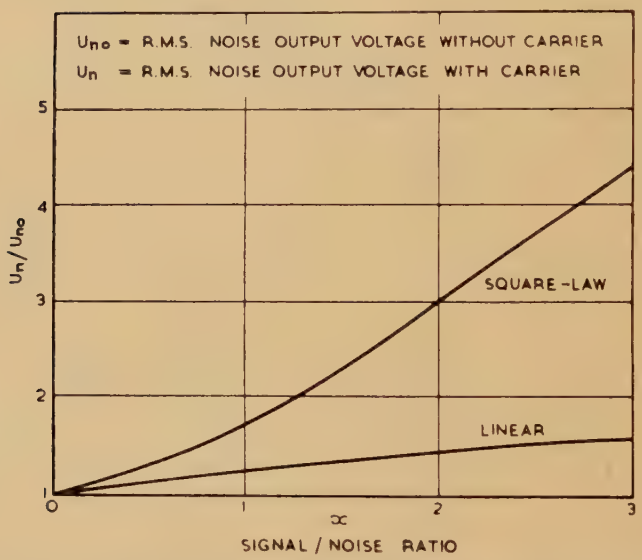

Increase of noise output from a linear and from a square-law rectifier on the introduction of a C.W. signal.

which shows that the noise output rises uniformly as the signal is increased instead of tending to a limit as in the case of the linear rectifier. The ratio of the r.m.s. output noise voltage with signal present to that with signal absent is shown in fig. 4 as a function of the signal/noise x.

§5. Frequency Spectrum of the Output Noise.

The formulæ given in the last section for u_n^2 are for the total mean square output noise voltage ; in point of fact the noise is spread out in a continuous spectrum whose integral is equal to u_n^2. The form of this spectrum is of importance in determining the effect which post-detector selectivity will have on the noise voltage and on its ratio to a signal.

The frequency distribution of the output noise can be conveniently expressed in terms of the spectrum $G(\omega_a)$ where ω_a is the audio frequency. This spectrum is such that the mean square noise voltage in a frequency interval $d\omega_a$ is given by $G(\omega_a)d\omega_a$ with

$$\int_0^\infty G(\omega_a) \, . \, d\omega_a = u_n^2. \quad . \quad . \quad . \quad . \quad . \quad . \quad . \quad (27)$$

Clearly the spectrum of the output noise is a function of the spectrum applied to the input of the rectifier; since the noise impulses at their origin are extremely short, the input spectrum is determined by the frequency characteristics of the amplifier between the noise source and the rectifier. The rate at which the envelope of the noise varies from moment to moment is inversely dependent upon the bandwidth of the amplifier since the narrower the bandwidth the greater the lengthening of the impulses and hence the closer the correlation at successive instants of time. The correlation function of a random disturbance and its power spectrum are connected by the Fourier cosine transform.

The frequency spectrum of the input noise to the detector denoted by $F(\omega)$ is defined in a manner similar to that used above for the output noise, namely, that the mean square voltage in a frequency interval $d\omega$ is $F(\omega) \, . \, d\omega$. Then

$$\int_0^\infty F(\omega) \, . \, d\omega = E^2, \quad . \quad . \quad . \quad . \quad . \quad . \quad . \quad (28)$$

where E^2 is the mean square noise voltage.

If ω_0 is the mid-band frequency, it is possible to specify an effective bandwidth β for the noise at the input of the rectifier:

$$\beta = \frac{\int_0^\infty F(\omega) \, . \, d\omega}{F(\omega_0)} = \frac{E^2}{F(\omega_0)}. \quad . \quad . \quad . \quad . \quad . \quad . \quad (29)$$

Consider first the response of the square-law rectifier to a mixture of noise and signal. If the rectifier characteristic is given by

$$u = A^2$$

it is seen that when two sinusoidal voltages $A_1 \sin \omega_1 t$ and $A_2 \sin \omega_2 t$ are applied, the rectified voltage can be written

$$u = [A_1^2 + A_2^2 + 2A_1A_2 \cos (\omega_1 - \omega_2)t],$$

which has a pure modulation product of amplitude $2A_1A_2$. Hence, if any number of sinusoidal voltages are applied to the square-law rectifier, the low frequency products will be *linearly superposed*, so that the components of u have the general form

$$u = 2 \sum_r \sum_s A_r A_s \cos (\omega_r - \omega_s)t. \quad . \quad . \quad . \quad . \quad . \quad (30)$$

The mean square output voltage thus has the form

$$\overline{u^2}=2\sum_r\sum_s A_r^2A_s^2. \quad . \quad . \quad . \quad . \quad . \quad . \quad . \quad . \quad . \quad (31)$$

In these summations the products are only to occur once so that A_sA_r is taken as being included in A_rA_s.

If now fluctuation noise of spectrum $F(\omega)$ and a sinusoidal signal of amplitude S and frequency ω_0 are applied to the rectifier the mean square noise output in an interval ω_a to $\omega_a+d\omega_a$ has two components—that arising from the cross-products of the noise terms and given by

$$2\int_0^\infty 2F(\omega) \, . \, 2F(\omega+\omega_a) \, . \, d\omega \, . \, d\omega_a$$

and that arising from the product of the signal and the noise :

$$2S^2[2F(\omega_0+\omega_a)+2F(\omega_0-\omega_a)]d\omega_a.$$

Thus the output noise spectrum is given by

$$G(\omega_a)=4\left[2\int_0^\infty F(\omega)F(\omega+\omega_a) \, . \, d\omega+S^2\{F(\omega_0+\omega_a)+F(\omega_0-\omega_a)\}\right].$$

For simplicity it will be assumed that the input noise spectrum is symmetrical about ω_0 and thus

$$G(\omega_a)=8\left[\int_0^\infty F(\omega)F(\omega+\omega_a) \, . \, d\omega+S^2F(\omega_0+\omega_a)\right]. \quad . \quad . \quad (32)$$

This formula will be applied to a rectangular input noise spectrum corresponding to an ideal band-pass characteristic.

If the pass band is β it is seen from equation (29) that within this band the input spectrum is given by

$$F(\omega)=E^2/\beta \quad . \quad . \quad . \quad . \quad . \quad . \quad . \quad . \quad . \quad (33)$$

and is zero outside it.

Hence equation (32) gives for the output spectrum

$$\left.\begin{aligned} G(\omega_a)&=8E^4\left[\frac{\beta-\omega_a}{\beta^2}+\frac{2x^2}{\beta}\right] \text{ for } \omega_a<\frac{\beta}{2},\\ G(\omega_a)&=8E^4\frac{\beta-\omega_a}{\beta^2} \quad \text{for } \frac{\beta}{2}<\omega_a<\beta,\\ G(\omega_a)&=0 \quad \text{for } \beta<\omega_a. \end{aligned}\right\} \quad . \quad . \quad . \quad . \quad (34)$$

The integration of $G(\omega_a)$ gives

$$u_n^2=\int_0^\infty G(\omega_a) \, . \, d\omega_a=\int_0^\beta G(\omega_a) \, . \, d\omega_a=4E^4(1+2x^2)$$

in accordance with equation (26) for the mean square noise output from a square-law rectifier.

Fig. 5 shows the output spectrum for a number of values of signal/noise ratio. It is seen that in the absence of a signal the spectrum is triangular and of width β at the base which is twice as wide as the input spectrum about its central frequency ω_0. As the signal increases the output spectrum progressively tends to coincide with the bisected input spectrum. These results can be easily understood from a physical point of view by

Fig 5

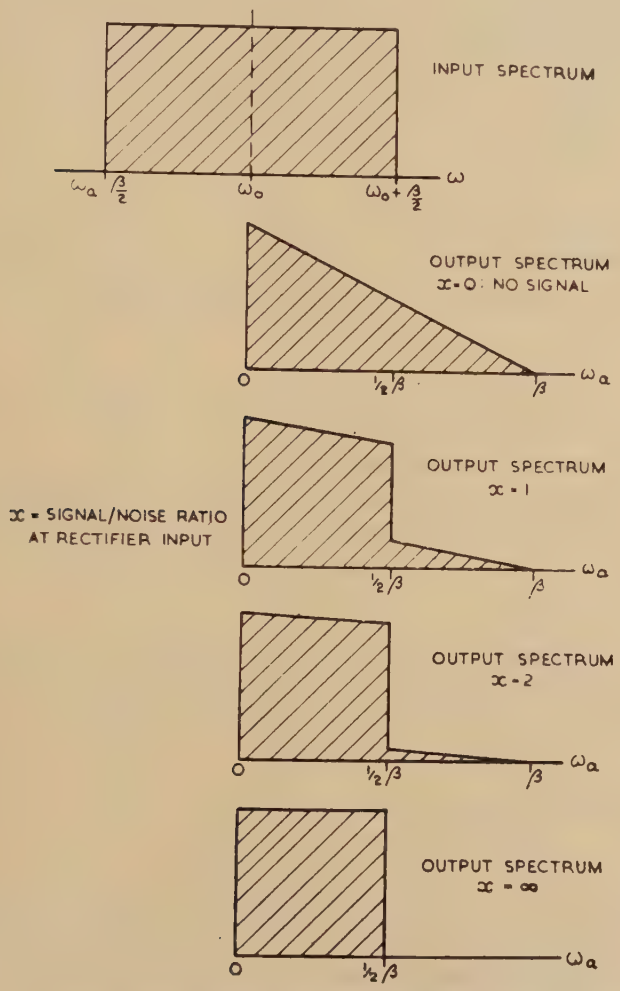

Output noise spectrum from a square-law rectifier when the input spectrum is rectangular.

consideration of the relative contribution to the output by the various cross-products of the noise components with each other and with the signal.

The results derived above apply to the square-law detector and are of practical application, since for small values of applied voltage detectors

tend to behave as square-law rather than linear devices. It is of interest, however, to know how the output spectrum from the linear detector differs from that from the square-law detector; the difference between the output noise spectra of the two detectors is least when a large sinusoidal signal is present, since the input spectrum is faithfully reproduced. On the other hand, if the detector is supplied with noise having a rectangular spectrum and no signal is present, then, as is shown in § 8, the output spectrum of the linear detector is very little different from the triangular spectrum given by the square-law detector. Therefore, a good approximation to the frequency distribution is obtained if equation (22) is used for the total output noise instead of equation (26) and the output spectrum shape is assumed to be the same as for the square-law detector.

§6. Signal/noise Ratio for Reception of Modulated Waves.

If the signal of carrier frequency ω_0 and amplitude S_0 is modulated at frequency ω_m to a depth m, the wave can be written

$$S_0(1+m\cos\omega_m t)\cos\omega_0 t$$

$$=S_0\left[\cos\omega_0 t+\frac{m}{2}\cos(\omega_0-\omega_m)t+\frac{m}{2}\cos(\omega_0+\omega_m)t\right],$$

whose r.m.s. value is $\frac{1}{2}S_0^2(1+\frac{1}{2}m^2)$.

It will be assumed that the input spectrum is rectangular and of width β and the detector is square-law, and furthermore, that

$$\omega_m<\frac{\beta}{2},$$

since otherwise the sidebands would not be passed to the detector.

The fundamental component of the rectified output at frequency ω_m has the form

$$2mS_0^2\cos\omega_m t$$

the mean square value of which is

$$u_s^2=2m^2S_0^4=8m^2x_0^4E^4$$

taking $x_0=S_0/\sqrt{(2)}E$, the r.m.s. carrier/noise ratio. The ratio of the r.m.s. values of the modulated signal to the noise is then $x=x_0(1+\frac{1}{2}m^2)^{\frac{1}{2}}$.

Now the mean square noise output due to the components of the noise mixing with each other and with the carrier is given by the value already found:

$$4E^4(1+2x_0^2).$$

The mean square noise output due to the components of the noise mixing with the two sidebands is easily shown to be

$$4E^4m^2x_0^2.$$

The total mean square noise output is therefore

$$u_n^2 = 4E^4(1+m^2x_0^2+2x_0^2). \quad . \quad . \quad . \quad . \quad . \quad . \quad . \quad (35)$$

Thus the output signal/noise ratio is given by

$$\frac{u_s}{u_n} = \frac{mx_0^2}{\sqrt{[\frac{1}{2}+x_0^2(1+\frac{1}{2}m^2)]}}, \quad . \quad . \quad . \quad . \quad . \quad . \quad (36)$$

which is the ratio of the r.m.s. audio output voltage of frequency ω_m to the total r.m.s. output noise voltage. Fig. 6 shows the variation of u_s/u_n with the carrier/noise ratio x_0 at the input for $m=1$, 0·5 and 0·2.

Fig. 6.

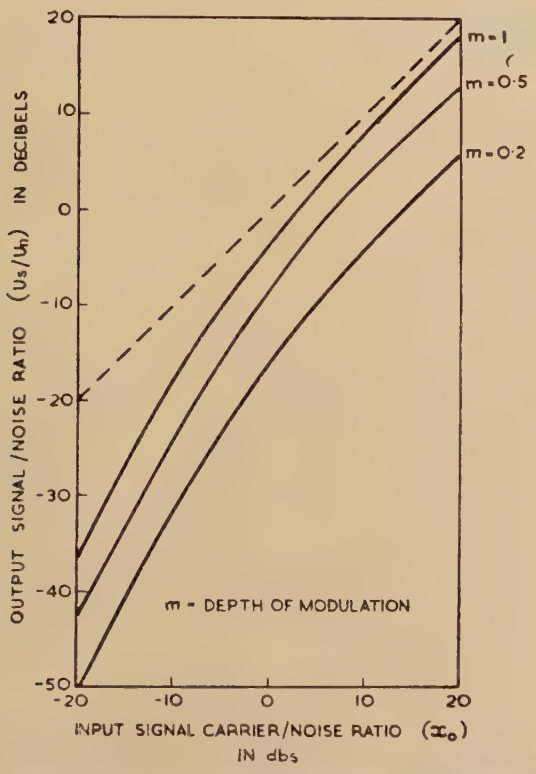

Relation between the signal/noise ratio at the output and input of a square-law detector for an amplitude modulated signal.

Even the best case ($m=1$, x_0 large) the loss in signal/noise ratio is 1·8 db., but it can be much greater than this in conditions of small input signal/noise ratio x, since then u_s/u_n is proportional to x_0^2. This suppression of the signal by the noise when the latter preponderates is clearly seen in fig. 6 as a change of slope as x_0 decreases through unity (0 db).

In this analysis any contribution of the second harmonic $2\omega_m$ to the useful signal output has been ignored, since its inclusion would only increase u_s by a factor of $(1+m^2/16)^{\frac{1}{2}}$ which is always negligible.

§ 7. Signal/noise Ratio for Heterodyne Reception of C.W. Signal.

A commonly used method of reception of a C.W. signal consists in producing an audible beat tone by heterodyning the signal at the detector by means of a local oscillator. Let the local oscillation be of amplitude H and the signal of amplitude S and let their frequencies lie with the rectangular pass-band $(\omega_0-\beta/2)$ to $(\omega_0+\beta/2)$ of the amplifier preceding the detector.

The amplitude of the beat note produced by a square-law detector is 2 HS and so the mean square signal output voltage is

$$u_s^2=2\mathrm{H}^2\mathrm{S}^2. \quad . \quad . \quad . \quad . \quad . \quad . \quad . \quad . \quad (37)$$

The mean square noise output voltage can easily be derived from the results of the earlier sections :

$$u_n^2=4\mathrm{E}^2(\mathrm{E}^2+\mathrm{H}^2+\mathrm{S}^2). \quad . \quad . \quad . \quad . \quad . \quad . \quad (38)$$

Thus putting

$$h=\frac{\mathrm{H}}{\sqrt{(2)}\mathrm{E}},$$

the output signal/noise ratio is found to be

$$\frac{u_s}{u_n}=\frac{hx}{\sqrt{(h^2+x^2+\frac{1}{2})}}. \quad . \quad . \quad . \quad . \quad . \quad . \quad (39)$$

Fig. 7 shows the signal/noise ratios at the input and at the output of the square-law detector as a function of the heterodying voltage. If this voltage is large compared with both the noise and signal voltages, the signal/noise ratio is seen to be unimpaired by the detector ; in fact the detector behaves as a linear frequency changer and leaves the spectra and the relative magnitudes of the signal and noise components unaffected apart from a common translation in frequency.

This equality of signal/noise ratio before and after detection for large values of heterodyning voltage also applies to the linear detector ; in fact for any type of detector the transfer ratio will tend to unity if the heterodyning voltage is made sufficiently large.

These remarks apply to the frequency-changing stage of a super-heterodyne as well as to the audible beat method of C.W. reception. However, it should be remembered that the present analysis is not concerned with the effect of any noise introduced by the heterodyning detector itself.

§ 8. The Response of a Detector to Noise or to Noise with a Weak Signal.

The preceding sections have dealt with the detection of a mixture of signal and noise with particular emphasis on square-law detectors and a general ratio of signal to noise. However, when the signal is weak compared with the noise as is the practical case in many problems of

marginal reception we have seen (equation (9)) that the amplitude of the mixture is statistically similar to that of random noise having a mean square value equal to the sum of the mean square values of the signal and the noise. Thus results may be derived for the output from an nth power envelope detector which are reasonably accurate and indicate the behaviour of such a detector in the observation of signals below noise level.

In order to derive the output spectrum of a detector to which random noise has been applied it is quickest to calculate the autocorrelation function of the output voltage and then form its cosine transform. Now in the nth power detector the output voltage is given by

$$u=\mathrm{A}^n$$

Fig 7.

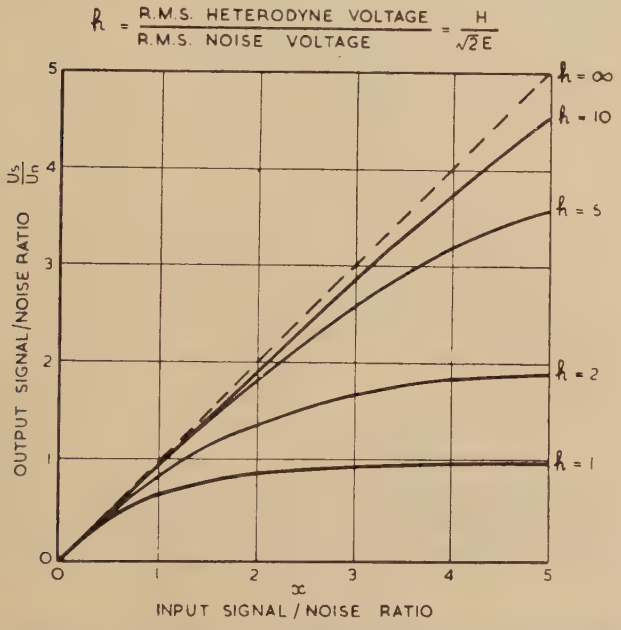

Relation between the signal/noise ratio at the input and at the output of a square-law detector for heterodyne reception of a C.W. signal.

and hence the autocorrelation function

$$\overline{u_1u_2}=\overline{\mathrm{A}_1{}^n\mathrm{A}_2{}^n}$$

where the suffices 1 and 2 refer to instants of time separated by an interval τ. Then it is shown in Appendix 2 that

$$\overline{u_1u_2}=2^n\mathrm{E}^{2n}(\tfrac{1}{2}n)\,!^2\,\mathrm{F}\left(-\frac{n}{2},\quad -\frac{n}{2},\quad 1,\quad \mathrm{R}^2\right),\qquad (40)$$

where F is the hypergeometric function and R is a function of τ having the form

$$R(\tau)=\frac{\sin \frac{1}{2}\beta\tau}{\frac{1}{2}\beta\tau}, \quad \ldots\ldots\ldots \quad (41)$$

in the case of a rectangular input noise spectrum of width β.

The audio output spectrum then has the form

$$G(\omega_a)=\frac{2}{\pi}\int_0^\infty (\overline{u_1u_2}-\overline{u}^2)\cos\omega_a\tau\,.\,d\tau. \quad \ldots\ldots \quad (42)$$

Now since $\overline{u_1u_2}$ is a series in R^2 it may be written

$$\overline{u_1u_2}=a_0+a_1R^2+a_2R^4+\ldots. \quad \ldots\ldots \quad (43)$$

which will terminate if n is an even integer and be an infinite series otherwise. Each term in this series can be regarded as producing its own component spectrum

$$G(\omega_a)=\frac{2}{\pi}\int_0^\infty \sum_1^\infty a_m\left(\frac{\sin\frac{1}{2}\beta\tau}{\frac{1}{2}\beta\tau}\right)^{2m}\cos\omega_a\tau\,.\,d\tau$$

$$=\sum_1^\infty a_m f_{2m}(\omega_a), \quad \ldots\ldots\ldots \quad (44)$$

where

$$f_p(\omega_a)=\frac{2}{\pi}\int_0^\infty\left(\frac{\sin\frac{1}{2}\beta\tau}{\frac{1}{2}\beta\tau}\right)^p\cos\omega_a\tau\,.\,d\tau \quad \ldots\ldots \quad (45)$$

is the pth normalized component spectrum each of which is a function of ω_a/β alone and has unit content, *i. e.*

$$\int_0^\infty f_p(\omega_a)\,.\,d\omega_a=1.$$

The properties of these spectra have been investigated by Fränz (1940) and some of these are given in Appendix III.

From equation (43) the d.c. component of the output voltage is

$$\overline{u}=u_0=\sqrt{(a_0)}, \quad \ldots\ldots\ldots \quad (46)$$

while the mean square output voltage is

$$\overline{u^2}=a_0+a_1+a_2+\ldots. \quad \ldots\ldots\ldots \quad (47)$$

and the mean square L.F. output voltage is therefore

$$\overline{u^2}-u_0^2=a_1+a_2+\ldots.=\int_0^\infty G(\omega_a)\,.\,d\omega_a. \quad \ldots \quad (48)$$

For an nth law detector

$$u_0=[\sqrt{(2)}E]^n(\tfrac{1}{2}n)\,! \quad \ldots\ldots\ldots \quad (49)$$

$$\overline{u^2}=(2E^2)^n(\tfrac{1}{2}n)\,!^2\,F\left(-\frac{n}{2},-\frac{n}{2},1,1\right)=n\,!\,(2E^2)^n \quad . \quad (50)$$

and the mean square noise output is hence

$$\overline{u^2}-u_0^2=[n\,!-(\tfrac{1}{2}n)\,!^2](2\mathrm{E}^2)^n. \quad . \quad . \quad . \quad . \quad . \quad . \quad . \quad (51)$$

The last three relations are consistent with equations (11) and (13) derived earlier and can in fact be obtained directly from the Rayleigh distribution. The spectral composition of u will now be considered in more detail. The low frequency limit of the L.F. spectrum is given by

$$\mathrm{G}(\mathrm{O})=\sum_1^\infty a_m f_{2m}(\mathrm{O}).$$

This must not be confused with the d.c. component of the detector output which corresponds to a spectral " line " at zero frequency of infinitesimal width but finite content.

The square-law detector will be discussed briefly first, since it has already been dealt with in an elementary fashion in § 5. For this case

$$\overline{u_1u_2}=4\mathrm{E}^4(1+\mathrm{R}^2), \quad . \quad . \quad . \quad . \quad . \quad . \quad . \quad . \quad (52)$$

whence the mean square L.F. noise voltage output is

$$\overline{u^2}-u_0^2=4\mathrm{E}^4 \quad . \quad . \quad . \quad . \quad . \quad . \quad . \quad . \quad (53)$$

and the spectrum therefore has only one component :

$$\mathrm{G}(\omega_a)=4\mathrm{E}^4 f_2(\omega_a)=\frac{8\mathrm{E}^4}{\beta}\left(1-\frac{\omega_a}{\beta}\right), \quad . \quad . \quad . \quad . \quad (54)$$

which agrees with the earlier equation (34) when the signal is put equal to zero ($x=0$).

The effect of varying the bandwidth β of the predetector circuits on the detector output spectrum is seen to be to increase both the height and the width of spectrum proportionally to β since $\mathrm{E}^2/\beta=\mathrm{F}$ (the input noise spectral density) is assumed to be constant.

It is noted from equations (52) and (53) that the autocorrelation coefficient of the output of a square-law detector (*i.e.* of the square of amplitude of a noise voltage) is given simply by

$$\rho_2(\tau)=\frac{\overline{u_1u_2}-u_0^2}{\overline{u^2}-u_0^2}=\mathrm{R}^2. \quad . \quad . \quad . \quad . \quad . \quad . \quad (55)$$

In the linear envelope detector ($n=1$) the output voltage is equal to the envelope of the noise current and its autocorrelation function is

$$\begin{aligned}\overline{u_1u_2}&=\frac{\pi}{2}\mathrm{E}^2\mathrm{F}(-\tfrac{1}{2},\,-\tfrac{1}{2},\,1,\,\mathrm{R}^2)\\&=\frac{\pi}{2}\mathrm{E}^2\left(1+\frac{\mathrm{R}^2}{4}+\frac{\mathrm{R}^4}{64}+\frac{\mathrm{R}^6}{256}+\ldots.\right). \quad . \quad . \quad . \quad (56)\end{aligned}$$

The mean square L.F. noise output voltage is

$$\overline{u^2}-u_0^2=\frac{\pi}{2}\mathrm{E}^2[\mathrm{F}(-\tfrac{1}{2},\,-\tfrac{1}{2},\,1,\,1)-1]=\left(2-\frac{\pi}{2}\right)\mathrm{E}^2, \quad . \quad . \quad (57)$$

which is consistent with the results of § 4.

Now the spectrum of the L.F. noise output is obtained from equations (45) and (56)

$$G(\omega_a) = \sum_1^\infty a_m f_{2m} = \frac{\pi}{2} E^2 \sum_1^\infty \frac{(m-3/2)!^2}{4\pi\, m!^2} f_{2m}(\omega_a). \quad . \quad . \quad . \quad (58)$$

Since the content of the first spectral component $a_1 f_2$ is 16 times that of the following component $a_2 f_n$ (for $a_2 = a_1/16$ and all the f_n have unit content) it is seen that this component provides a close approximation to the noise output spectrum

$$G(\omega_a) \approx \frac{\pi}{8} E^2 f_2(\omega_a) = \frac{\pi}{8} E^2 \frac{2}{\beta}\left(1 - \frac{\omega_a}{\beta}\right) \quad . \quad . \quad . \quad . \quad (59)$$

Fig. 8.

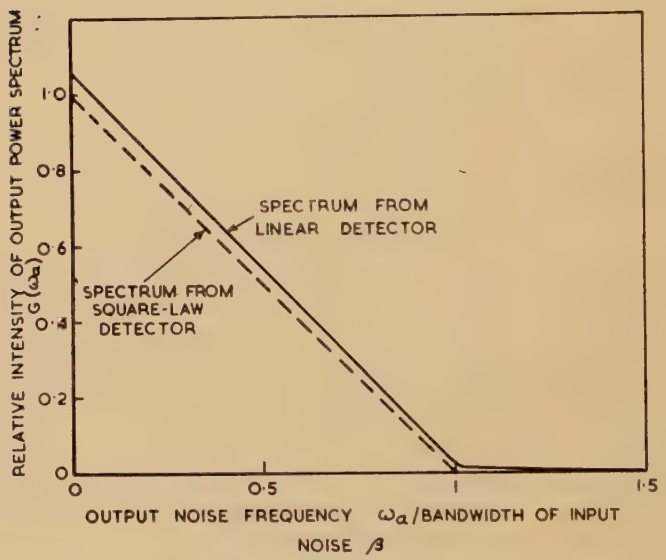

Spectral distribution of noise output from linear and square-law detectors when input noise has rectangular spectrum of width β.

up to β, and zero beyond. This is in fact of just the triangular form which is realized exactly with a square-law detector. The higher order component spectra represent the small departure from the triangular shape but their combined content is under 8 per cent of the total L.F. noise given by (57).

One point of difference from the square-law detector is that in the linear detector, when the bandwidth β of the input noise is increased (leaving its spectral density E^2/β constant), the height of the spectrum does not change although its width increases proportionately with β. Fig. 8 illustrates the very close similarity in form of the output noise spectra from the linear and square-law detector.

From equation (56) it is seen that the autocorrelation coefficient of the envelope of a noise voltage is given by

$$\rho_1(\tau)=\frac{\overline{u_1u_2}-u_0^2}{\overline{u^2}-u_0^2}=\frac{\pi}{4(4-\pi)}\left(\mathrm{R}^2+\frac{\mathrm{R}^4}{16}+\frac{\mathrm{R}^6}{64}+\ldots.\right). \quad . \quad (60)$$

The numerical factor $\pi/4(4-\pi)=0{\cdot}91$ and it is seen that the autocorrelation coefficient of the amplitude will always lie between $0{\cdot}91\ \mathrm{R}^2$ (for R small, τ large) and R^2 (R nearly unity, τ small), and is therefore only slightly different from that of the square of the amplitude.

§ 9. Signal/noise Discrimination of a Detector.

In a receiver used for the observation or measurement of weak signals the law of the detector plays a part in determining the discrimination against noise since upon it depends both the incremental output for a small applied signal and the fluctuations of output due to the applied noise.

In the case of meter indication a weak signal would be observed by first noting the reading in the absence, and then in the presence of the signal, the difference of reading providing a measure of the signal intensity. The initial reading due to the noise can be "backed off" (*i.e.* compensated electrically or mechanically) and the sensitivity of measurement so increased since a more sensitive meter may now be used. The limit to this process is set by the fluctuations of the meter readings about their average positions arising from the noise. These fluctuations may be reduced by the use of a meter of long time constant but correspondingly the duration of a measurement is prolonged; the effect of the meter time constant is discussed in the next section.

The signal/noise discrimination of a detector can be objectively expressed in terms of the ratio of the increase of the average (or d.c.) output on applying a certain signal to the r.m.s. fluctuation of the output (*i.e.* the L.F. output) about the average. The effect of long-term observation and averaging on the discrimination is considered in the next section.

Usually in the condition of limiting sensitivity the signal/noise ratio at the detector is small and this enables a simpler parameter to be obtained to express the discrimination of a detector in terms of its law. If the noise of r.m.s. voltage E is accompanied by a signal $\mathrm{S}\cos\omega_0 t$ and is applied to an nth power-law detector the d.c. output voltage is given by

$$u_0=[\sqrt{(2)}\mathrm{E}]^n\left(\frac{n}{2}\right)!\ {}_1\mathrm{F}_1\left(-\frac{n}{2},\ 1,\ -x^2\right), \quad . \quad . \quad . \quad (11)$$

where

$$x=\frac{\mathrm{S}}{\sqrt{(2)}\mathrm{E}}$$

is the signal/noise ratio as before.

The total mean-square output voltage from the detector is given by

$$u^2=2^n\mathrm{E}^{2n}n\ !\ {}_1\mathrm{F}_1(-n,\ 1,\ -x^2).$$

For the signal/noise ratio x small the mean-square fluctuation of the output will be given approximately by

$$u_n^2=(2\mathrm{E}^2)^n\left[n\,!-\left(\frac{n}{2}\right)!^2\right]$$

as already given by equation (51).

The increase of d.c. output voltage due to the signal is found from equation (11) to be

$$u_0(x)-u_0(0)=[\sqrt{(2)}\mathrm{E}]^n(\tfrac{1}{2}n)\,!\,\frac{n}{2}x^2 \quad . \quad . \quad . \quad . \quad . \quad (61)$$

for x small. It is noted that the detector behaves as a square-law device as regards the increase of output due to a weak signal owing to the suppression effect of the stronger noise.

A convenient parameter for expressing the detector discrimination for *very small signals* is thus:

$$\mathrm{Q}=\frac{u_0(x)-u_0(0)}{u_n x^2}=\frac{\frac{1}{2}n}{\left[\dfrac{n\,!}{(n/2)\,!^2}-1\right]^{\frac{1}{2}}}. \quad . \quad . \quad . \quad . \quad (62)$$

It is found that Q has a maximum of unity at $n=2$ but this maximum is very flat, so that, in practice, superiority of a square-law detector in this respect is of no significance. For example:

$$n=\tfrac{1}{2},\quad \mathrm{Q}=0{\cdot}90.$$
$$n=1,\quad \mathrm{Q}=0{\cdot}96,$$
$$n=2,\quad \mathrm{Q}=1,$$
$$n=4,\quad \mathrm{Q}=0{\cdot}89.$$

A greater practical advantage of the square-law detector is that the d.c. output for a signal and noise input is given by

$$u_0=2\mathrm{E}^2(1+x^2)=2(\mathrm{E}^2+\tfrac{1}{2}\mathrm{S}^2),$$

showing that whatever the signal/noise ratio x, a change of indication can be directly interpreted as a change of mean-square input voltage.

§10. Influence of the Meter Time Constant and Integration Time on Sensitivity.

If the time constant of the indicating instrument connected to the detector output be increased the disturbing effect of the fluctuation of indication is reduced, so giving enhanced sensitivity at the expense of speed of measurement, or in statistical language, we would say that the random variations of the measured quantity are smoothed out by sampling over a longer time.

If the time constant of the meter is T the mean-square fluctuation of the output voltage is reduced in the ratio

$$\frac{1}{\mathrm{M}^2}=\frac{\displaystyle\int_0^\infty \frac{\mathrm{G}(\omega_a)\,.\,d\omega_a}{1+\omega_a{}^2\mathrm{T}^2}}{u_n^2}=\frac{\pi\mathrm{G}(0)}{2\mathrm{T}u_n^2} \quad \text{very nearly,}$$

if the receiver bandwidth is large compared with the reciprocal of the meter time constant. It is assumed that the signal is small compared with the noise so that the output spectrum is substantially the same as that found earlier for a noise input only.

The improvement factor due to the meter time constant is thus

$$\mathrm{M}=\sqrt{\left[\frac{2\mathrm{T}u_n^2}{\pi G(0)}\right]}, \qquad \ldots\ldots\ldots \quad (63)$$

which for a square-law detector is found from equations (53) and (54) to be

$$\mathrm{M}_2=\sqrt{(\beta\mathrm{T}/\pi)}=\sqrt{(2\mathrm{BT})}. \qquad \ldots\ldots \quad (64)$$

While for a linear detector from equations (57) and (58)

$$\mathrm{M}_1=1{\cdot}03\sqrt{(2\mathrm{BT})}, \qquad \ldots\ldots\ldots \quad (65)$$

which is negligibly different from the value for the square-law detector.

Thus combining these results with those of the previous section the ratio of the increase of indication to the r.m.s. fluctuation is

$$\frac{u_0(x)-u_0(0)}{u_n/\mathrm{M}}=x^2\mathrm{QM}=x^2\sqrt{(2\mathrm{BT})} \qquad \ldots\ldots \quad (66)$$

to a close approximation for both square-law and linear detectors.

Since the signal/noise power ratio x^2 is inversely proportional to the receiver bandwidth B, the discrimination y is seen to be proportional to $\sqrt{(\mathrm{T/B})}$. Hence, halving the receiver bandwidth or doubling the meter time constant is equivalent to a 1·5 db increase of signal voltage.

Another method of improving the sensitivity of measurement of a weak signal in noise is by taking the average of meter readings over a time T_0 long compared with the meter time constant T and so extending the period of integration. Clearly it is pointless to take readings too frequently in a given period since the closeness of correlation between successive values will prevent any further improvement in accuracy being obtained.

Consider the case in which N readings of the meter indication θ are taken. Their average is

$$\bar{\theta}=\frac{1}{\mathrm{N}}\sum_{\nu=1}^{\mathrm{N}}\theta_\nu$$

and the standard deviation σ of this average due to the random fluctuations in θ about its true average θ_0 is given by

$$\sigma_{\mathrm{N}}^2=\overline{\left[\frac{1}{\mathrm{N}}\sum_{1}^{\mathrm{N}}(\theta_\nu-\theta_0)\right]^2}$$

$$=\frac{1}{\mathrm{N}^2}\left[\mathrm{N}\sigma_1^2+2\sigma_1^2\sum_{1}^{\mathrm{N}-1}(\mathrm{N}-\mu)r_\mu\right], \qquad \ldots\ldots \quad (67)$$

where σ_1 is the standard deviation of a single reading and r_μ is the correlation coefficient between readings spaced μ apart. In the case of readings evenly spaced by a time s and a meter time constant T

$$r_\mu = \exp(-\mu s/T)$$

and

$$\frac{\sigma_N}{\sigma_1} = \frac{\sqrt{[N(1-r_1^2)-2r_1(1-r_1^N)]}}{N(1-r_1)}, \quad \ldots\ldots \quad (68)$$

where $r_1 = \exp(-s/T)$ is the correlation coefficient between successive readings. Naturally when this tends to unity corresponding to readings taken in very close succession $\sigma_N = \sigma_1$ and there is no improvement due to averaging.

At the other limit σ_N tends to $\sigma_1/\sqrt{(N)}$ as the correlation tends to zero and this factor $\sqrt{(N)}$ represents the maximum improvement obtainable. Fig. 9 shows the smoothing factor as a function of N for various degrees

Fig. 9.

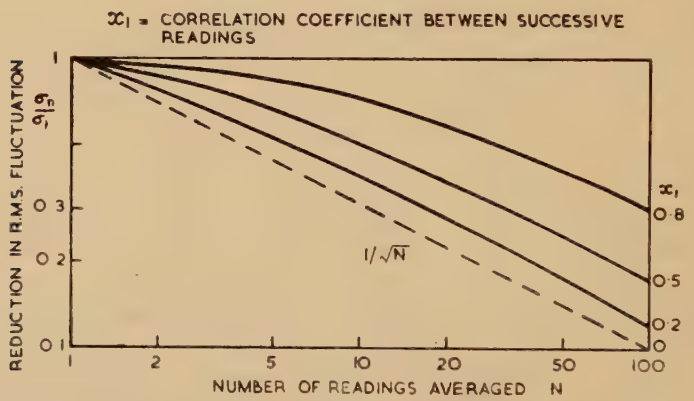

Reduction of fluctuation by averaging N regularly spaced readings.

of correlation. However, it is more useful to know what improvement can be obtained in a given observing time T_0 than with a given number of observations.

Imagine an integrating circuit which at any moment continuously provides the average value of the indications over the previous period of length T_0, that is, it forms the quantity

$$z = \frac{1}{T_0}\int_{t_0-T_0}^{t_0} \theta \, . \, dt$$

at the time t_0 of observation. The fluctuations in z can be calculated directly or as a limit to the summation given by equation (67) when discrete observations are made at infinitesimal spacings. It is found that the mean square deviation in z is given by

$$\sigma_{T_0}^2 = \frac{2\sigma_1^2}{T^2}\int_0^T (T-t)r(t) \, . \, dt, \quad \ldots\ldots \quad (69)$$

which for an exponential correlation $r(t)= \exp(-t/T)$ of indications gives

$$\frac{\sigma_{T_0}}{\sigma_1} = \sqrt{\left[\frac{2T}{T_0}\left(1+\frac{T}{T_0}\exp(-T_0/T)-\frac{T}{T_0}\right)\right]}, \quad . \quad . \quad (70)$$

which is shown in fig. 10.

Now from equations (63), (64) and (65), $\sigma_1=u_n/M$, and thus the overall improvement due to the meter time constant T and continuous averaging over T_0 which is assumed large compared with T is given by

$$\frac{u_n}{\sigma_{T_0}} = M\sqrt{\left(\frac{T_0}{2T}\right)} = \sqrt{(BT_0)}. \quad . \quad . \quad . \quad . \quad . \quad (71)$$

Fig. 10.

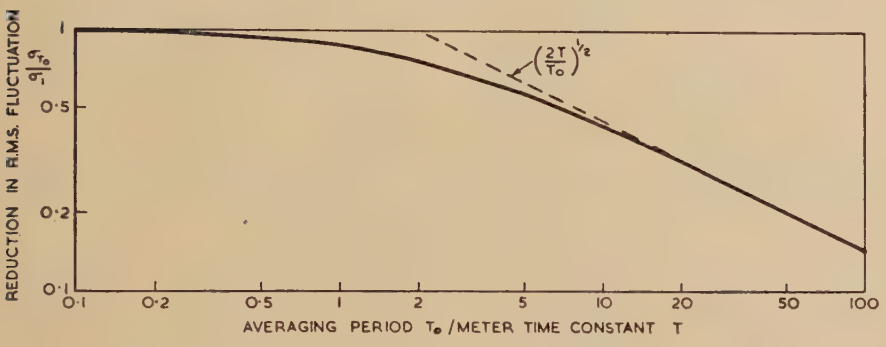

Reduction of fluctuation by continuous averaging over time T_0.

Acknowledgments.

The work described was carried out as part of the programme of the Radio Research Board to whom it was communicated in confidential reports in 1944 and 1945. It is published by permission of the Director of the National Physical Laboratory and of the Director of Radio Research of the Department of Scientific and Industrial Research.

References.

Fränz, K., 1940, *Elekt. Nachr.-tech.*, **17**, 215–230; 1941, *Hochfreq. tech. u. Elektroak.*, **57**, 146–151.

Ragazzini, J. R., 1942, *Proc. Instn. Radio Engrs., N.Y.*, **30**, 277–288.

APPENDIX I.

Probability Distribution of C.W. Signal Plus Narrow-Band Noise.

The instantaneous amplitude A of the mixture of signal and noise is given by

$$A^2=(X+S)^2+Y^2.$$

Now (X+S) and Y have independent normal distributions each of standard deviation E and centred on S and zero respectively. Putting $\xi=(X+S)^2$, $\eta=Y^2$ and $\alpha=A^2=\xi+\eta$, we see that

$$P(\xi)=\frac{1}{2E\sqrt{(2\pi\xi)}}\left\{\exp\left[-\frac{[\sqrt{(\xi)}-S]^2}{2E^2}\right]+\exp\left[-\frac{[-\sqrt{(\xi)}-S]^2}{2E^2}\right]\right\}$$

$$=\frac{1}{E\sqrt{(2\pi\xi)}}\exp\left(-\frac{\xi+S^2}{2E^2}\right)\cosh\left[\frac{S\sqrt{(\xi)}}{E^2}\right],$$

$$P(\eta)=\frac{1}{E\sqrt{(2\pi\eta)}}\exp\left(-\frac{\eta}{2E^2}\right),$$

whence

$$P(\alpha)=\frac{1}{2\pi E^2}\int_0^\alpha\frac{1}{\sqrt{[\xi(\alpha-\xi)]}}\exp\left(-\frac{\eta+\xi+S^2}{2E^2}\right)\cosh\frac{S\sqrt{\xi}}{E^2}\,.\,d\xi$$

$$=\frac{1}{2\pi E^2}\exp\left(-\frac{\alpha+S^2}{2E^2}\right)\int_0^{\pi/2}2\cosh\left[\frac{S\sqrt{(\alpha)}\sin\theta}{E^2}\right].\,d\theta$$

$$=\frac{1}{2E^2}\exp\left(-\frac{\alpha+S^2}{2E^2}\right)I_0\left[\frac{S\sqrt{(\alpha)}}{E^2}\right].$$

Thus the probability distribution for the amplitude $A=\alpha^{\frac{1}{2}}$ is

$$P(A)=\frac{A}{E^2}\exp\left(-\frac{A^2+S^2}{2E^2}\right)I_0\left(\frac{SA}{E^2}\right),$$

which is equation (7) of the text.

APPENDIX II.

Autocorrelation Function for the Nth Power of the Noise Amplitude.

If

$$v_1=X_1\cos\omega_0t_1+Y_1\sin\omega_0t_1,$$

$$v_2=X_2\cos\omega_0t_2+Y_2\sin\omega_0t_2$$

are the noise voltages at times spaced by $(t_2-t_1)=\tau$, their autocorrelation is

$$E^2r(\tau)=\overline{v_1v_2}=\tfrac{1}{2}(\overline{X_1X_2}+\overline{Y_1Y_2})\cos\omega_0\tau$$

when the spectrum is symmetrical, *i.e.* $\overline{X_1Y_2}=\overline{X_2Y_1}=0$. In the case of a rectangular spectrum $F(\omega)=E^2/\beta$ and

$$r(\tau)=\frac{1}{\beta}\int_{\omega_0-\frac{1}{2}\beta}^{\omega_0+\frac{1}{2}\beta}\cos\omega\tau\,.\,d\omega=\frac{\sin\frac{1}{2}\beta\tau}{\frac{1}{2}\beta\tau}\cos\omega_0\tau.$$

Thus

$$\overline{X_1X_2}=\overline{Y_1Y_2}=E^2\frac{\sin\frac{1}{2}\beta\tau}{\frac{1}{2}\beta\tau}=E^2R(\tau),$$

where

$$R(\tau)=\frac{\sin\frac{1}{2}\beta\tau}{\frac{1}{2}\beta\tau}$$

is the " envelope " of the correlation function $r(\tau)$.

The joint distribution of $X_1Y_1X_2Y_2$ is thus the product of two bivariate normal distributions

$$P(X_1, Y_1, X_2, Y_2)$$
$$= \frac{1}{4\pi^2 E^4(1-R^2)} \exp\left[-\frac{X_1^2+X_2^2-2RX_1X_2+Y_1^2+Y_2^2-2RY_1Y_2}{2E^2(1-R^2)}\right].$$

Now we require the autocorrelation of

$$A^n=(X^2+Y^2)^{n/2}$$

which is given by

$$\overline{A_1^n A_2^n} = \int\int\int\int_{-\infty}^{+\infty} (X_1^2+Y_1^2)^{n/2}(X_2^2+Y_2^2)^{n/2} P(X_1, Y_1, X_2, Y_2)\, dX_1\, dY_1\, dX_2\, dY_2.$$

In order to evaluate this, a convenient substitution is

$$X_1^2=qe^p E^2(1-R^2)\cos^2\phi_1, \qquad Y_1^2=qe^p E^2(1-R^2)\sin^2\phi_1,$$
$$X_2^2=qe^{-p} E^2(1-R^2)\cos^2\phi_2, \qquad Y_2^2=qe^{-p} E^2(1-R^2)\sin^2\phi_2,$$

which for the transformation to the variables p, q, ϕ_1 and ϕ_2 has the Jacobian

$$|J|=qE^4(1-R^2)^2,$$

whence

$$\overline{A_1^n A_2^n} = \frac{E^{2n}(1-R^2)^{n+1}}{4\pi^2} \int_0^\infty dq \int_0^\infty dp \int_0^{2\pi} d\phi_1 \int_0^{2\pi} d\phi_2 \cdot q^{n+1}$$
$$\times \exp\left[-q\cosh p - qR\cos(\phi_2-\phi_1)\right]$$
$$= E^{2n}(1-R^2)^{n+1} \int_0^\infty q^{n+1} K_0(q) I_0(qR)\, dq$$
$$= (2E^2)^n (1-R^2)^{n+1} \left(\frac{n}{2}\right)!^2 F\left(\frac{n+1}{2}; \frac{n+1}{2}; 1; -R^2\right)$$
$$= (2E^2)^n \left(\frac{n}{2}\right)!^2 F\left(-\frac{n}{2}, -\frac{n}{2}, 1, -R^2\right),$$

which is equation (40) of the text.

APPENDIX III.

The Components of the Output Spectrum due to a Rectangular Input Spectrum.

The component spectra of the detector output voltage are defined by

$$f_p(\omega_a) = \frac{2}{\pi} \int_0^\infty \left(\frac{\sin \frac{1}{2}\beta\tau}{\frac{1}{2}\beta\tau}\right)^p \cos \omega_a \tau \cdot d\tau.$$

They have the normalizing property

$$\int_0^\infty f_p(\omega_a) \, . \, d\omega_a = 1.$$

Each f_p is represented by a polynomial in ω_a/β with coefficients changing at each integral value of this variable. Furthermore, each f_{2m} cuts off at $m\beta$ beyond which it is identically zero. The first three even spectra are as follows :

$$f_2(\omega_a) = \frac{2}{\beta}\left(1-\frac{\omega_a}{\beta}\right),$$

$$f_4(\omega_a) = \frac{1}{3\beta}\left[\left(2-\frac{\omega_a}{\beta}\right)^3 - 4\left(1-\frac{\omega_a}{\beta}\right)^3\right] \qquad 0<\omega_a<\beta$$

$$= \frac{1}{3\beta}\left(2-\frac{\omega_a}{\beta}\right)^3, \qquad \beta<\omega_a<2\beta$$

$$f_6(\omega_a) = \frac{1}{60\beta}\left[\left(3-\frac{\omega_a}{\beta}\right)^5 - 6\left(2-\frac{\omega_a}{\beta}\right)^5 + 15\left(1-\frac{\omega_a}{\beta}\right)^5\right] \qquad 0<\omega_a<\beta$$

$$= \frac{1}{60\beta}\left[\left(3-\frac{\omega_a}{\beta}\right)^5 - 6\left(2-\frac{\omega_a}{\beta}\right)^5\right] \qquad \beta<\omega_a<2\beta$$

$$= \frac{1}{60\beta}\left(3-\frac{\omega_a}{\beta}\right)^5, \qquad 2\beta<\omega_a<3\beta$$

The higher order normal spectra tend rapidly to the Gaussian form since

$$\left(\frac{\sin z}{z}\right)^p \sim \exp\left(-pz^2/6\right) \text{ for } p \text{ large},$$

whence

$$f_p(\omega_a) \sim \frac{2}{\beta}\sqrt{\left(\frac{6}{\pi p}\right)}\exp\left(-\frac{6\omega_a^2}{p\beta^2}\right).$$

APPENDIX IV.

Rectification Efficiency of a Diode Detector.

For small applied voltages (*i. e.* such that the anode is not more positive than $+0{\cdot}2$ V. with respect to the cathode) the current *vs* voltage characteristic of typical diodes is of the exponential form appropriate to the retarding-field region with negligible space charge :

$$\mathrm{i} = c \exp(\mathrm{KV}),$$

where $\mathrm{K} = (\epsilon/k\mathrm{T}_c)$ is usually about 10 volt^{-1},

ϵ = electronic charge,

k = Boltzmann's constant,

T_c = cathode temperature.

If now a sinusoidal voltage A sin ωt is applied to the detector and $\bar{i}$ is the mean current over one cycle

$$V = A \sin \omega t - \bar{i}R,$$

$$\bar{i} = \frac{c}{2\pi}\int_0^{2\pi} \exp\left[K(A \sin \omega t - \bar{i}R)\right] d(\omega t) = c \exp(-K\bar{i}R) I_0(KA).$$

In the absence of an applied voltage there is an initial diode current i_0 given by

$$i_0 = c \exp(-K i_0 R).$$

The rectified voltage is thus given implicitly by

$$u = (\bar{i} - i_0)R = i_0 R[\exp(-Ku) I_0(KA) - 1].$$

If $KA \ll 1$, $I_0(KA) \approx 1 + \frac{1}{4}K^2A^2$, $\exp(-Ku) \approx 1 - Ku$,

whence

$$u \approx \frac{K^2 i_0 R}{4(1 + K i_0 R)} A^2,$$

demonstrating the square-law behaviour of the detector.

At large amplitude $KA \gg 1$,

$$I_0(KA) \approx \frac{\exp(KA)}{(2\pi KA)^{\frac{1}{2}}}$$

and thus

$$1 - \frac{u}{A} = \frac{1}{KA}\log_e\left(1 + \frac{u}{i_0 R}\right) + \frac{\log_e 2\pi KA}{KA},$$

showing that the rectification efficiency u/A approaches unity as KA becomes large. When A becomes very large the exponential law no longer holds for the diode and the current tends to be more nearly proportional to the voltage. It is easy to show that in this condition the rectified voltage approaches more and more closely to proportionality with the amplitude of the applied wave.

LIV. *A Radio Echo Apparatus for the Delineation of Meteor Radiants.*

By A. Aspinall, J. A. Clegg, Ph.D., and G. S. Hawkins,
Jodrell Bank Experimental Station, University of Manchester*.

[Received February 13, 1951.]

[Plates XVIII. & XIX.]

Abstract.

This paper describes a radio echo apparatus for the continuous recording of meteor activity, and the determination of the coordinates of active meteor radiants. It has been in operation since September 1949, and the occurrence of well known night time showers during this period have provided an opportunity to estimate its performance. The results obtained during the Geminid shower of 1949 and 1950 are described as an example, and its accuracy and resolving power are discussed.

§1. Introduction.

The radio echo technique has been used extensively during the past five years to detect meteor ionization in the atmosphere, and with the development of methods of radiant determination (Hey and Stewart 1947, Clegg 1948, McKinley and Millman 1949) and velocity measurement Hey and Stewart 1947, Ellyett and Davies 1948, Manning, Villard and Peterson 1949), has proved valuable in the observation of meteors under conditions which render visual watching impossible. The earlier radio investigations were concerned primarily with the well-known night time meteor showers, but the experiments of Hey and Stewart (1947) and Prentice, Lovell and Banwell (1947) revealed a high level of daytime activity during the summer months of 1945 and 1946, and more comprehensive surveys in 1947 (Clegg, Hughes and Lovell 1947) and 1948 (Aspinall, Clegg and Lovell 1949) confirmed the existence of a number of rich meteor streams incident on the sunlit side of the earth between May and July. This work has now been extended, and an apparatus has been developed to record meteor activity continuously throughout the whole year. It is designed to determine the radiants of the major daytime and night time showers occurring in the Northern hemisphere, to detect the minor streams, and to measure the hourly rate of sporadic meteors.

The method of radiant determination is similar to that described by Clegg (1948); but in order to obtain a more complete record the single rotatable aerial used in earlier experiments (Lovell, Banwell and Clegg 1947)

* Communicated by Dr. A. C. B. Lovell.

has been replaced by two fixed arrays which operate independently, producing low elevation beams, one directed towards the North of West and the other towards the South of West. The radiant coordinates are calculated from the times at which echoes appear at maximum range on the two systems.

The equipment has been fully operational since September 1949, and the results of the continuous survey and of the work on the summer daytime streams which has been carried out since that date will be discussed in detail elsewhere (Aspinall and Hawkins 1951). The purpose of the present paper is to describe the apparatus and to discuss the accuracy and limitations of the method of radiant determination employed.

Fig. 1.

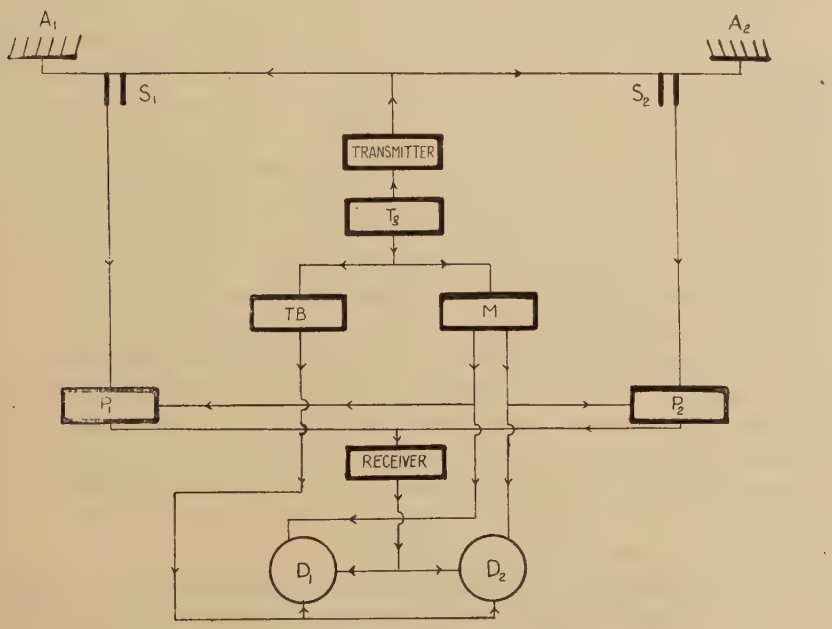

A brief account of the observations made during the Geminid meteor shower is included, however, in order to illustrate its performance.

§2. Apparatus.

A schematic diagram of the apparatus is shown in fig. 1. It operates on a frequency of 72 Mc./s., and comprises two independent beamed aerials A_1 and A_2, which are directed at low elevation, on azimuthal bearings of 242° and 292° respectively *. These arrays are common to the transmitter and receiver, and the pulses from the transmitter are radiated simultaneously by both. The received signals are fed through

* The azimuthal directions being measured in degrees East of North.

the transmitter–receiver switches, S_1 S_2, into the preamplifying stages, P_1, P_2, and after further amplification and detection are applied to the grids of the intensity modulated display tubes, D_1 and D_2. The sequence of operations is initiated from a master control unit by the unit T_g, which provides pulses to trigger the transmitter, the multivibrator M, and the common time base TB of the two display tubes. The square waves from the multivibrator are used to suppress the preamplifying stages P_1 and P_2 alternately, and are also applied to the grids of the cathode ray tubes D_1 and D_2, so that the signals from each aerial are displayed separately side by side, and are photographed on a film which moves continuously in a direction perpendicular to that of the time bases.

The unit T_g is capable of providing pulses with a number of different recurrence frequencies, and the apparatus can be triggered in a variety of ways. For normal observations the transmitter is usually operated at a pulse recurrence frequency of 150 c./s. and the time base unit at a frequency of 75 c./s. Under these circumstances the transmitter pulses appear twice on each display, at the beginning of each time base and at a range of 1000 Kms. This serves as a useful check on the range calibration, although subsidiary range markers can be supplied from the triggering system at intervals of 200 or 250 Kms. along the time base. One of the most serious difficulties encountered during the early experiments was that of differentiating between short duration echoes and the random noise impulses which present a similar appearance on the photographic record. This form of interference was considerably reduced by inserting a discriminator unit, similar to that used by Davies and Ellyett (1949), in the output of the receiver, but it has also been found advisable to trigger the transmitter with a pair of pulses separated by approximately 300 μsec., so that a true echo appears as a double. A portion of a record, taken with a film speed of 12 cms. per hour, is shown in fig. 2 (Pl. XVIII). The continuous lines A, B, A′, B′ correspond to the double transmitter pulses, and a number of echoes are visible as at C, D and E.

The photograph in fig. 3 (Pl. XIX.) shows the general arrangement of the two aerial systems, which are situated at longitude 2° 18′ W., latitude 53° 14′ N., and are placed symmetrically on either side of the building housing the transmitter and receiver. Each array consists of 6 Yagi aerials mounted at horizontal distances of $1{\cdot}2\lambda$ apart and at a height of $1{\cdot}57\lambda$ above the ground. They produce identical beams of elevation 8·5° and of half amplitude width $\pm 5°$ and have a power gain of 165 over a half wave dipole. The horizontal and vertical radiation patterns are shown in figs. 4*a* and 4*b*.

The minimum detectable signal at the receiver is 7×10^{-14} w., and in normal operation the peak power of the transmitter is 5 Kw., with a pulse length of 8 μs. Simultaneous visual and radio observations have shown that under these conditions the echo rate produced by an active shower, when the radiant is at 90° elongation to either of the aerial beams, corresponds closely to the rate of occurrence of visual meteors.

§3. The Determination of Meteor Radiants.

The method of radiant determination has been described previously (Clegg 1948) and only a brief description of its application to the present apparatus will be given.

Fig. 4*a*.

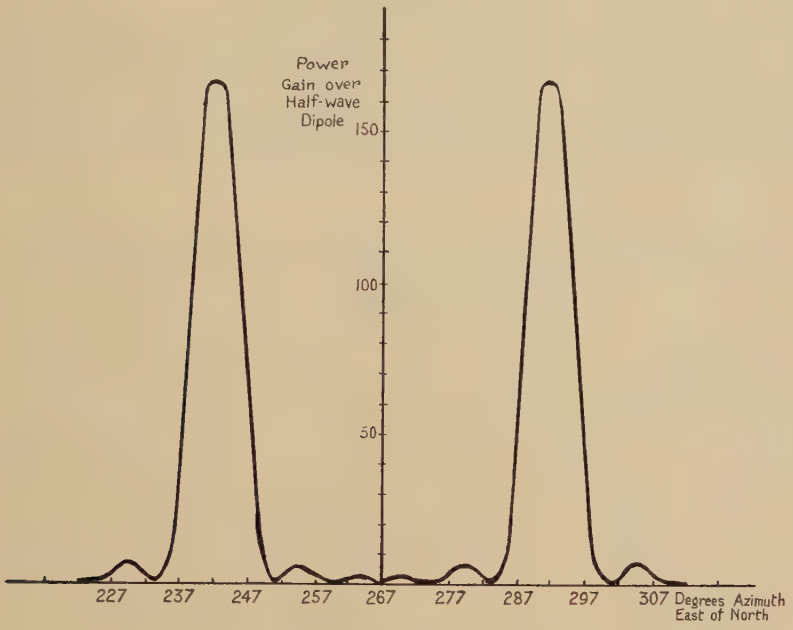

Fig. 4*b*.

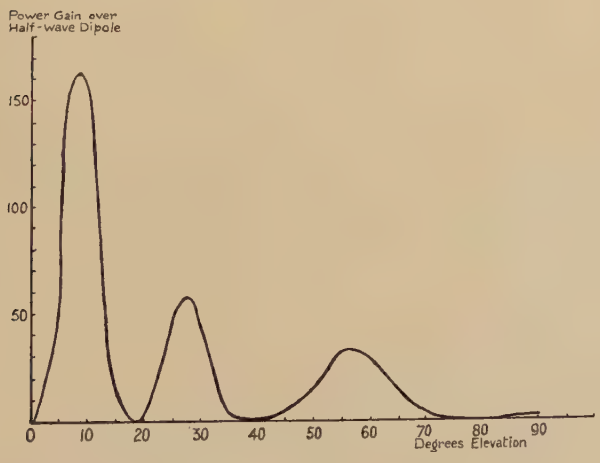

It follows from the condition of specular reflection (Hey and Stewart 1947, Lovell, Banwell and Clegg 1947), that when the earth passes through an active meteor stream, the radio echoes observed on frequencies of the

order of 72 Mc./s. are returned from a narrow zone of the atmosphere, of limited depth, which lies in a plane passing through the observing station and perpendicular to the direction of the radiant. The rate of occurrence and ranges of the echoes depend on the position and orientation of this plane relative to the aerial coverage, and vary with time as the radiant moves across the sky. It can be shown that with an aerial directed at low elevation on an azimuthal bearing of 270°, echoes attain a maximum range when the radiant is close to the central meridian. For a radiant close to upper culmination, the passage of the echo zone through the beam is accompanied by the initial appearance of echoes at short ranges, followed by a gradual increase in range to a maximum value R_{max}, and a final sudden decay in the echo rate.

Fig. 5.

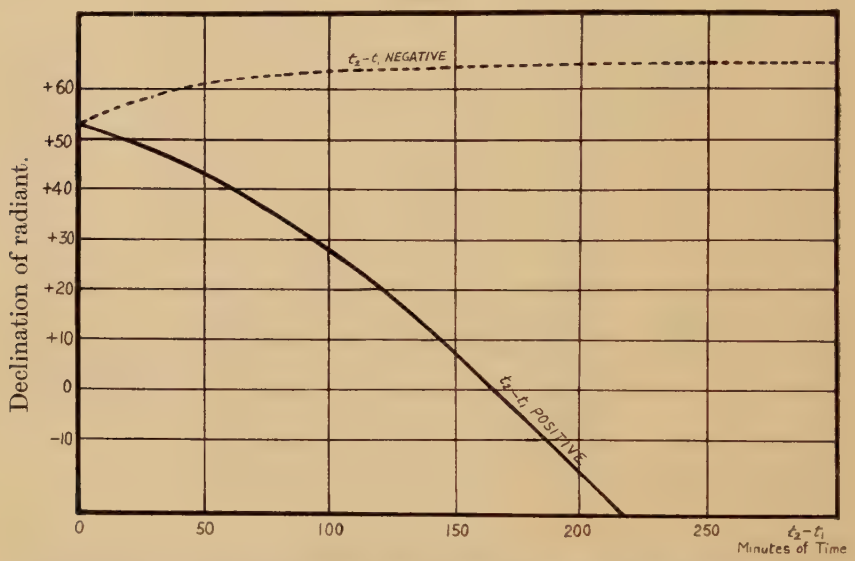

If the aerial characteristics are such that echoes can be detected down to the horizon, R_{max} is equal to the distance at which the meteor zone cuts the horizon circle of the station, and for a typical shower of medium velocity, for which the mean height of the zone can be taken as approximately 95 Kms., $R_{max}=1100$ Kms. Under these circumstances the time of maximum range, T, is the time at which the azimuth of the radiant differs from that of the beam by 90° and corresponds to the transit of the radiant. For aerials directed along azimuths $270°+\theta_1$ and $270°+\theta_2$, the echoes reach a maximum range at times $T+t_1$ and $T+t_2$. The time difference t_2-t_1 is a function of the declination, δ, of the radiant, θ_1, θ_2, and the latitude of the station. This function is plotted in fig. 5 for the case of $\theta_1=-28°$, $\theta_2=+22°$ and lat.$=53°$N., and from this curve the declination of the radiant may be found. From the curve labelled 1100 Kms. in fig. 6, t_1 and t_2 may be determined separately and the time of transit then found from the observed values of $T+t_1$ and $T+t_2$.

It may be noted that t_1 is negative for radiants which transit south of the zenith and echoes appear first in aerial 1 and then in aerial 2. For radiants which transit north of the zenith (dec. $>53°$) this order is reversed, and t_2-t_1 becomes negative. If the declination is greater than 76° the echo zone never enters the coverage of aerial 2, but remains for many hours in the beam of aerial 1. A radiant position can still be determined however by fitting theoretical range curves to the range/time plots.

In practice, owing to the conditions governing the reflection of radio waves from the surface of the earth, the aerial sensitivity falls off rapidly in directions close to the horizontal, and echoes are never observed out to ranges exceeding 1000 Kms. Under these circumstances the times of occurrence of echoes of maximum range are advanced by an amount

Fig. 6.

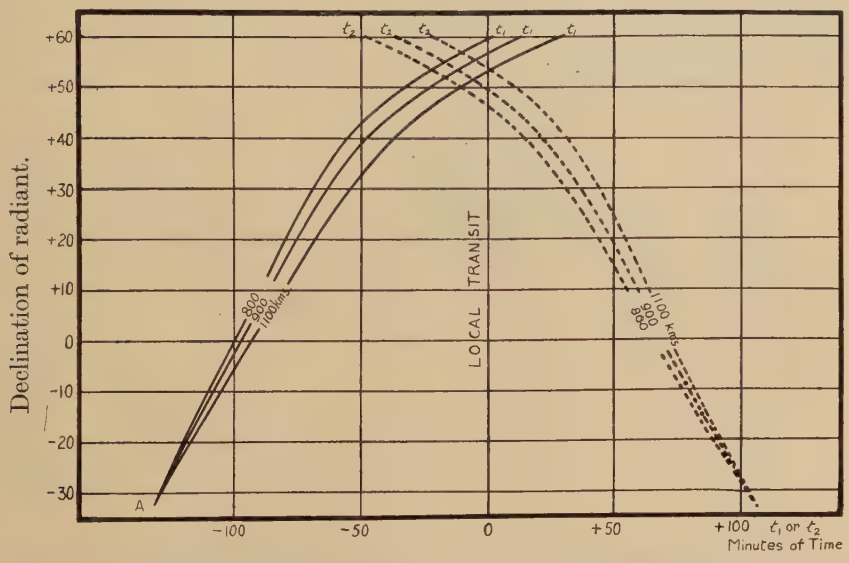

depending on the declination of the radiant and the observed value of R_{max}. This has been taken into account in the curves labelled 900 and 800 Kms. in fig. 6, from which the time of transit is found, but since the displacement is to a close approximation the same for both aerials, the curve of fig. 5 and determination of declination is not affected. Finally, a small correction has to be applied if the mean height of the meteors in a stream is not 95 Kms. This correction, which affects only the time of transit, is given in Table I.

§4. Results Obtained During The Geminid Meteor Shower.

The range-time plots obtained during the Geminid shower of 1949 and 1950, which are shown in fig. 7, provide a typical example of the results obtained with the apparatus. Times are shown as absicissæ, and the ranges of individual echoes are indicated by the lengths of the vertical lines. The results obtained on each aerial, between 0000 and 0400 U.T. on Dec. 13, 1949 and Dec. 13, 1950 are shown separately.

These plots indicate clearly the general variation in echo rate and range which occur as the echo zone sweeps through each beam in turn. The occurrence of echoes at maximum range, and the subsequent sharp fall in rate, appear at approximately 0110 U.T. on the first aerial, and at approximately 0240 U.T. on the second aerial. The radiant positions obtained from these plots are as follows :—

	Time of local transit.	*Radiant coordinates.*
Dec. 13, 1949	0214 U.T.	R.A. 111·5°, Dec. 32·5° U.T.
Dec. 13, 1950	0218 U.T.	R.A. 112·2°, Dec. 32·5° U.T.

When the radiant position has been determined, theoretical range-time curves can be constructed. These are shown as dotted lines in fig. 7. In the case of an ideal point radiant, in the absence of sporadic meteor activity, these envelopes should contain all the echoes, and they provide a useful indication of the diffuseness of the radiant.

TABLE I.

Correction in minutes of time to be applied to time of transit.

Height kms. \ δ	−20°	−10°	0°	10°	20°	30°	40°	50°	60°
115	2	3	4	5	6	7	8	10	12
110	1	2	3	3	4	4	5	7	8
105	0	1	1	1	1	1	2	2	3
95	0	0	0	0	0	0	0	0	0
85	−0	−1	−1	−1	−1	−1	−2	−2	−3
80	−1	−2	−3	−3	−4	−4	−5	−7	−8
75	−2	−3	−4	−5	−6	−7	−8	−10	−12

§5. ACCURACY OF RADIANT DETERMINATION.

The results obtained with this apparatus during the major daytime and night time showers have shown that when the echo rate, during the passage of the echo zone through the beam, exceeds 30 per hour, times t_1 and t_2 can be measured to within ± 5 minutes. This corresponds to an error of $\pm 1°$ in right ascension and $\pm 1{\cdot}5°$ in declination. In the exceptional case of a major stream with a radiant lying within 20° of the celestial pole, the position must be determined by the curve fitting method, and the accuracy is necessarily reduced.

For weaker streams the accuracy of radiant determination falls off markedly with decreasing echo rate, particularly if the shower rate does not exceed that of the sporadic background by a sufficiently high factor. Indeed, in the case of minor streams occurring during times of high sporadic activity, it is often difficult to distinguish between true and spurious

Fig. 7*a*.

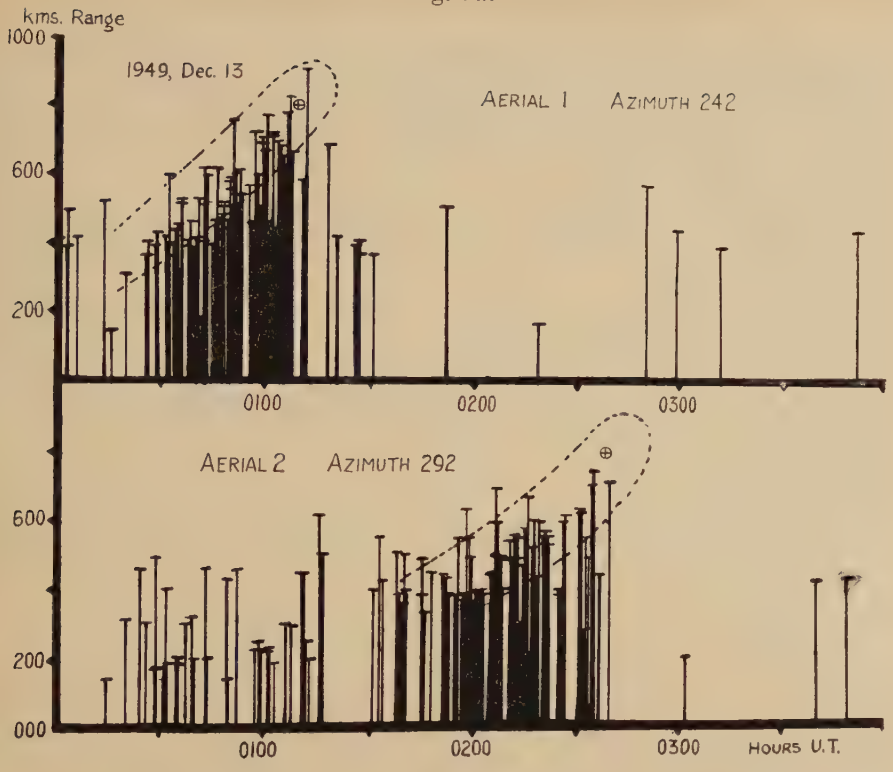
kms. Range
1000
600
200
1949, Dec. 13
AERIAL 1 AZIMUTH 242
0100
0200
0300
AERIAL 2 AZIMUTH 292
600
200
000
0100
0200
0300
HOURS U.T.

Fig. 7*b*.

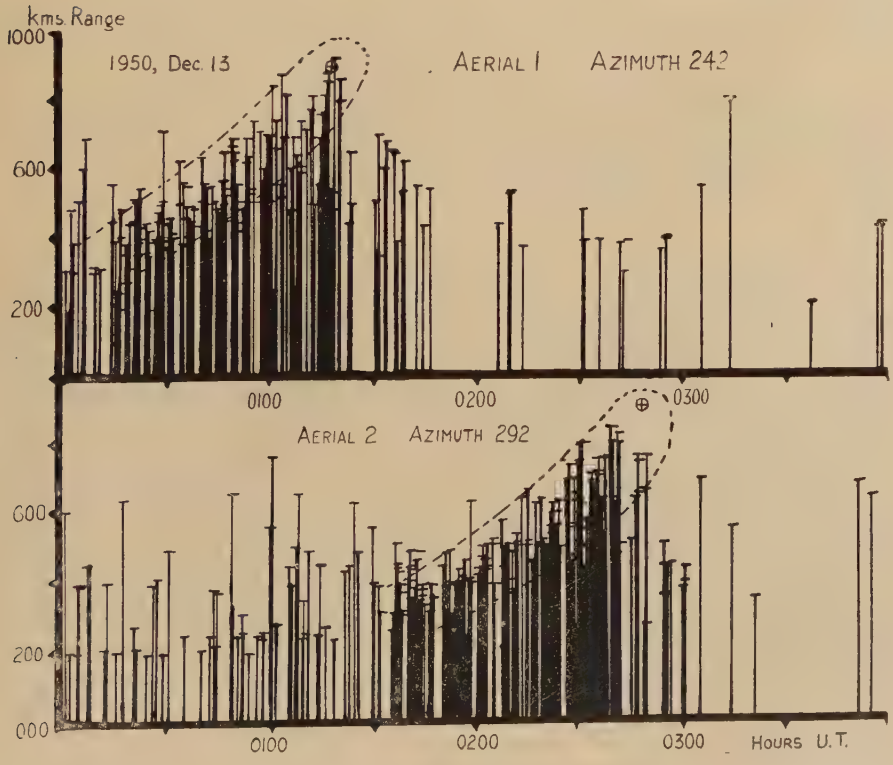
kms. Range
1000
600
200
1950, Dec. 13
AERIAL 1 AZIMUTH 242
0100
0200
0300
AERIAL 2 AZIMUTH 292
600
200
000
0100
0200
0300
HOURS U.T.

radiants, and for this reason it has been found necessary to classify showers for the purposes of radiant determination in the following way :

Class A, which comprises the most active and prominent showers, and which is defined by the following criteria :

(1) During the passage of the echo zones through the two beams there must be at least 3 echoes of range greater than 700 Kms. appearing on each aerial.

(2) Two-thirds of the total number of echoes observed must fall within the theoretical range envelopes.

A statistical analysis shows that the probability of a radiant of this class being spurious is less than 1/100, so that all showers which fulfil the foregoing conditions may be taken to be real.

Class B. This is defined as follows :—

(1) During the passage of the echo zone through the two beams there must be at least 3 echoes of range greater than 600 Kms. appearing on each aerial.

(2) One-half of the total number of echoes observed must fall within the theoretical range envelope.

A range-time plot fulfilling these criteria is not by itself considered to afford definite proof of the existence of a shower, but only to provide confirmatory evidence in cases where a Class A radiant appears on the previous or the following day.

Class C. This Class is used to monitor the meteor activity from a region of the sky containing a suspected radiant for which the plots do not fulfil the conditions required by A and B.

In estimating the radiant position of a shower which is active for several days, a mean of individual radiant positions is taken, weighting the plots of Class A, B and C in order of importance in the ratio 2 : 1 : 0.

§6. Resolving Power.

It occasionally happens, particularly during the summer daytime streams, that two radiants are simultaneously active ; and if the apparatus is to resolve between two such centres, their range-time plots on at least one of the two aerials must be separated by approximately 30 minutes. This time separation depends on the relative positions of the two radiants, and is most conveniently expressed in terms of their angular separation, s, and their relative position angle, ϕ, as indicated in fig. 8. This figure represents a small portion of the celestial sphere, viewed internally, with two radiants situated at R_1 and R_2. If ABC is the meridian bisecting the great circle arc $R_1 R_2$ at B, then the position angle ϕ is defined as the angle ABR_2.

Fig. 9 shows the angular separation s required for resolution on each of the two aerials, plotted as a function of ϕ for different values of the declination of the radiant R_1. It is evident from these curves than any

pair of radiants whose angular separation is greater than 20° can be resolved by at least one of the two aerials, while for more favourable cases the degree of resolution is considerably higher than this.

Fig. 8.

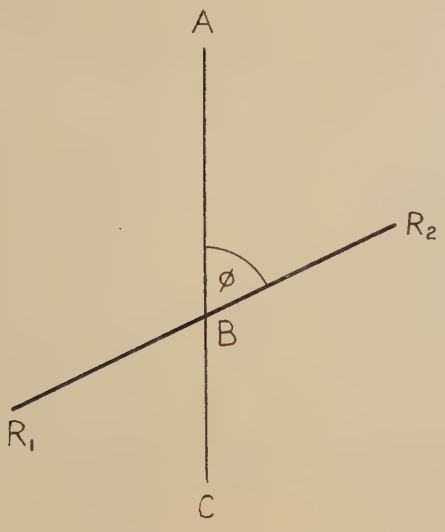

Fig. 9.

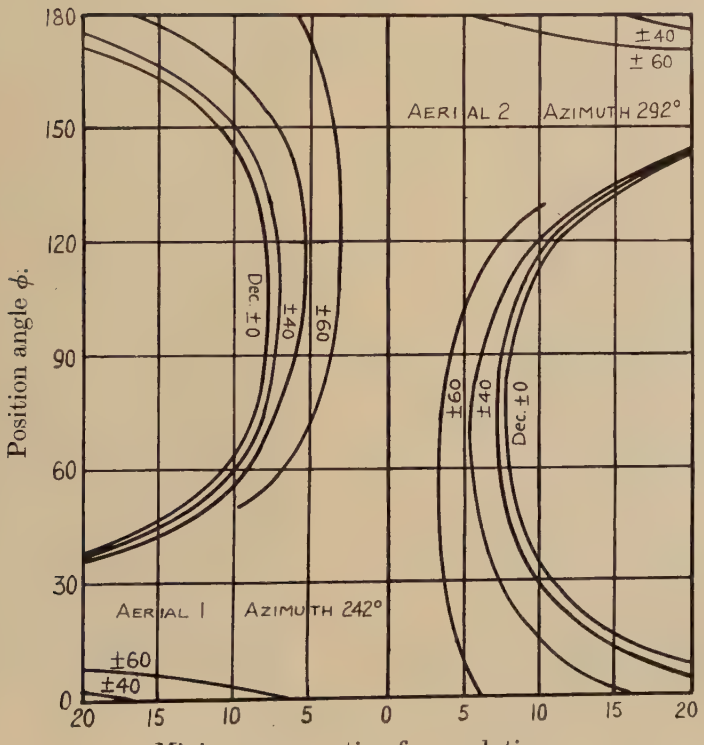

ACKNOWLEDGMENTS.

This apparatus has been built at the Jodrell Bank Experimental Station of the University of Manchester under the auspices of Dr. A. C. B. Lovell, whose advice and encouragement has been appreciated. Much of the capital expenditure has been borne by the Department of Scientific and Industrial Research, and two of the authors (A.A., G.S.H.) are indebted to the Department individually for the award of maintenance grants.

REFERENCES.

ASPINALL, A., CLEGG, J. A., and LOVELL, A. C. B., 1949, *Mon. Not. Roy. Astr. Soc.*, **109,** 352.

ASPINALL, A., and HAWKINS, G. S., 1951, *Mon. Not. Roy. Astr. Soc.*, in publication.

CLEGG, J. A., 1948, *Phil. Mag.*, **39,** 577.

CLEGG, J. A., HUGHES, V. A., and LOVELL, A. C. B., 1947, *Mon. Not. Roy. Astr. Soc.*, **107,** 369.

DAVIES, J. G., and ELLYETT, C. D., 1949, *Phil. Mag.*, **40,** 614.

ELLYETT, C. D., and DAVIES, J. G., 1948, *Nature, Lond.*, **161,** 596.

HAWKINS, G. S., and MARY ALMOND, 1950, *J. Brit. Astr. Ass.*, **60,** 251.

HAWKINS, G. S., and ASPINALL, A., 1951, in preparation.

HEY, J. S., and STEWART, G. S., 1947, *Proc. Phys. Soc.*, **59,** 858.

LOVELL, A. C. B., BANWELL, C. J., and CLEGG, J. A., 1947, *Mon. Not. Roy. Astr. Soc.*, **107,** 164.

MANNING, L. A., VILLARD, O. G., and PETERSON, A. M., 1949, *J. Appl. Phys.*, **20,** 475.

MCKINLEY, D. W. R., and MILLMAN, P. M., 1949 a, *Canad. J. Res.*, **27A,** 53; 1949 b, *Proc. Inst. Radio Engrs.*, **37,** 364.

PRENTICE, J. P. M., LOVELL, A. C. B., and BANWELL, C. J., 1947, *Mon. Not. Roy. Astr. Soc.*, **107,** 155.

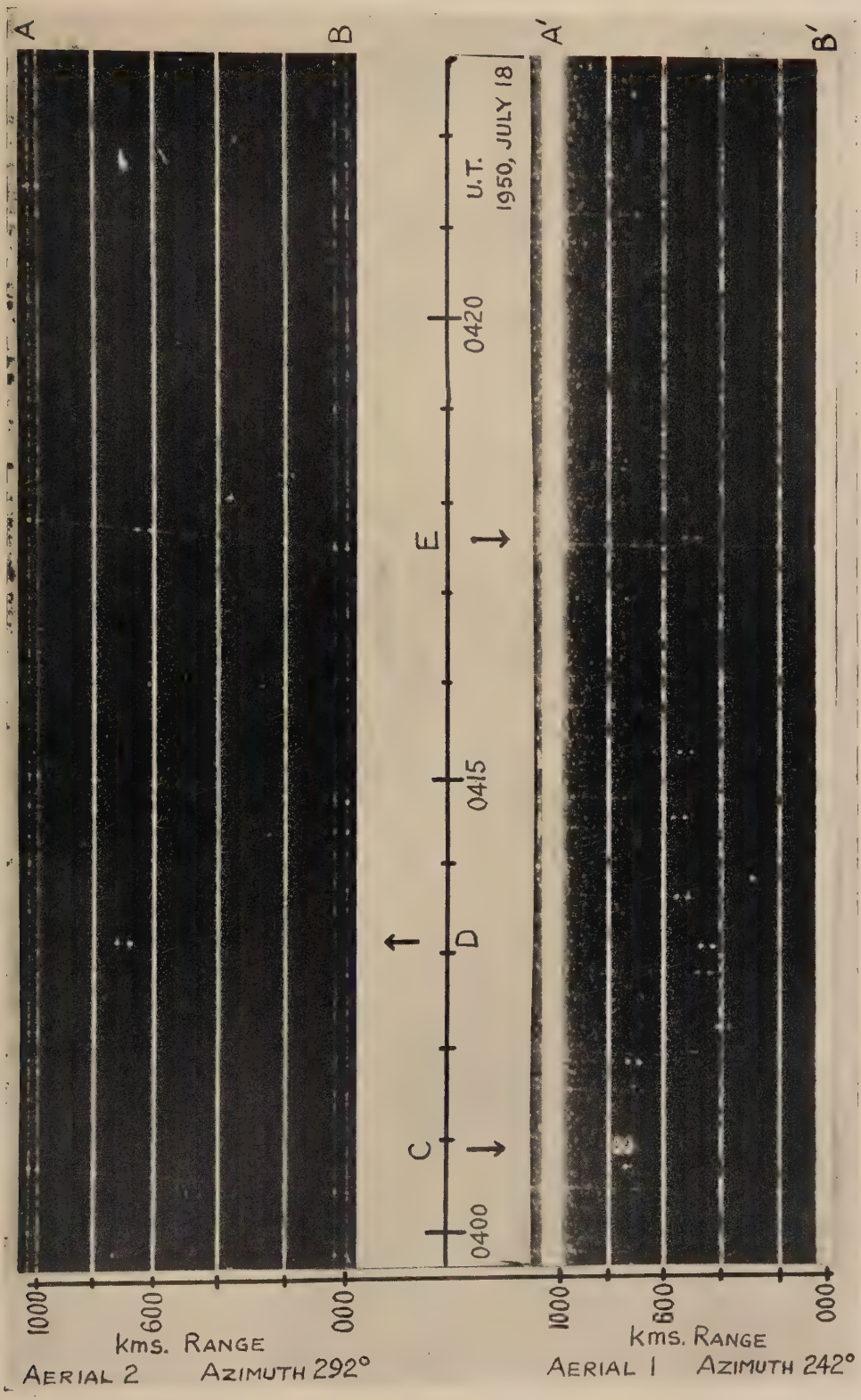

To face page 514

FIG. 3.

LV. *Transit-time Phenomena in Electron Streams.*—III. *The Electron-Ion Plasma and Beam Fluctuations.*

By D. K. C. MacDonald,
Clarendon Laboratory, Oxford*.

[Received February 13, 1951.]

Abstract.

Continuing the investigation started in earlier papers, we analyse here the equilibrium (isothermal) fluctuations ("noise") in a travelling electron beam taking into account full space-charge interaction. The results are then considered in relation to a number of practical electron valve problems. Because of its relevance to the general problem we also present first a short discussion of the characteristics of electron-ion and electron plasmas based on a "lattice" model.

§1. Introduction.

In two previous papers in this Journal (MacDonald 1949, 1950) we have studied systematically the problem of fluctuations ("noise") in a travelling electron beam and their growth. In the first paper we neglected interaction entirely while in the second an average, or "smoothed", potential-variation due to space-charge (*e. g.* Child's law) was taken into account. In the present paper we derive the equilibrium shot noise in a travelling beam where the complete fluctuating interaction is included insofar as this is expressed by Poisson's law at any instant. A general expression emerges which enables a number of very suggestive comparisons to be made with a range of valve problems.

When undertaking this work we were naturally led to consider models for an electron-plasma and in particular found a "lattice" model illuminating in several respects. We have therefore thought it relevant at this time to present first a brief discussion of such a model although it should be emphasized that the fluctuations analysis which follows is essentially independent of this model, being in fact based on quite general premisses.

§2. Plasma Models.

In the past it has been customary (*e. g.* Tonks and Langmuir 1929, Bohm and Gross 1949, Twiss 1950, Gabor 1950) to consider an electron plasma or electron-ion plasma as a quasi-continuum of essentially gas-like (*cf.* also v. Laue 1918) properties. If we assume the average inter-charge distance to be d then the potential energy per charge will be in the order of e^2/d, while at temperature T the random kinetic energy$\sim kT$. Since generally in electron-tube problems $kT \gg e^2/d(=(\rho e^5)^{1/3})$ the gas (or rather

* Communicated by the Author.

perhaps fluid) approximation is essentially justified. However, it appears useful, as has often been done in the corresponding metallic "electron-gas" problem, to consider the properties—particularly as regards the frequency spectrum—of a "rigid" charge lattice of inter-atomic distance d. The well known difficulties associated with three-dimensional lattices restrict us to a linear lattice, following closely Brillouin (1946).

2.1. *Electron-Ion Lattice.*

Consider then a linear chain of ions (mass M, charge $+e$) and electrons (mass m, charge $-e$). In order to maintain this chain in a stable state it will be necessary to assume some repulsive force in addition to the Coulomb attraction*. Born assumed a potential law of the form A/r^n when dealing with the alkali-halide solid and we shall follow him here.

Let d be the distance between *electrons*, and let U be the potential energy between an adjacent electron-ion pair. Then it may readily be shown (*cf.* Brillouin, *loc. cit.*, Cap 3) that two separate modes of vibration of the lattice can occur. In the lower-frequency branch, generally known as the "acoustical" branch, neighbouring electrons and ions will essentially be oscillating in phase with one another while, after a "forbidden-zone" of frequencies, we arrive at an upper branch—the "optical" branch—where electrons and ions will effectively be in anti-phase.

If, as a first approximation, we consider only "nearest-neighbour" interaction then the frequency/wavelength relations for the two branches are given by

$$\omega_a^2=\left(\frac{\partial^2 U}{\partial r^2}\right)_0\left\{\frac{1}{m}+\frac{1}{M}-\left[\left(\frac{1}{m}+\frac{1}{M}\right)^2-\frac{4\sin^2\frac{\pi d}{\lambda}}{mM}\right]^{1/2}\right\}, \quad . \quad (1)$$

$$\omega_0^2=\left(\frac{\partial^2 U}{\partial r^2}\right)_0\left\{\frac{1}{m}+\frac{1}{M}+\left[\left(\frac{1}{m}+\frac{1}{M}\right)^2-\frac{4\sin^2\frac{\pi d}{\lambda}}{mM}\right]^{1/2}\right\}, \quad . \quad (2)$$

where r is the distance between an electron-ion pair, ω_a and ω_0 are the (angular) acoustical and optical frequencies and the differentials are to be evaluated at $r=d/2$.

Since $m/M \ll 1$, these reduce to

$$\omega_a=\sqrt{\left[\frac{2}{M}\left(\frac{\partial^2 U}{\partial r^2}\right)_0\right]}\cdot\sin\frac{\pi d}{\lambda} \quad . \quad . \quad . \quad . \quad . \quad . \quad (3)$$

and

$$\omega_0=\sqrt{\left[\frac{2}{m}\left(\frac{\partial^2 U}{\partial r^2}\right)_0\right]}. \quad . \quad . \quad . \quad . \quad . \quad . \quad . \quad . \quad (4)$$

Now with the foregoing assumptions we may set

$$(\partial^2 U/\partial r^2)_0=8(n-1)e^2/d^3=8(n-1)e\rho,$$

* It should be emphasized that this is merely a convenient *ad hoc* assumption to enable us to treat the problem effectively as a lattice. In fact, the thermal energy of the plasma could be regarded for our purpose as playing in part the rôle of this repulsive potential. If T is too small, then electron-ion recombination will simply occur.

where ρ is the density of electrons (or ions) in the corresponding three-dimensional " lattice ". For $\lambda \gg d$, (3) may then be written

$$\omega_a = \sqrt{\left[\frac{16(n-1)e\rho}{M}\right]} \cdot \frac{\pi d}{\lambda} \quad . \quad . \quad . \quad . \quad . \quad . \quad (3a)$$

corresponding to travelling waves with a phase—(and group)—) velocity

$$v = \frac{d}{2}\sqrt{\left(\frac{16\gamma e\rho}{M}\right)}, \quad . \quad . \quad . \quad . \quad . \quad . \quad . \quad . \quad (5)$$

where $\gamma = n-1$.

For $\lambda \sim d$, dispersion becomes evident and a limiting frequency, $\hat{\omega}_a$, occurs for $\lambda = 2d$ where the group-velocity becomes zero (standing waves):

$$\hat{\omega}_a = \sqrt{\left(\frac{16\gamma e\rho}{M}\right)}. \quad . \quad . \quad . \quad . \quad . \quad . \quad . \quad (3b)$$

This may be compared with the " plasma-ion (angular) frequency " (*cf.* Tonks and Langmuir, *loc. cit*) given by

$$\Omega p = \sqrt{\left(\frac{4\pi e\rho}{M}\right)}. \quad . \quad . \quad . \quad . \quad . \quad . \quad . \quad (3c)$$

From (4) above it is clear that the " optical " frequency branch has degenerated into a single standing-wave vibration with

$$\omega_0 = \sqrt{\left(\frac{16\gamma e\rho}{m}\right)}, \quad . \quad . \quad . \quad . \quad . \quad . \quad . \quad (4a)$$

which then corresponds directly to the " plasma-electron frequency ". To our approximation the wavelength may then assume any value greater than $2d$ which is the common limit for both classes of oscillation.

2.2. *Electron Lattice.*

With a linear lattice consisting purely of electrons, only the acoustical branch can exist and we have now, to the " nearest-neighbour " approximation,

$$\omega = \sqrt{\left[\frac{4}{m}\left(\frac{\partial^2 U}{\partial r^2}\right)_0\right]} \sin\frac{\pi d}{\lambda}. \quad . \quad . \quad . \quad . \quad . \quad . \quad (6)$$

Taking now U, the potential energy between two adjacent electrons, as simply e^2/d in this case we see that for $\lambda \gg d$ we have *travelling* waves with phase —, and group —, velocity

$$v = \frac{d}{2}\sqrt{\left(\frac{8e\rho}{m}\right)}, \quad . \quad . \quad . \quad . \quad . \quad . \quad . \quad . \quad (7a)$$

(7*a*) may also be written :

$$\tfrac{1}{2}mv^2 = \frac{e^2}{d}. \quad . \quad . \quad . \quad . \quad . \quad . \quad . \quad . \quad . \quad (7b)$$

Again a maximum frequency (*standing* waves) occurs for

$$\hat{\omega} = \sqrt{\left(\frac{8e\rho}{m}\right)} \quad . \quad . \quad . \quad . \quad . \quad . \quad . \quad . \quad (6a)$$

and

$$\lambda_{min} = 2d, \quad . \quad . \quad . \quad . \quad . \quad . \quad . \quad . \quad . \quad (6b)$$

which may again be compared with the familiar plasma-electron frequency.

2.3. *Effect of Thermal Energy.*

So long as kT is less than, or the order of e^2/d—the electrostatic energy—we shall not expect in our model appreciable deviation from these results within their degree of approximation. When, however, kT exceeds e^2/d significantly we should expect the velocity in (7) to be given now rather by

$$\tfrac{1}{2}mv_t^2 \sim \frac{k\mathrm{T}}{2}, \qquad i.\,e. \quad v_t \sim \sqrt{\left(\frac{k\mathrm{T}}{m}\right)}, \quad . \quad . \quad (8)$$

while $$\lambda_{\min} \sim \frac{v_t}{\hat{f}} \sim \sqrt{\left(\frac{k\mathrm{T}}{m}\right)}\left[2\pi\sqrt{\left(\frac{m}{8e\rho}\right)}\right], \quad \sim 2\pi\sqrt{\left(\frac{k\mathrm{T}}{8e\rho}\right)}. \quad . \quad (9a)$$

If in fact we set $$\hat{\omega} = \sqrt{\left(\frac{4\pi e\rho}{m}\right)},$$

the plasma electron frequency, we have

$$\lambda_{\min} = \sqrt{\left(\frac{k\mathrm{T}}{m}\right)}\left[2\pi\sqrt{\left(\frac{m}{4\pi e\rho}\right)}\right] = 2\pi\sqrt{\left(\frac{k\mathrm{T}}{4\pi e\rho}\right)}, \quad . \quad . \quad (9b)$$

which is essentially just the Debye characteristic length (*cf. e. g.* Bohm and Gross, *loc. cit.*)

3. *Noise in Travelling Electron Beams.*

We turn now to a beam travelling as a whole with velocity v_0 such that $\frac{1}{2}mv_0^2 = \Phi$, say. We wish to determine the *equilibrium* observable current fluctuations in such a beam due to thermal agitation. The "atomicity" of electricity (*cf.* the "shot effect") will introduce itself naturally as a consequence of the frequency characteristics of the discrete lattice discussed above.

Consider then an electron beam of mean density, ρ_0, velocity v_0, which has been travelling "for a sufficiently long time", to be regarded as being in thermal equilibrium at a temperature*, T. Let us also take a length, L, of the beam of "sufficient" extent for the end conditions to be neglected and let us assume an arbitrary disturbance of electron density, ρ, and of velocity, v, which has been analysed into Fourier components over this interval. Let the component at (angular) frequency, ω, say, of electron-density be

$$\tilde{\rho}_\omega = \rho_\omega \sin\left(\omega\left(t - \frac{x}{v_0}\right) + \theta\right), \quad . \quad . \quad . \quad . \quad . \quad (10a)$$

and of velocity be

$$\tilde{v}_\omega = v_\omega \sin\left(\omega\left(t - \frac{x}{v_0}\right) + \phi\right). \quad . \quad . \quad . \quad . \quad . \quad (10b)$$

The corresponding component of current is given by

$$\left.\begin{aligned} \tilde{\mathrm{I}}_\omega &= \mathrm{A}(\tilde{\rho}_\omega v_0 + \rho_0 \tilde{v}_\omega) \\ &\text{(where this is essentially a vector addition)} \\ &= \tilde{\mathrm{I}}_{1\omega} + \tilde{\mathrm{I}}_{2\omega}, \quad \text{say} \end{aligned}\right\} \quad . \quad . \quad . \quad (11)$$

where A is cross sectional area of the beam.

* The question of the actual temperature appropriate to a beam is returned to briefly later.

From (10a) using Poisson's equation we derive the corresponding potential variation, and hence that the perturbation energy corresponding to (11) is *

$$\mathrm{E}=\frac{\pi v_0^2\rho_\omega^2\mathrm{AL}}{\omega^2}+\frac{\rho_0 v_\omega^2\mathrm{AL}}{4}\frac{m}{e}. \quad . \quad . \quad . \quad . \quad . \quad . \quad . \quad (12)$$

We can then write down immediately the probability distribution function for the beam current components and phases

$$f(\mathrm{I}_1, \mathrm{I}_2;\ \theta, \phi)\, d\mathrm{I}_1\, d\mathrm{I}_2\, d\theta\, d\phi$$
$$=\left(\frac{\mathrm{L}}{\mathrm{A}\omega^2 k\mathrm{T}}\right)\left(\frac{\mathrm{L}m}{4\pi e\rho_0\mathrm{A}k\mathrm{T}}\right)\mathrm{I}_1\epsilon^{-\frac{\pi\mathrm{L}\mathrm{I}_1^2}{\mathrm{A}\omega^2 k\mathrm{T}}}\cdot\mathrm{I}_2\epsilon^{-\frac{m\mathrm{L}\mathrm{I}_2^2}{4e\rho_0\mathrm{A}k\mathrm{T}}}\, d\mathrm{I}_1\, d\mathrm{I}_2\, d\theta\, d\phi. \quad (13)\dagger$$

And, in particular,

$$\overline{\mathrm{I}_1^2}=\frac{\omega^2 k\mathrm{TA}}{\pi\mathrm{L}};\quad \overline{\mathrm{I}_2^2}=\frac{4e\rho_0\mathrm{A}k\mathrm{T}}{m\mathrm{L}}. \quad . \quad . \quad . \quad . \quad . \quad (14)$$

Since, further, in a bandwidth B there will be BL/v_0 components, we may write

$$\overline{\delta\mathrm{I}_f^2}\left[\equiv\frac{\mathrm{BL}}{v_0}\left(\frac{\overline{\mathrm{I}_1^2}+\overline{\mathrm{I}_2^2}}{2}\right)\right]=\left(\frac{\omega^2 k\mathrm{TA}}{2\pi v_0}+\frac{2e\rho_0\mathrm{A}k\mathrm{T}}{mv_0}\right)\mathrm{B}, \quad . \quad . \quad (15)$$

which may finally be arranged as

$$\overline{\delta\mathrm{I}_f^2}=\frac{k\mathrm{T}}{2\Phi}\left[1+\left(\frac{\omega}{\omega_p}\right)^2\right]2e\mathrm{I}_0\mathrm{B}, \quad . \quad . \quad . \quad . \quad . \quad (16)$$

noting that I_0 (the d.c. current)$=\rho_0 v_0\mathrm{A}$, and that ω_p, the electron plasma frequency, is given by $\omega_p^2=4\pi e\rho_0/m$.

3.1. *Discussion of Derived Formula* ‡.

In an actual thermionic valve one may expect that the above expression for $\overline{\delta\mathrm{I}_f^2}$ should lead to a lower limit for the average value of current noise which will be observed. Let us consider first a parallel-plane diode at low frequencies (thus $\omega\ll\omega_p$) ; in the strongly space-charge limited condition let us assume Child's Law to hold as a sufficient approximation

$$\mathrm{I}_0=\mathrm{C}\mathrm{V}_a^{3/2},$$

therefore

$$\frac{1}{\mathrm{V}_a}=\frac{2}{3}g_a/\mathrm{I}_0,\quad \left(g_a=\frac{\partial\mathrm{I}_0}{\partial\mathrm{V}_a}\right).$$

---

* The omission in the first integration of a term linear in x corresponds of course to the " removal " of a d.c. potential variation which is irrelevant.

† We are using here the well-known result that for a system in thermal equilibrium characterized by canonical coordinates p_i, q_i, say, the distribution function for these coordinates is given by

$$f(p_i, q_i)\, dp_i\, dq_i \sim \epsilon^{-\mathrm{E}(p_i, q_i)/k\mathrm{T}}\, dp_i\, dq_i.$$

‡ This comparison of our derived formula with particular valve problems is to be considered as essentially heuristic in nature rather than in any way rigorous ; we mention below some aspects which require further careful consideration.

Now eV_a represents the *final* anode energy and it might seem therefore rather more appropriate to insert in (16) some effective average value for Φ. A direct time-average, for example, for Φ yields in fact $\Phi_{\text{eff}}=\frac{1}{5}\Phi$ whence, substituting, we find

$$\overline{\delta I_f^2}=4kTg_a\left(\frac{5}{6}\right)B. \quad . \quad . \quad . \quad . \quad . \quad . \quad . \quad (17)$$

This may be compared with the classical detailed analysis of North *et al.* (1940) and Schottky and Spenke (1937) of the noise in a diode at low frequencies which under extreme space-charge limitation yields

$$\overline{\delta I_f^2}=4kTg_a\left[3\left(1-\frac{\pi}{4}\right)\right]B. \quad . \quad . \quad . \quad . \quad . \quad (18)$$

We might therefore suggest that the diode *under strong space-charge limitation* behaves very much as a current stream in thermal equilibrium. That is, we may consider that the available accelerating energy is used efficiently in a quasi-reversible manner through the medium of the space-charge barrier to maintain the noise at practically its lower thermal level.

Again, the electron-current in a diode under purely retarding-field conditions has its x-component of velocity given everywhere by $\frac{1}{2}m\overline{v_x^2}=kT$, and it seems not unreasonable in this case to define Φ, the effective transport energy, by $\frac{1}{2}m\overline{v_x^2}-kT/2$, $=kT/2$, whence from (16) we have

$$\delta I_f^2=2eI_0B \quad . \quad . \quad . \quad . \quad . \quad . \quad . \quad . \quad (19)$$

in agreement with other approaches to the problem and with experiment (MacDonald and Fürth 1947).

On the other hand, in the case of a *saturated* diode (*i. e.* having a high enough anode voltage to prevent the formation of any potential minimum) where experiment and theory show that $\overline{\delta I_f^2}=2eI_0B$ it is clear from comparison with (16) that the system is then *very far from thermal equilibrium*, as is otherwise quite evident.

The discussion above of the space-charge limited diode suggests that a cylindrical, or, *a fortiori*, a spherical-structure would exhibit lower noise since in that case the final energy is effectively achieved in transit more quickly than in the parallel-plane valve. A detailed analysis by Wainstein (1947) of the cylindrical diode based on the concept of a single-valued velocity-equivalent of the random thermal energy as first introduced by Rack (1938) proposed this and his analysis indicates that for $r_a/r_c\gtrsim 20$, the reduction factor over the parallel-plane diode would be as low as $\sim(0{\cdot}4)^2=0{\cdot}16$. On the other hand, a direct application of our equations (16) and (17) suggests that one might expect a lower limit to be given by

$$\overline{\delta I_f^2}\gtrsim 4kTg_a\left(\frac{1}{6}\right)B. \quad . \quad . \quad . \quad . \quad . \quad . \quad . \quad (20)$$

Turning to the general travelling beam problem without restriction on frequency, it is clear from the first part of this paper that (16) will only be valid up to an (externally "observed") frequency $f=v_0/\lambda_{\min}$, where $\lambda_{\min}$ is

defined by (9*b*). v_0 is given by $\frac{1}{2}mv_0^2=\Phi$ or—more strictly it appears—for a beam originally emitted from a cathode at temp. T, by $\frac{1}{2}mv_0^2=\Phi-k\mathrm{T}/2$.

Thus
$$\frac{\hat{\omega}^2}{\omega_p^2}=\frac{mv_0^2}{k\mathrm{T}},$$

therefore
$$1+\frac{\hat{\omega}^2}{\omega_p^2}=2\Phi,$$

and thus at this frequency limit we have

$$\overline{\delta \mathrm{I}_f^2}=2e\mathrm{I}_0\mathrm{B}, \quad \ldots\ldots\ldots \quad (21)$$

characteristic of a purely random electron flow (pure " shot effect ").

Thus, generally,

$$\left.\begin{aligned}\overline{\delta \mathrm{I}_f^2}&=\frac{k\mathrm{T}}{2\Phi}\left(1+\frac{\omega^2}{\omega_p^2}\right)2e\mathrm{I}_0\mathrm{B} \quad \ldots\ldots \quad (16a)\\ \text{for}\quad &\left[\omega<\sim\sqrt{\left(\frac{4\pi e\rho v_0^2}{k\mathrm{T}}\right)}\right]\\ &=2e\mathrm{I}_0\mathrm{B}\left[\omega>\sim\sqrt{\left(\frac{4\pi e\rho v_0^2}{k\mathrm{T}}\right)}\right]. \quad \ldots \quad (16b)\end{aligned}\right\}$$

The introduction of the limiting frequency and the approximation of spectral variation in (16*a*, *b*) are closely analogous to the limiting frequency involved in the Debye treatment of the specific heat of a crystalline solid.

It is very interesting to notice here also that Pierce, Smullin (1949) and Robinson (1950) have recently derived an expression for the noise current at high frequencies *emerging from an electron gun*, again on the basis of Rack's approximation in combination with a detailed analysis of the gun as a diode at high frequencies (*cf.* Llewellyn and Peterson : 1944).

They find

$$\overline{\delta \mathrm{I}_f^2}=(4-\pi)\left(\frac{\omega^2}{\omega_p^2}\right)\left(\frac{k\mathrm{T}}{2\Phi}\right)2e\mathrm{I}_0\mathrm{B}, \quad \ldots\ldots \quad (22)$$

which may again be compared with our (16).

The analysis and experiment (Cutler and Quate 1949) also indicate that if the beam then drifts freely the noise magnitude will show an oscillatory variation along the drift-space about this value. Ultimately, however, this variation must decay with transit time, τ, due to the thermal velocity spread ; the decay time will be given approximately by $\tau\sim 1/2\pi f\,(k\mathrm{T}/2\Phi)$ (*cf.* MacDonald 1949).

3.2 : *Outstanding Considerations.*

A more precise application of our results to valve structures would require a rather careful consideration of the influence of the boundary conditions at the cathode in terms of the effective degrees of freedom of the system. The situation then is of course very similar to that encountered in a discussion of the thermal energy and specific heat of a crystal,

but in the *latter* cases we are not indeed interested in the actual behaviour in the neighbourhood of the physical boundaries but only in so far as it may affect our specification of the normal modes of vibration. Consequently, an idealized artifice such as Born's "Cyclic crystal" is adequate in that situation. It appears in fact to the writer that if one specifies the current emerging from a thermionic cathode by $I=A\rho v$ then only v may be regarded as an independent degree of freedom, "near" the cathode.

Since also electron beams in practice presumably correspond more nearly to adiabatic than isothermal systems care would also be necessary in ascribing an equilibrium temperature in a particular situation and more work remains to be done on both these aspects of the problem.

Acknowledgments.

I should like to thank Dr. R. Kompfner and Mr. F. N. H. Robinson very sincerely for their continued interest and for stimulating discussions in this work.

References.

Brillouin, L., 1946, *Wave Propagation in Periodic Structures* (New York: McGraw-Hill).
Bohm, D., and Gross, E. P., 1949, *Phys. Rev.*, **75,** 1851.
Cutler, C. C., and Quate, C. F., 1949, *Bell Lab. Memo. MM*-49–160–36 (20/12/49).
Gabor, D., 1950, *A Survey of the Present State of Plasma Oscillations and Electron Interaction* (Imperial College of Science and Technology).
v. Laue, M., 1918, *Jahrb. d. Radioakt. u. Elek.*, **15,** 205.
Llewellyn, F. B., and Peterson, 1944, *Proc. Inst. Rad. Eng.*, **32,** 144.
MacDonald, D. K. C., and Fürth, R., 1947, *Proc. Phys. Soc.*, **59,** 375.
Macdonald, D. K. C., 1949, *Phil. Mag.*, **40,** 561; 1950. *Ibid.*, **41,** 863.
North, D. O., *et al.*, 1940, *R.C.A. Rev.*, **4, 5.**
Rack, A. J., 1938, *Bell Syst. Tech. Journ.*, **17,** 592.
Robinson, F. N. H., 1950, *S.E.R.L. Memo* 23/5/50.
Schottky, W., and Spenke, E., 1937, *Wiss. Veroff a. d. Siem. Werk.*, **16,** 127.
Smullin, L. D., 1949, *M.I.T. Tech. Report* 142 (24/10/49).
Tonks, L., and Langmuir, I., 1929, *Phys. Rev.*, **33,** 195.
Twiss, R. Q., 1950, *Extract Quart. Journ. S.E.R.L.*
Wainstein, L. A., 1947, *Journ. Tech. Phys.* (*U.S.S.R.*), **17,** 1035.

LVI. *The Production of Mesons in Proton–Proton Collisions.*

By J. C. Gunn, E. A. Power and B. F. Touschek,
Department of Natural Philosophy, University of Glasgow*.

[Received February 14, 1951.]

Summary.

A method of estimating the cross-sections for meson production in proton–proton collisions near the threshold is outlined, together with detailed calculations for spin zero meson fields under certain simplifying assumptions concerning the nuclear forces. It is found that, for the final continuous neutron–proton system, a low energy for the neutron–proton relative motion is favoured; this, together with a large contribution from transitions to a final bound deuteron, leads to a meson spectrum well peaked at the highest allowed energies in agreement with recent experiments. While the total cross-section is dependent more on the shape and size of the inter-nucleon potential than on the meson type, the spectrum at a given angle and, more particularly, the angular distribution are critically dependent on the parity of the produced meson. Comparison with experiment favours scalar mesons.

§1. Introduction.

The problem of the production of mesons in nucleon–nucleon collisions has previously received treatment by Heitler (1943–5) and his collaborators, and more recently by Morette (1949) and by Foldy and Marshak (1949). The emphasis of earlier work is on the effect of strong radiation damping of the meson field in reducing the otherwise divergent cross-sections calculated by perturbation theory. In the present paper we do not intend to deal with the case where the nucleon kinetic energies become greater than their rest mass, so that some approximate non-relativistic treatment should be applicable to the nucleon motion. The mesons, however, are given relativistic treatment. Recent measurements by Cartwright *et al.* (1950) and Peterson *et al.* (1950) at 345 MeV. are such as to come within our treatment. It is natural to make the further step of replacing the inter-nucleon interaction by a phenomenological one. In doing so we ignore the fact that nuclear forces are, at least in part, due to π-meson exchange. This approach has already been adopted by Foldy and Marshak, who discuss briefly the errors likely to be introduced as compared with a full field theoretic treatment, such as that of Morette. (These questions have been more fully investigated by one of us (E.A.P.) and will be reported elsewhere.) The advantage of the phenomenological approach is that the internucleon wave functions can then be described with an accuracy

* Communicated by the Authors.

limited only by the inadequacy of existing data on scattering to provide nuclear potentials. These scattering experiments have been very much studied recently, and the analysis of the experimental results by various authors, see for example Jackson and Blatt (1950), has led to several at least qualitative conclusions regarding the internucleon potential.

In the present paper we take as a working assumption that :—

1. The interaction in states of odd parity is so small that it may be neglected. This assumption has been introduced by Serber and is based on the approximate symmetry about 90° of the angular distributions in n–p scattering.

2. The interaction in states of even parity is charge independent and may be best represented by a singular form of potential with a long tail.

No account is taken of tensor forces, or of possible spin orbit forces. Some such addition is clearly necessary to account for the observed p–p scattering and will be considered in later calculations. We further confine attention to the production of positive mesons in proton–proton collisions, limiting ourselves to scalar and pseudo-scalar meson fields.

§2. General Formalism.

The Hamiltonian of the interaction between the nucleon and meson fields will generally be represented by

$$\mathrm{H}' = \int \psi^\dagger(x) \mathrm{Q} \phi(x) \psi(x)\, dx + \text{adjoint}, \quad . \quad . \quad . \quad . \quad . \quad (1)$$

where ψ is the field operator of the nucleons and ϕ the field operator of the mesons. The operator Q differs according to charge and spin dependence of the meson theory. The matrix-elements of the Hamiltonian (1) may be evaluated following a method discussed by Becker and Leibfried (1946), the term appropriate to a transition from an initial state o to a final state f each with A nucleons being

$$\mathrm{H}' = \int dx_1 \ldots \int dx_\mathrm{A} \psi_0^\dagger(x_1 \ldots . x_\mathrm{A}) \left\{ \sum_{i=1}^{\mathrm{A}} (\mathrm{Q}_i \phi(x_i) + \mathrm{Q}_i^\dagger \phi^\dagger(x_i)) \right\} \psi_f(x_1 \ldots x_\mathrm{A}).$$

$$. \quad . \quad . \quad (2)$$

Here ψ_0 and ψ_f are the properly antisymmetrized and normalized wave-functions of the initial and final states of the nucleon system, expressed as functions of the space, spin and charge variables. The term with $\phi^\dagger$ corresponds to the annihilation, the term with ϕ to the creation of a π^+ meson.

Calculations have been carried out in detail for scalar and pseudo-scalar meson fields, using a scalar coupling in the first case and a pseudo-vector coupling in the second. The equivalence theorem shows that, in the approximation used here, pseudo-scalar and pseudo-vector coupling should give identical results in the pseudo-scalar meson theory. With the usual Fourier expansion of the meson field we then find for the matrix-element

describing the emission of a positive π-meson with momentum k and energy ω from a two nucleon system :

$$H'_{0f}=g\sqrt{\frac{2\pi}{\omega}}\int\int d\mathbf{r}_1 d\mathbf{r}_2 \psi_0^\dagger(\mathbf{r}_i,\tau_i,s_i)\left\{\sum_{i=1}^{2} \Pi^{(i)}\beta^{(i)}\exp(i\mathbf{k}\,.\,\mathbf{r}_i)\right\}\psi_f(\mathbf{r}_i,\tau_i,s_i), \quad . \; . \; . \quad (3\,\mathrm{S})$$

for scalar mesons and

$$H'_{0f}=\frac{if}{\mu}\sqrt{\frac{2\pi}{\omega}}\int\int d\mathbf{r}_1 d\mathbf{r}_2 \psi_0^\dagger\left\{\sum_{i=1}^{2} \Pi^{(i)}(\boldsymbol{\sigma}^{(i)}\,.\,\mathbf{k}-\rho_1^{(i)}\omega)\exp(i\mathbf{k}\,.\,\mathbf{r}_i)\right\}\psi_f. \quad . \; . \; . \quad (3\,\mathrm{P})$$

Here and in the following S denotes scalar mesons, P pseudo-scalar ones ; $\beta^{(i)}$, $\boldsymbol{\sigma}^{(i)}$, $\rho_1^{(i)}$, are the usual Dirac matrices applicable to the ith nucleon, $\Pi^{(i)}$ is the charge operator changing nucleon i from a neutron into a proton, τ_i and s_i are the isotopic and spin variables of the ith nucleon, μ is the rest energy of the meson and we work in natural units with $\hbar=c=1$.

The frame of reference will be chosen so that in the initial state the total momentum is zero, *i. e.* if $\mathbf{p}_1$, $\mathbf{p}_2$ denote the momenta of the two nucleons

$$(\mathbf{p}_1)_0=-(\mathbf{p}_2)_0=\mathbf{p}_0.$$

In the final state it follows from the conservation of energy and momentum that

$$(\mathbf{p}_1+\mathbf{p}_2)_f=\mathbf{P}=-\mathbf{k}.$$

The motion of the nucleon mass centre corresponding to $\mathbf{P}$ is fairly slow (*i. e.* non relativistic), so that we may suppose an approximate separation

$$\psi_f(\mathbf{r}_1,\mathbf{r}_2;\; s_i,\tau_i)=\exp(i\mathbf{P}\,.\,\mathbf{R})\,u_f(\mathbf{r},s_i,\tau_i), \quad . \; . \; . \; . \quad (4)$$

where $\mathbf{R}$ is the position of the mass-centre and $\mathbf{r}$ the relative position vector of the two nucleons. The isotopic factor in u_0 and u_f may also be separated out. In the problem considered the initial state contains two protons so that $\psi_0=u_0(\mathbf{r},s_i)\,{}^3(\tau)_1$; the final state may be either the charge singlet ${}^1(\tau)_0$ or charge triplet ${}^3(\tau)_0$ state. Using the properties

$$\Pi^{(1)}\,{}^1(\tau)_0=-\Pi^{(2)}\,{}^1(\tau)_0=-\frac{1}{\sqrt{2}}\,{}^3(\tau)_1,$$

$$\Pi^{(1)}\,{}^3(\tau)_0=\;\;\Pi^{(2)}\,{}^3(\tau)_0=\;\;\frac{1}{\sqrt{2}}\,{}^3(\tau)_1$$

of the change of charge operator Π, one may write for the matrix elements (3)

$$H'_{0f}=g\sqrt{(\pi/\omega)}\int d\mathbf{r} u_0^\dagger(\mathbf{r},s_i)\{\mp\beta^{(1)}\exp(\tfrac{1}{2}i\mathbf{k}\,.\,\mathbf{r})+\beta^{(2)}\exp(-\tfrac{1}{2}i\mathbf{k}\,.\,\mathbf{r})\}u_f(\mathbf{r},s_i) \quad . \; . \; . \quad (5\,\mathrm{S})$$

$$H'_{0f}=if/\mu\sqrt{(\pi/\omega)}\int d\mathbf{r} u_0^\dagger\{\mp(\boldsymbol{\sigma}^{(1)}\,.\,\mathbf{k}-\omega\rho_1^{(1)})\exp(\tfrac{1}{2}i\mathbf{k}\,.\,\mathbf{r}) + (\boldsymbol{\sigma}^{(2)}\,.\,\mathbf{k}-\omega\rho_1^{(2)})\exp(-\tfrac{1}{2}i\mathbf{k}\,.\,\mathbf{r})\}u_f. \quad . \; . \quad (5\,\mathrm{P})$$

In these expressions the alternative $-$ and $+$ signs hold for the final charge singlet and charge triplet states respectively. In accordance with approximate non-relativistic treatment of the nuclear motion the wave-function u_0 and u_f may be reduced to their large components. To the first order in the velocity this corresponds to replacing β and $\boldsymbol{\sigma}$ (which do not mix large and small components) by 1 and the 2×2 $\boldsymbol{\sigma}$-matrices respectively. On the other hand

$$u_0^\dagger \rho_1^{(1)} u_f \simeq i/2\mathrm{M} v_0^\dagger \boldsymbol{\sigma}^{(1)} . (\overleftarrow{\nabla} - \overrightarrow{\nabla}) v_f, \quad \mathrm{M}=\text{nucleon mass},$$

where v_0 and v_f denote the large components of u_0 and u_f and ∇ is the gradient with respect to the relative coordinate $\mathbf{r}$. Introducing these expressions into (5 S) and (5 P) we arrive at the final approximate form for the matrix elements

$$\mathrm{H}'_{0f} = g\sqrt{(\pi/\omega)} \int d\mathbf{r}\, v_0^\dagger \{\mp \exp(\tfrac{1}{2}i\mathbf{k} . \mathbf{r}) + \exp(-\tfrac{1}{2}i\mathbf{k} . \mathbf{r})\} v_f, \quad . \quad (6\,\mathrm{S})$$

$$\mathrm{H}'_{0f} = if/\mu\sqrt{(\pi/\omega)} \int d\mathbf{r}\, v_0^\dagger \{\mp \boldsymbol{\sigma}^{(1)} . [\mathbf{k} - (i\omega/\mathrm{M})\overleftarrow{\nabla}] \exp(\tfrac{1}{2}i\mathbf{k} . \mathbf{r})$$
$$+ \boldsymbol{\sigma}^{(2)} . [\mathbf{k} + (i\omega/\mathrm{M})\overleftarrow{\nabla}] \exp(-\tfrac{1}{2}i\mathbf{k} . \mathbf{r})\} v_f \quad . \quad . \quad . \quad (6\,\mathrm{P})$$

for scalar and pseudo-scalar meson theories. The $-$ and $+$ signs hold for the final charge singlet and triplet states respectively.

The cross-sections for the various processes by which a pair of protons may produce a positive meson must now be evaluated by using equations (6). The chief problem that remains is the selection of suitable wave-functions to describe the motion of the nucleons. In this we shall be guided by the information acquired in the fitting of the deuteron and two body scattering data by internuclear potentials. We shall find that the cross-sections are in fact rather sensitive to the choice of potential.

§ 3. Transitions to the Discrete State.

We first consider the production of a meson when the transition of the nucleons leads to the ground state of the deuteron. Separate consideration must be given to the two possibilities that the protons are initially in the spin triplet or spin singlet states. In the case of an intial spin triplet the wave function v_0 will be of the form

$$v_0 = {}^3(\sigma)_{m_s} v_0(\mathbf{r})$$

so that the matrix element in the pseudo-scalar case becomes

$$\mathrm{H}'_{0f} = if/\mu\sqrt{(\pi/\omega)} \int d\mathbf{r}\, {}^3(\sigma)_{m_s} v_0^* \{-\mathbf{k} . [\boldsymbol{\sigma}^{(1)} \exp(\tfrac{1}{2}i\mathbf{k} . \mathbf{r}) - \boldsymbol{\sigma}^{(2)} \exp(-\tfrac{1}{2}i\mathbf{k} . \mathbf{r})]$$
$$+ i\omega/\mathrm{M}[\boldsymbol{\sigma}^{(1)} . \overleftarrow{\nabla} \exp(\tfrac{1}{2}i\mathbf{k} . \mathbf{r}) + \boldsymbol{\sigma}^{(2)} . \overleftarrow{\nabla} \exp(-\tfrac{1}{2}i\mathbf{k} . \mathbf{r})]\}\, {}^3(\sigma)_{m_s'} v_f.$$

The evaluation of this matrix element will in general require the consideration of integrals such as

$$\int v_0^* \exp(\tfrac{1}{2}i\mathbf{k} . \mathbf{r}) v_f\, d\mathbf{r}, \quad \int \nabla v_0^* \exp(\tfrac{1}{2}i\mathbf{k} . \mathbf{r}) v_f\, d\mathbf{r}, \quad . \quad . \quad . \quad (8)$$

where v_0 and v_f are solutions of Schrödinger-equations, say,

$$\left.\begin{aligned}\nabla^2 v_0+(p_0^2+\mathrm{M}U_0)v_0=0,\\ \nabla^2 v_f+(p_f^2+\mathrm{M}U_f)v_f=0,\end{aligned}\right\}\ \mathrm{M}=\text{nucleon-mass.} \quad . \ . \ . \quad (9)$$

The potential functions U_0 and U_f will in general be different on account of the spin and charge dependence of nuclear forces. We shall, however, always restrict ourselves to central forces of the same range and shape, so that

$$U_0=J_0 w(r) \quad \text{and} \quad U_f=J_f w(r),$$

where the J's are constants of the dimension of an energy and $w(r)$ is a dimensionless function of r depending only on one parameter — the range of the forces.

It can immediately be shown from equation (9) that

$$(p_0^2-p_f^2)\int v_0^* v_f\, d\mathbf{r}=\mathrm{M}\int(U_f-U_0)v_0^* v_f\, d\mathbf{r} \quad . \ . \ . \ . \quad (10)$$

and this identity allows one to restrict the space integration to an interval of the order of the range of the nuclear forces. There is, however, no transformation directly available for the integrals (8). It is here that the assumption of " no interaction " in odd parity states leads to some simplification, for according to this assumption, $U_0=0$ in the initial spin triplet states, and we may write

$$v_0=[\exp(i\mathbf{p}_0\,.\,\mathbf{r})-\exp(-i\mathbf{p}_0\,.\,\mathbf{r})]/\sqrt{2}.$$

The matrix element (7 P) can now be written

$$\mathrm{H}'_{0f}=-if/\mu\sqrt{(\pi/\omega)}\,\langle {}^3\sigma_{m_s}\,|\,\boldsymbol{\sigma}^{(1)}+\boldsymbol{\sigma}^{(2)}\,|\,{}^3\sigma_{m_{s'}}\rangle\,.\,[\mathbf{k}\{\mathrm{I}(\mathbf{p}_0+\tfrac{1}{2}\mathbf{k})-\mathrm{I}(\mathbf{p}_0-\tfrac{1}{2}\mathbf{k})\}$$
$$+(\omega/\mathrm{M})\mathbf{p}_0\{\mathrm{I}(\mathbf{p}_0+\tfrac{1}{2}\mathbf{k})+\mathrm{I}(\mathbf{p}_0-\tfrac{1}{2}\mathbf{k})\}], \quad . \ . \ . \quad (11\,\mathrm{P})$$

where as an abbreviation we have put

$$\mathrm{I}(\mathbf{p}_0)=\int\exp(i\mathbf{p}_0\,.\,\mathbf{r})v_f\, d\mathbf{r}. \quad . \ . \ . \ . \ . \quad (12)$$

If the initial state is a singlet state its parity will be even, so that $U_0\neq 0$ and no simple approximation will be possible to the integrals (8). However, as an estimate of the order of magnitude of the even parity contribution we shall make use of the approximation

$$\mathrm{H}'_{0f}=-\frac{if}{\mu}\sqrt{\left(\frac{2\pi}{\omega}\right)}\frac{(J_f-J_0)}{J_f}\,\langle {}^1(\sigma)_0\,|\,\boldsymbol{\sigma}^{(1)}-\boldsymbol{\sigma}^{(2)}\,|\,{}^3(\sigma)_{m_{s'}}\rangle\,.\,\mathrm{I}(\mathbf{p}_0)\mathbf{k}, \quad . \ . \quad (13)$$

which is equivalent to assuming that of all states with even parity only the 2 proton S-state contributes, and that the momentum of the meson in the integrals (8) can be neglected. The expression (13) can then be expected to give the right order of magnitude and to represent an upper limit in the sense that consideration of the meson momentum will tend to decrease the value of the integrals (8).

For the calculation of the cross-section we need $\Sigma|H'_{0f}|^2$ summed over the final spin states of the deuteron and averaged over the orientations of the original spin. This is now given by

$$\Sigma|H'_{0f}|^2=\frac{\pi f^2}{\mu^2\omega}\left[\left\{\mathbf{k}(I(\mathbf{p}_0+\tfrac{1}{2}\mathbf{k})-I(\mathbf{p}_0-\tfrac{1}{2}\mathbf{k}))+\frac{\omega}{M}\mathbf{p}_0(I(\mathbf{p}_0+\tfrac{1}{2}\mathbf{k})+I(\mathbf{p}_0-\tfrac{1}{2}\mathbf{k}))\right\}^2\right.$$
$$\left.+2k^2I(\mathbf{p}_0)^2\left(\frac{\Delta J}{J}\right)^2\right],$$

where $\Delta J=J_f-J_0$, and we have written J for J_f.

The differential cross-section can be determined from

$$\frac{d\sigma}{d\Omega}=\frac{k\omega}{4\pi^2V}\sum_f|H'_{0f}|^2, \quad \ldots\ldots\ldots \quad (14)$$

where V is the initial relative velocity of the nucleons and $d\Omega$ is the element of solid angle for the meson.

For the evaluation of I some assumption has to be made about the inter-nucleon potential. Present scattering evidence on the whole favours a fairly singular, long tailed potential for which we may use as a simple analytical expression the potential suggested by Hulthén (1942):

$$U(r)=J\exp(-\kappa r)/[1-\exp(-\kappa r)]. \quad \ldots\ldots \quad (15)$$

The normalized wave function of the ground state of the deuteron is then

$$v_f(r)=\sqrt{\left\{\frac{\kappa b(b^2-1)}{8\pi}\right\}}\frac{1}{r}\exp[-\tfrac{1}{2}(b-1)\kappa r][1-\exp(-\kappa r)]$$

with
$$b=MJ/\kappa^2. \quad \ldots\ldots\ldots \quad (16)$$

The depth and range of the potential well must be adjusted so as to fit the deuteron data. We shall use the values

$$1/\kappa=1.17\times10^{-13}\text{ cm.}, \qquad {}^{(3)}J=46.6\text{ MeV.}, \qquad {}^{(1)}J=27.2\text{ MeV.},$$

where $^{(3)}J$ and $^{(1)}J$ refer to the spin triplet and singlet states respectively. The integral I from equation (12) may now be easily evaluated yielding

$$I(\mathbf{p}_0)=\frac{\sqrt{\{2\pi b^3(b^2+1)\kappa^5\}}}{(p_0^2+MW_D)(p_0^2+\left(\frac{b+1}{2}\right)^2\kappa^2)}.$$

In the energy region which we can compare with experiment we find $p_0\simeq400$ MeV. and $k\simeq90$ MeV., and, therefore, in good approximation

$$I(\mathbf{p}_0+\tfrac{1}{2}\mathbf{k})+I(\mathbf{p}_0-\tfrac{1}{2}\mathbf{k})\simeq2I(\mathbf{p}_0),$$
$$I(\mathbf{p}_0+\tfrac{1}{2}\mathbf{k})-I(\mathbf{p}_0-\tfrac{1}{2}\mathbf{k})\simeq-(4k/p_0)\cos\theta\, I(\mathbf{p}_0),$$

where θ is the angle between $\mathbf{k}$ and $\mathbf{p}_0$. This gives finally an approximate expression for the cross-section describing the formation of a deuteron under meson emission

$$\frac{d\sigma}{d\Omega}=\frac{f^2}{V\mu^2}\frac{b^3(b^2-1)}{\left\{1+\frac{(b+1)^2\kappa^2}{4p_0^2}\right\}^2}\frac{k^3\kappa^5}{p_0^8}\left\{\left(\frac{\Delta J}{J}\right)^2+2\left(\frac{\omega p_0}{kM}\right)^2-\frac{8\omega}{M}\cos^2\theta\right\}, \quad (17\text{ P})$$

where f^2 denotes the square of the coupling constant in "ordinary" units. A numerical discussion of this result will be given in § 5.

The corresponding result for scalar meson theory is

$$\frac{d\sigma}{d\Omega} = \frac{12g^2}{V} \frac{b^3(b^2-1)}{\left\{1+\frac{(b+1)^2\kappa^2}{4p_0^2}\right\}^2} \frac{k^3\kappa^5}{p_0^{10}} \cos^2\theta. \quad . \quad . \quad . \quad (17\,S)$$

In this case no nuclear spin changes are allowed owing to the assumed central character of the forces. The only effective initial states, therefore, are triplet states. For the transition to be allowed the mesons must be emitted in states of odd parity. The approximate formula (17 S) represents the emission of a p-wave meson, though some contributions from interference with higher angular momentum waves are included. The cross-section for scalar mesons increases more slowly just above the threshold than that for pseudo-scalar mesons which may be emitted in s-waves. However, with 345 MeV. protons (in the laboratory system) the two cross-sections have become comparable. If $g^2=f^2$ the pseudo-scalar total cross-section is about twice the scalar at this energy. In the forward direction, however, the differential scalar cross-section is larger than the pseudo-scalar one. The angular variation $\cos^2\theta$ of the cross-section for scalar mesons is more in accord with present experimental evidence than that for pseudo-scalar mesons, where interference between s- and d-waves leads to an approximate cancellation in the forward direction.

§ 4. Transitions to Continuous States.

The transitions to the continuous final states of the proton–neutron system can be treated in a manner very similar to that applied in the discrete case. In the energy region considered the relative motion of neutron and proton in the final state is very slow, so that it will be sufficient to deal only with final S-states of the neutron–proton system. For pseudo-scalar mesons the final S-states of the n–p system can be reached either from the odd initial triplet states under emission of an even parity meson, or from the even initial singlet states with emission of an odd parity meson. The ^{1}S final states can only be reached from initial triplet states, the transition $^1\text{S}\rightarrow{}^1\text{S}$ being totally forbidden. The contribution to the total cross-section from transitions to the final nucleon ^{1}S-states will be found to be negligible. For scalar mesons the only allowed transitions are triplet–triplet and singlet–singlet transitions, the latter giving a negligible contribution.

Turning to the detailed treatment of the case of pseudo-scalar mesons we deal first with transitions to the final triplet states. The matrix elements may be calculated as in the previous section. The integrals can be taken over, provided that v_f is normalized so that

$$v_f \sim (1/pr) \sin(pr+\delta) \quad . \quad . \quad . \quad . \quad . \quad . \quad . \quad (18)$$

asymptotically, where p denotes the momentum of relative motion of the nucleons in the final state. In the evaluation of I a transformation of the

type (10) is always made so that only the behaviour of v_f near the origin is important. In this region v_f can be adequately represented by the form of the ground-state solution

$$v_f=(\mathrm{N}/r)\exp\left[-\tfrac{1}{2}(b-1)\kappa r\right]\left[1-\exp\left(-\kappa r\right)\right].$$

The normalization factor N has to be derived from the asymptotic behaviour of the true continuous s-waves in a Hulthen potential. It is then found that

$$\mathrm{N}=\frac{1}{\kappa}\left[\frac{b\pi\sinh 2\pi\alpha}{\alpha\{\cosh 2\pi\alpha-\cos 2\pi\sqrt{(b-\alpha^2)}\}}\right]^{\frac{1}{2}}, \quad . \quad . \quad . \quad (19)$$

where $\alpha=p/\kappa$ and b has been defined in equation (16). In the region of interest we may simply put

$$\mathrm{N}=(b\pi/\kappa p)^{\frac{1}{2}}, \quad . \quad . \quad . \quad . \quad . \quad . \quad . \quad (19^1)$$

and it is then found that

$$\mathrm{I}(\mathbf{q})=\frac{4}{p_0^4}\left(\frac{\pi^3 b^3\kappa^3}{p}\right)^{\frac{1}{2}}\mathrm{F}(\mathbf{q}), \quad . \quad . \quad . \quad . \quad . \quad . \quad (20)$$

where

$$\mathrm{F}(\mathbf{q})=\frac{p_0^4}{(p_0^2-q^2)\left(p_0^2+\dfrac{(b+1)^2\kappa^2}{4}\right)}. \quad . \quad . \quad . \quad . \quad . \quad (20^1)$$

The differential cross-section for a transition to a final ^{3}S state with the production of a meson in the energy interval ω to $\omega+d\omega$ is then given by

$$\frac{d\sigma}{d\omega d\Omega}=\frac{f^2b^3}{\mathrm{V}}\frac{k\mathrm{M}\kappa^3}{\mu^2p_0^8}\Big[\{\mathbf{k}(\mathrm{F}(\mathbf{p}_0-\tfrac{1}{2}\mathbf{k})-\mathrm{F}(\mathbf{p}_0-\tfrac{1}{2}\mathbf{k}))$$
$$+\frac{\omega}{\mathrm{M}}\mathbf{p}_0(\mathrm{F}(\mathbf{p}_0+\tfrac{1}{2}\mathbf{k})+\mathrm{F}(\mathbf{p}_0-\tfrac{1}{2}\mathbf{k}))\}^2+2k^2\left(\frac{\Delta\mathrm{J}}{\mathrm{J}}\right)^2\mathrm{F}(\mathbf{p}_0)^2\Big]. \quad (21\,\mathrm{P})$$

Using the same approximation as in the treatment of the discrete state one obtains

$$\frac{d\sigma}{d\omega d\Omega}=\frac{4f^2}{\mathrm{V}}\frac{b^3}{\left\{1+\dfrac{(b+1)^2\kappa^2}{4p_0^2}\right\}^2}\frac{k\kappa^3\omega}{\mu^2p_0^6}\left\{\frac{\omega}{\mathrm{M}}-4\frac{k^2}{p_0^2}\cos^2\theta+\frac{2k^2\mathrm{M}}{p_0^2\omega}\left(\frac{\Delta\mathrm{J}}{\mathrm{J}}\right)^2\right\}. \quad (22\,\mathrm{P})$$

The result exhibits the same tendency towards cancellation in the forward direction as was found for the cross-section in the discrete case.

Transitions to the final ^{1}S states can be similarly treated. The resulting cross-section, however, as is evident from equation (22 P), is proportional to the cube of the well depth of the final state. This reduces the contributions from singlet transitions by a factor of at least 8 and as a result they may be neglected in calculations of the present approximate character.

In the case of scalar mesons the same method leads to a cross-section

$$\frac{d\sigma}{d\omega d\Omega}=\frac{3g^2}{2\mathrm{V}}\frac{b^3k\kappa^3\mathrm{M}}{p_0^8}\{\mathrm{F}(\mathbf{p}_0+\tfrac{1}{2}\mathbf{k})-\mathrm{F}(\mathbf{p}_0-\tfrac{1}{2}\mathbf{k})\}^2, \quad . \quad . \quad (21\,\mathrm{S})$$

which can be approximated by

$$\frac{d\sigma}{d\omega\, d\Omega} = 24\frac{g^2}{V}\frac{b^3}{\left\{1+\frac{(b+1)^2\kappa^2}{4p_0^2}\right\}^2}\frac{k^3\kappa^3 M}{p_0^{10}}\cos^2\theta. \quad . \quad . \quad (22\,S)$$

§5. Numerical Results.

We have first calculated the variation of the total cross-section for the production of scalar and pseudo-scalar mesons in a transition to the ground-state of the deuteron as a function of the energy of the incident proton in

Fig. 1.

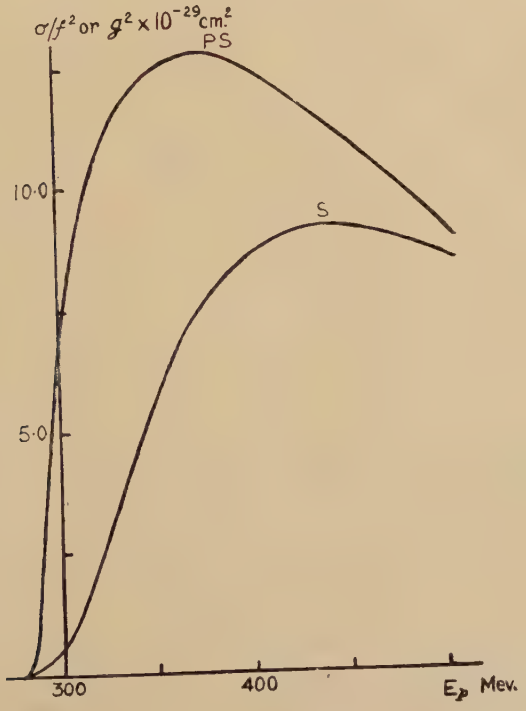

The cross-sections for meson production, scalar and pseudo-scalar, in proton–proton collisions against energies of incident proton, in cases where final nucleons form a bound system.

the laboratory system. The results are shown in fig. 1. Corresponding to the possibility of production of the mesons in an s-state the cross-section for pseudo-scalar mesons is considerably higher near the threshold ($E_p = 290$ MeV.). A maximum is reached at $E_p = 370$ MeV. At $E_p = 350$ MeV., $\sigma_{sc} \simeq 5g^2 \times 10^{-29}$ cm.^{2}, $\sigma_{ps} \simeq 12f^2 \times 10^{-29}$ cm.^{2}. It has already been noted that the results are rather dependent on the internucleon

well shape. For comparison these cross-sections have also been evaluated for a square well potential

$$^{(3)}\mathrm{J}=41 \text{ MeV.}; \quad a=1.85\times10^{-13} \text{ cm.}$$

and yield results smaller by a factor 1/25.

Fig. 2 represents the energy dependence of the integrated total cross-section for transitions to the continuous part of the deuteron spectrum. The result in each case naturally increases more slowly above the threshold than in the discrete case. At $E_p=350$ MeV. approx.—the energy of the Berkeley experiments—σ_{cont} is about half of σ_{disc} for scalar mesons and about $\frac{3}{4}$ for pseudo-scalar mesons. The fall in the continuous cross-section

Fig. 2.

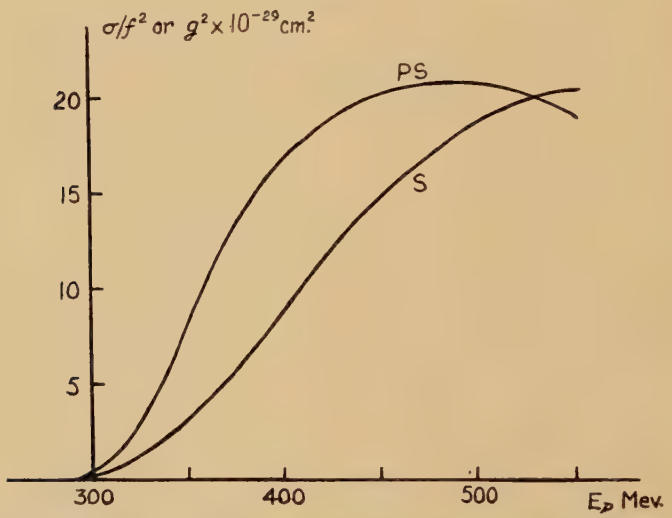

The integrated cross-sections for meson production in proton–proton collisions against energies of incident proton, in cases where final neutron–proton system is in a continuous state.

indicated in fig. 1 should not be taken too seriously. At these energies higher angular momentum contributions as well as higher order corrections to the meson field must be considered. The ratio of the continuous to the discrete cross-section is consistent with experiment for both types of meson.

The transformation to the laboratory system has the effect of throwing more mesons into the forward direction. We shall now denote by k', ω', θ', the momentum, energy and the angle at which the meson is emitted in the centre of mass system and by k, ω and θ, the corresponding quantities in the laboratory system. Taking, for example, the differential cross-section for the production of scalar discrete mesons to be

$$d\sigma/d\Omega'=\mathrm{A}\cos^2\theta'$$

in the centre of mass system, the corresponding cross-section in the laboratory system is

$$d\sigma/d\Omega = A\gamma \frac{k^2}{k'^3} \frac{(k\cos\theta - v\omega)^2}{(k - v\omega\cos\theta)},$$

where v is the relative velocity of the two frames of reference and $\gamma=(1-v^2)^{-\frac{1}{2}}$. The results have been evaluated for incident 350 MeV. protons for the production of both types of mesons. They are shown in fig. 3. The cross-section for scalar mesons is strongly peaked in the forward

Fig. 3.

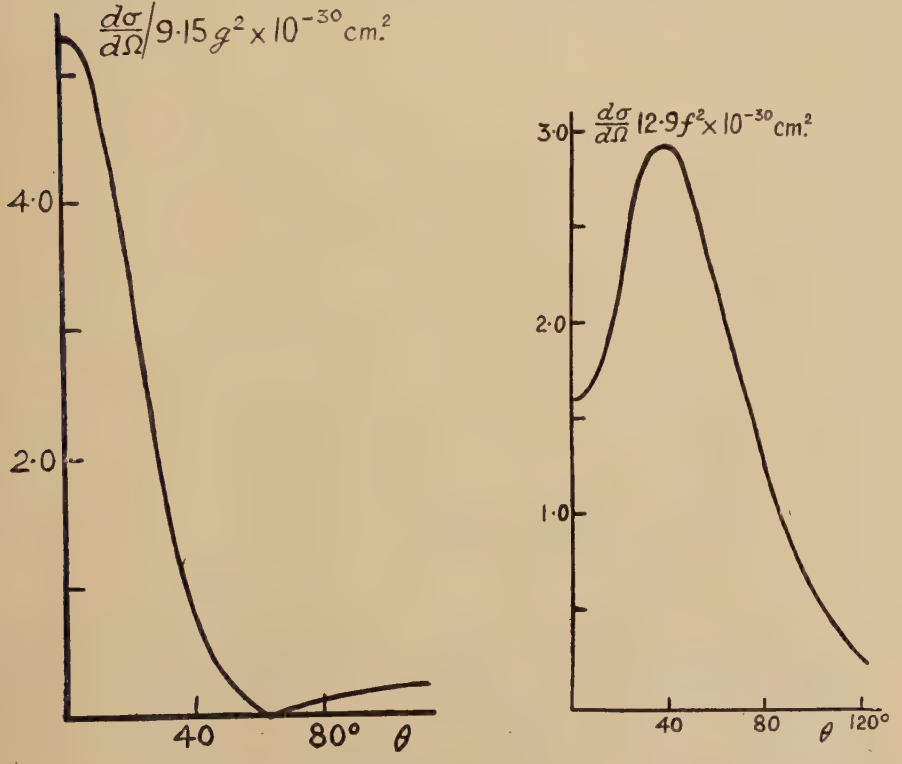

(*a*) Scalar. (*b*) Pseudoscalar.

Variation of the differential cross-section for meson production with the angle of emission of the meson, in laboratory system, is shown for incident 350 MeV. protons and mesons of maximum energy.

direction where it obtains its maximum value of $49g^2\times10^{-30}$ cm.^{2}/sterad. The cancellation in the forward direction for pseudo-scalar mesons is still apparent in the laboratory system. The maximum of the angular distribution of $39\,f^2\times10^{-30}$ cm.^{2}/sterad. is reached at an angle of between 30° and 40°.

The determination of the continuous contributions in the laboratory system is more laborious. In fig. 4 $d\sigma/d\omega d\Omega$ is plotted against the kinetic energy for scalar mesons—assuming a proton energy of 350 MeV. for observations at 0° and 30°. The differential cross-sections are both peaked towards the upper end favouring high meson energies. Integrating over all energies we find at 0°,

$$\frac{d\sigma}{d\Omega} = 32g^2 \times 10^{-30} \text{ cm.}^2\text{/sterad. and at } 30°, \frac{d\sigma}{d\Omega} = 3{\cdot}4g^2 \times 10^{-30} \text{ cm.}^2\text{/sterad.}$$

Fig. 4.

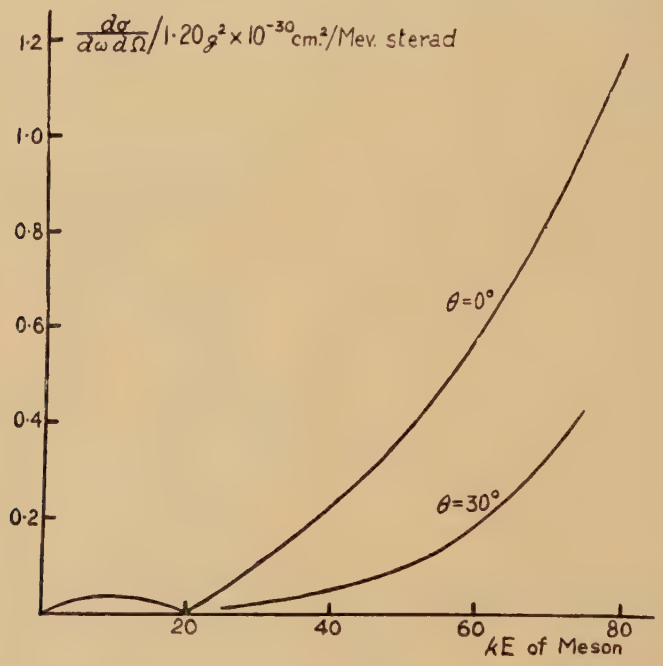

The cross-section per sterad. per unit energy is shown against the kinetic energy of the emitted scalar meson in the forward direction and at 30° to the beam of incident 350 MeV. protons. The differential cross-section in angle falls off rapidly from the forward direction as the results show, *e.g.*

$$\left(\frac{d\sigma}{d\Omega}\right)_{30°} \sim \frac{1}{10}\left(\frac{d\sigma}{d\Omega}\right)_{0°}.$$

The cross-section falls away very rapidly from the forward direction. Pseudo-scalar mesons show a very differently shaped differential cross-section, approximately proportional to $(\omega - \mu)^{\frac{1}{2}}$ so that there is not the same favouring of high meson energies. The approximate integrated contributions to the differential cross-section are for pseudo-scalar mesons

at $\theta = 0$, $\frac{d\sigma}{d\Omega} = 30f^2 \times 10^{-30}$ cm.²/sterad,

$\theta = 30°$, $\frac{d\sigma}{d\Omega} = 20f^2 \times 10^{-30}$ cm.²/sterad.

Recent experiments have all been carried out with 345 MeV. protons and so the correct dependence of the cross-sections on energy cannot yet be discussed. The angular distributions at this energy can, however, be compared with experiment as cross-sections have been reported at angles 0°, 18° and 30° to the beam. Agreement appears possible only with a $\cos^2\theta$ type of distribution at these angles, and so favours scalar rather than pseudo-scalar type mesons. Also the marked peak in the continuous spectrum at high meson energies is predicted by scalar theory.

The forward cross-sections appear to require rather a large coupling constant ($g^2 \simeq 3$, $f^2 \simeq 5$). However these cross-sections are rather susceptible to fine changes in shape and size of the nuclear well. It is perhaps also of interest to note that Brueckner (1950) found $f^2 \simeq 0.2$ to fit the observed meson production by photons (assuming the mesons to be pseudo-scalar).

§6. Conclusions.

It has not been the purpose of this paper to give the most complete description possible of meson production with the use of all the available data on the n–p and p–p interactions. Rather, by means of relatively simple analytical approximations for the potentials, and by using approximate methods, we have shown how important it is, in the low energy region (say up to 500 MeV.), to take accurate account of the nucleon wave functions. In this region indeed allowance for the detailed behaviour of the nucleons is likely to be more important than the inclusion of any field theoretical refinements. Increasingly at higher energies the neglect of higher order reactive terms from the meson field will affect the results and simultaneously the concept of internucleon potential will lose its validity. At the same time multiple meson production will begin affecting the results. We believe, however, that in the low energy region the methods applied in this paper should be expected to give at least qualitatively correct results.

If the use of Serber forces can be regarded as satisfactory then a considerable difference has been established between the behaviour of pseudo-scalar and scalar mesons. The angular distributions are quite different : for scalar mesons the distribution goes with $\cos^2\theta$ in the centre of mass system; for pseudo-scalar mesons the angular distribution though isotropic near the threshold has come nearer to a $\sin^2\theta$ law at the maximum of the total cross-sections. These results can only be fitted to present experimental evidence with the assumption of scalar mesons. It is interesting to compare this conclusion with that suggested by other meson processes. In making this comparison we disregard the information about the meson character which can be obtained from processes in which they are only involved as virtual particles—magnetic moments, nuclear forces, etc. This leaves the evidence from the production of mesons by photons, and from the various capture processes in hydrogen and deuterium. The first of these has recently been considered by Brueckner (1950), and his conclusions are decidedly against scalar mesons. The evidence from the capture processes is perhaps less certain. On the other

hand, we have made no exhaustive effort to discover how, by alteration of the internucleon potential—say by addition of spin orbit forces—the results for the pseudo-scalar meson theory in the present investigation might be affected.

One of us (E.A.P.) is indebted to the Department of Scientific and Industrial Reserach for a Maintenance Allowance during the tenure of which this work was carried out.

References.

Becker, R., and Liebfried, G., 1946, *Phys. Rev.*, **69,** 34.
Brueckner, K. A., 1950, *Phys. Rev.*, **79,** 641.
Cartwright, W. F., Richman, C., Whitehead, M. N., and Wilcox, H. A., 1950 a, *Phys. Rev.*, **78,** 823 ; 1950 b, *Bull. Amer. Phys. Soc.*, **25,** 6, 9.
Foldy, L. L., and Marshak, R. E., 1949, *Phys. Rev.*, **75,** 1493.
Heitler, W., and Peng, H. W., 1943, *Proc. Roy. Irish Acad.*, **49** A, 101.
Heitler, W., 1945, *Proc. Roy. Irish Acad.*, **50** A, 155.
Hulthén, L., 1942, *Arkiv. f. Mat. Ast. och Fysik*, **28** A, 5 ; **29** B, 1.
Jackson, J. D., and Blatt, J. M., 1950, *Rev. Mod. Phys.*, **22,** 77.
Morette, C., 1949, *Phys. Rev.*, **76,** 1432.
Peterson, V., Iloff, E., and Sherman, D., 1950, *Bull. Amer. Phys. Soc.*, **25,** 6, 4.

LVII. *The Energy Loss of Slow Deuterons in Heavy Ice.*

By A. P. French,
Cavendish Laboratory, Cambridge
and
F. G. P. Seidl,
Brookhaven National Laboratory, Upton, Long Island, U.S.A*.

[Received January 16, 1951.]

Abstract.

A review is made of experimental evidence on the energy losses of protons and deuterons in materials of low atomic number, at energies below about 350 keV. The discrepancies between results of different experiments are discussed, and an attempt is made to arrive at a plausible curve of energy loss as a function of energy for deuterons in heavy ice at energies below 700 keV. The region 0–100 keV., which is of considerable interest in the study of the D–D reaction, is given special attention.

§1. Introduction.

In this paper we shall attempt to deduce, from existing experimental evidence, the rate of energy loss of deuterons in a D_2O (heavy ice) target, for the special case of very low bombarding energies (10 to 100 keV.). The determination of this quantity is of obvious importance in obtaining D+D reaction cross-sections from measured values of thick target yields.

There are not, in fact, any published data on energy losses in ice. The nearest approach to what we need is contained in a paper by Crenshaw (1942), who studied the energy loss of deuterons in water vapour. Unfortunately, however, the lowest energy at which he worked was 60 keV.; for information on the rather critical region of lower energies we have to look elsewhere. We propose to review the low-energy data first, obtaining from them a tentative energy-loss curve which can then be compared with Crenshaw's results over the region common to both.

Setting aside Crenshaw's work for the moment, the data most pertinent to our problem are contained in several papers by Gerthsen (1930 a & b) and his collaborators (Eckardt 1930, and Reusse 1932), concerning the energy loss of slow protons in various media (air, hydrogen and celluloid). Their results may be applied in the present case, provided that one makes the following assumptions :—

(*a*) That the rates of energy loss of a proton and a deuteron having the same velocity are identical in any medium.

(*b*) That the atomic stopping powers of H and D are identical.

(*c*) That the molecular stopping power of D_2O can be found by suitably combining the atomic stopping powers of two atoms of D and one atom of O.

* Communicated by the Authors.

(*d*) That the stopping power of D_2O is independent of its physical state.

Although there has been no experimental verification of assumption (*a*) for the very lowest energies, Crenshaw (1942) found it to hold good between 60 keV. and 300 keV. deuteron energy ($\equiv$30 keV. and 150 keV. proton energy) for energy losses in hydrogen. Moreover, it is a general principle that a proton and a deuteron having the same velocity will lose energy through electronic interactions at equal rates, whatever the exact nature of the energy loss process*. We shall therefore take it that this assumption is rigorously justified. In general we shall speak in terms of proton energies ; any relation arrived at will then be true for deuterons of twice the energy.

With regard to (*b*), measurements have been made by Crenshaw (1942) and others (Joos 1942, Jussuf 1942, and Koops 1938) of the relative total amounts of ionization produced by protons and deuterons in hydrogen and deuterium gas. The sum total of the evidence is that a difference of ionizing effects, if it exists at all, is very slight, and becomes noticeable only at very low incident-particle velocities ($\sim 6 \cdot 10^7$cm./sec.) corresponding to 2 keV. protons or 4 keV. deuterons. Thus, for proton or deuteron velocities greater than $6 \cdot 10^7$ cm./sec., one may consider the atomic stopping powers of H and D to be equal.

Assumption (*c*) has purposely been written in a rather vague form. At high energies the suitable combination appears to be simple addition. The molecular stopping power of a chemical compound is equal (to about 2 per cent) to the sum of the atomic stopping powers of its constituent atoms. This result, however, is based upon measurements with alpha particles, and for such energies the difference in stopping power due to differences of chemical binding is expected on theoretical grounds to be less than 1 per cent. (The problem is more fully discussed in a review article by Gray (1944).) The situation is markedly changed at the energies in which we are here interested, and according to Crenshaw's measurements the stopping power of D_2O is significantly less than one would obtain by adding the component atomic stopping powers. We shall defer a full discussion of this matter until later in the paper.

The evidence to support assumption (*d*) is practically non-existent. There are some grounds for believing that the stopping powers of a substance in solid and gaseous forms are equal, but this result again is for alpha particles, for which no significant difference is expected theoretically. (References and discussion may be found in Gray's paper†.) By assuming that the stopping power of heavy ice is equal to that of water vapour we therefore subject ourselves to some uncertainty.

After this general introduction to the problem we will proceed to a survey and analysis of the experiments of Gerthsen, Eckardt and Reusse.

* See, for example, Livingston and Bethe (1937), *Rev. Mod. Phys.*, **9**, 271.

† See also Wilkinson, 1948, *Proc. Camb. Phil. Soc.*, **44**, 114 ; Appleyard, 1949, 1949, *Nature, Lond.*, **163**, 526.

§2. The Energy Loss of Slow Protons in Matter.

The experiments on the loss of energy of protons in matter can be classed into two types, *integral* and *differential*. In the first type of experiment the total range in a gas of a proton of given initial energy is measured. This is the experiment described by Gerthsen (1930 a & b). His results are shown in fig. 1 for the case of protons in air. The ranges R are expressed in cms. of air at 1 mm. pressure Hg, and the proton energies E in keV. Gerthsen found (*cf.* fig. 1) that R as a function of E could be very closely represented by the formula

$$R=\alpha E^{3/4}. \quad . \quad . \quad . \quad . \quad . \quad . \quad . \quad . \quad . \quad (1)$$

We have applied a least-squares analysis to his data and have found that the results are better fitted if the power of E is 0·773 ; this difference,

Fig. 1.

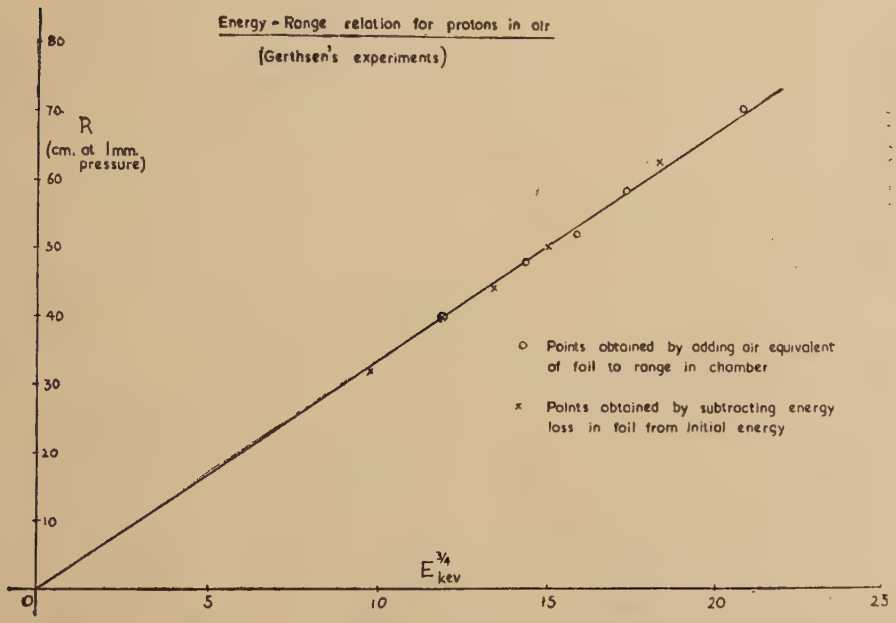

however, is scarcely significant Now the quantity of interest in determining the cross-section for a nuclear reaction is $-dE/dx$, the energy loss per unit distance in the target at a given energy If we accept Gerthsen's formula, we have

$$-\frac{dE}{dx}=\frac{4}{3\alpha}E^{1/4}=\text{const. } v^{1/2}, \quad . \quad . \quad . \quad . \quad . \quad . \quad (2)$$

dE/dx as a function of velocity is plotted in fig. 2.

In the differential experiments the loss of velocity of protons in traversing a very small quantity of matter is directly observed. This is the type of experiment described by Eckardt (1930) and Reusse (1932). A proton beam was passed through celluloid films of various thicknesses Δx. For a given film the energy loss ΔE in passing through it was

measured as a function of the initial energy E. The results are shown in fig. 3. By considering the results for the various films one can find

Fig. 2.

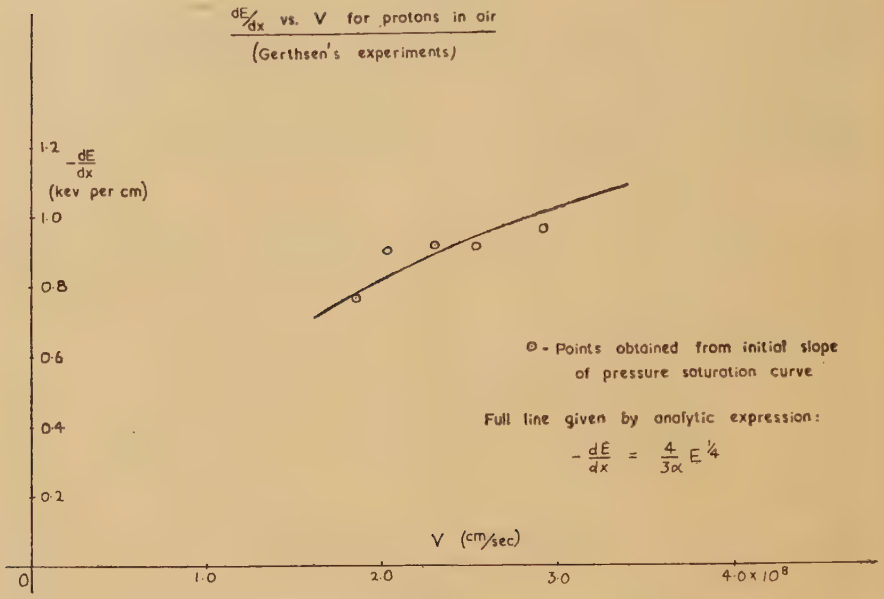

Fig. 3.

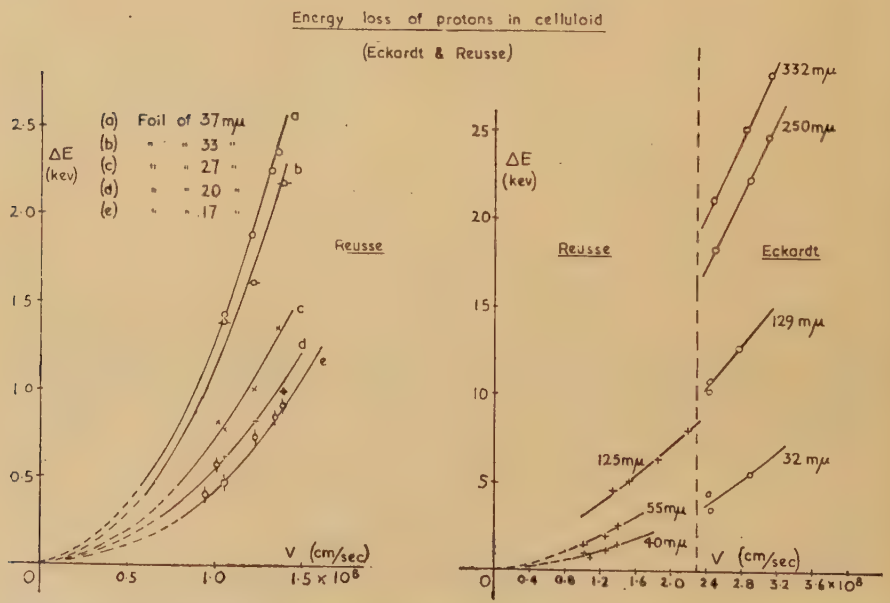

the magnitude of $\Delta E/\Delta x$ as a function of Δx for a given E. The relation between them is found to be linear, of the form

$$-\frac{\Delta E}{\Delta x} = a' - b'\Delta x. \qquad \ldots\ldots\ldots \quad (3)$$

By extrapolating the line to zero film thickness one finds the value of $d\mathrm{E}/dx$ at the initial energy E. By performing this analysis for a series of values of E one can obtain $d\mathrm{E}/dx$ as a function of velocity. We have treated all of the data of Eckardt and Reusse in this way, using least-squares solutions throughout, and find that they are consistent with a relation

$$-\frac{d\mathrm{E}}{dx}=\beta(v-v_0). \quad . \quad . \quad . \quad . \quad . \quad . \quad . \quad . \quad (4)$$

This is plotted in fig. 4.

Fig. 4.

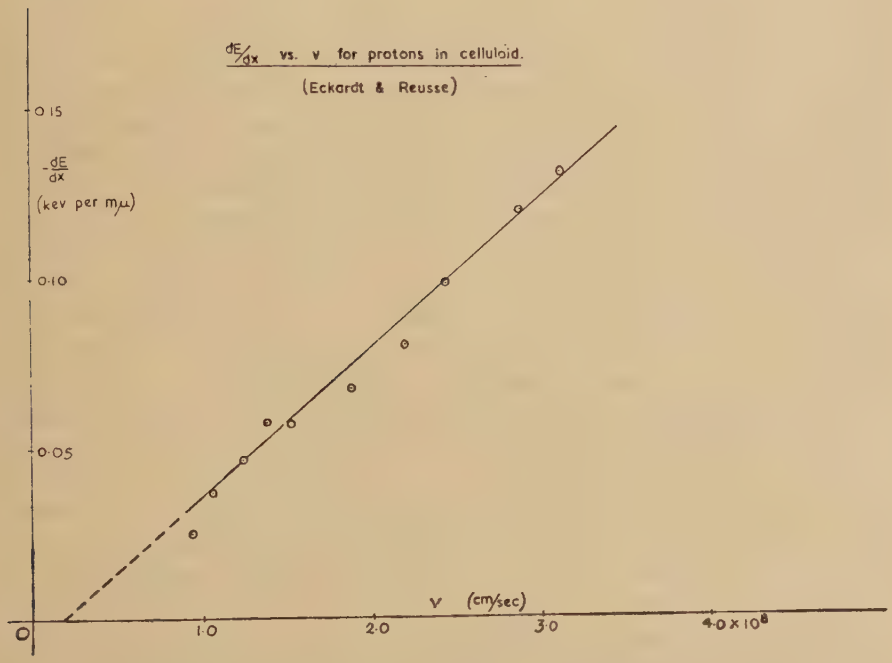

The discrepancy between the results of Gerthsen (equation (2)) and of Eckardt and Reusse (equation (4)) is very striking. From the one experiment one finds that $d\mathrm{E}/dx$ is proportional to the velocity, from the other to its square root. It is true that the values of $\Delta\mathrm{E}/\Delta x$, obtainable from the measurements of Eckardt and Reusse, lead more directly to a value for $d\mathrm{E}/dx$ than do Gerthsen's measurements of total range, but both experiments are open to criticism and merit more detailed consideration.

§3. The Experiment of Gerthsen.

A proton beam generated in a canal-ray tube was magnetically analysed and passed through a thin celluloid window situated at the centre of curvature of a hemispherical ionization chamber. The thickness of the window was 80 mμ (1 mμ = 10^{-6} mm. = 10 A.U.). The ionization chamber could be filled to any desired pressure (up to a few cms. Hg) with air or H_2. The positive ions produced by the protons in traversing the

chamber were collected on an electrode which was made negative with respect to the walls of the chamber. The charge collected in a given time was registered on an electrometer ; a second electrometer recorded the charge carried by the primary beam entering the chamber. The ionization current was found to increase steadily with increasing gas pressure up to a certain critical pressure p_c and thereafter remained constant. At the pressure p_c the protons are just failing to reach the walls of the chamber, so that for this and higher pressures they lose their whole energy in the gas. If the radius of the chamber is ρ the proton range r at unit gas pressure is ρp_c.

Gerthsen's experiment consisted in measuring p_c for air and H_2 for several values of E between 27 and 57 keV. He found that the range in H_2 at all energies was 2·50 times the corresponding range in air, so that the same form of the energy-range relation must hold for protons in air and in H_2. It is necessary to point out that the value of E was measured *before* the protons passed through the celluloid window. Gerthsen assumed that the window was equivalent to the same thickness δ of air at all energies, and calculated δ by considering the celluloid to be composed of hydrogen and " air-like " atoms. In this latter category he placed the C, N and O atoms which comprised 94·4 per cent by weight of the celluloid. δ was then added to each observed value of r to give the total range R. δ was about 10 per cent to 20 per cent of R, so that any error in its value could materially affect the final results.

There exists an additional way of evaluating dE/dx from Gerthsen's experiment, which he himself describes (1930 a). When the pressure in the ionization chamber was very low the ionization current was found to be a linear function of pressure. The slope of the current vs. pressure curve in this region gives directly the number of ion pairs, per mm. pressure of gas in the chamber, produced by the whole proton beam. Since the primary proton beam was simultaneously recorded, it is possible to state the number, n, of ion pairs per cm. of path, in gas at 1 mm. pressure, produced by *one* proton of energy E′, where E′ is the energy of a proton after it has lost energy ΔE in traversing the celluloid foil. With the assumed value of δ, ΔE and thence E′ could be calculated for various values of E.

To translate n into a rate of energy loss it is necessary to know the mean energy, W, required to produce an ion pair in the gas at the energy E′. Gerthsen could not determine W at a single energy, but by dividing the saturation current in the ion chamber by the current of primary protons, he could determine the total number N of ion pairs produced by a single proton of energy E′. The quotient E′/N then gave the average value of W over the energy range zero to E′. This ratio was found to be independent of the value of E′ ; it was therefore assumed that W itself was independent of energy and equal to the constant quotient E′/N. (From our evaluation of the data we find W=38 eV. Gerthsen gives W=35 eV., but we have cause to suspect the values of E on which this is based—see below.)

The rate of energy loss, $-dE'/dx$, of a proton of energy E′ is then given by the product nW (keV. per cm. of path at 1 mm. pressure).

Support for the assumed constancy of W is to be found in a paper of Joos (1942). He quotes an experiment in which the ratio E′/N for protons in H_2 is found constant for energies from 4 to 14 keV.

As Gerthsen has published his results, the values of dE/dx derived by this second method from his one experiment are very different from its values as derived from the first method mentioned earlier (dE/dx appears to be proportional to v, not to $v^{\frac{1}{2}}$ as required by equation (2)). Upon careful re-evaluation of the results we found that his values of ΔE, and hence of E′, were at variance with the integral energy-range relation (equation (1)). That is to say, the curve obtained by plotting $(r+\delta)$ against E does not coincide with the plot of r against $(E-\Delta E)$ if one uses the values of δ and ΔE postulated by Gerthsen. It would appear that the discrepancy may have arisen through numerical errors; in our own treatment of the data we have found that the values for dE/dx are essentially the same by either method of evaluation and satisfy the relation expressed by equation (2). (See fig. 2.) In determining ΔE we took the mean of values obtained by three different methods :—

(1) The method used by Gerthsen (1930 a.) (although our results differ from his and satisfy the integral energy-range relation).

(2) We assume that the loss of velocity, Δv, in the celluloid foil was independent of the energy of incidence E (a result found by Eckardt and Reusse, v. inf.) and accept Gerthsen's value for the air equivalent δ of the foil.

(3) We find directly from the data of Eckardt and Reusse the loss of energy suffered by a proton of various energies, E, in passing through a celluloid foil of 80 mμ thickness.

We consider that this point is sufficiently important to merit setting out the values obtained by the three methods, and this is done in Table I. below. One can see that the degree of concordance is quite satisfactory and gives some meaning to the average values of ΔE given in the last column :

TABLE I.

E keV.	ΔE keV. Method 1	Method 2	Method 3	Average
27·1	6·8	5·9	6·6	6·4
34·6	7·9	6·7	7·7	7·4
39·6	8·1	7·2	8·4	7·9
45	8·0	7·8	8·9	8·2
57	8·3	8·6	10·2	9·0

The outcome of Gerthsen's experiment would from this analysis appear to be that over the range 20 to 60 keV. the rate of energy loss of

protons in air or hydrogen is proportional to the square root of the velocity. The actual magnitude of this loss, in keV. per cm. of path in either gas at 1 mm. pressure, follows directly from the experimental results, and for air is given by

$$-\left(\frac{d\mathrm{E}}{dx}\right)_{\mathrm{air}} = (5{\cdot}90 \pm 0{\cdot}10) \times 10^{-5}\ v^{1/2}\ \text{keV. per cm., with } v \text{ in cm./sec.}$$

§4. The Experiments of Eckardt and Reusse.

A proton beam generated in a canal-ray tube was accelerated through an additional potential drop and was then magnetically analysed. Protons or H_2^+ ions of a specified velocity were thus selected. The range of proton energies covered was from 4 to 50 keV. After passing through a thin celluloid film the protons were subjected to a further magnetic analysis in order to determine their velocity upon emergence. There was of course a spread of energy in the emergent beam, but the velocity at the peak of the distribution was measured as the significant one. The experiment was repeated for celluloid films of various thicknesses (from 20 to 330 mμ).

It may be noted that the celluloid films were extremely thin, the thickest being only about 3000 A.U. Thus it was impossible to measure the thickness directly through the use of interference fringes. The method employed was (*a*) to note the change of interference colour when one of the thin films was placed over a relatively thick film of celluloid, or (*b*) to superpose portions cut from a single large foil until an interference colour was obtained. Unfortunately the account of the procedure as given by Eckardt (1930) is not very detailed, and its accuracy must remain open to question.

The conclusions reached by Eckardt and Reusse are (*a*) that for a given incident velocity, the loss of velocity in passing through a foil is proportional to its thickness, and (*b*) that in passing through a given foil the energy loss is a linear function of the incident velocity v. These results may be expressed by the following equations:

$$-\Delta v = a\,\Delta x, \qquad (5\,a)$$

$$-\Delta \mathrm{E} = bv - c. \qquad (5\,b)$$

It will be noted that equations (5) are not the same as the equations (3) and (4) which we have used in evaluating $d\mathrm{E}/dx$ as a function of velocity The two sets of equations may, however, be readily related. Suppose that the rate of energy loss is given by

$$-\frac{d\mathrm{E}}{dx} = f(v), \qquad (6)$$

i. e. $-m\,v\,dv = f(v)\,dx$, where m=mass of proton.

Then
$$\left.\begin{aligned} \Delta x &= -m\int_v^{v+\Delta v} \frac{v\,dv}{f(v)} = -m\int_v^{v+\Delta v} \phi'(v)\,dv, \quad \text{say,} \\ &= +m[\phi(v) - \phi(v+\Delta v)]. \end{aligned}\right\} \qquad (7)$$

If we accept equation (5*a*), we have

$$\Delta x = -\frac{1}{a}\Delta v, \text{ and hence the identity :}$$

$$-\frac{1}{a}\Delta v \equiv m[\phi(v)-\phi(v+\Delta v)]$$

$$= -m\phi'(v)\Delta v + \ldots$$

Consequently $$\phi(v) = +\frac{1}{am} = +\frac{v}{f(v)} \text{ (from (7))}$$

so that $$-\frac{dE}{dx} = amv, \text{ from (6).} \quad \ldots\ldots\ldots \quad (8)$$

Differentiating (8),

$$-\frac{d^2E}{dx^2} = am\frac{dv}{dx} = -a^2m, \text{ from (5}a\text{).} \quad \ldots\ldots \quad (9)$$

Now we may write $\Delta E \sim \frac{dE}{dx}\Delta x + \frac{1}{2}\frac{d^2E}{dx^2}(\Delta x)^2$, which by (8) and (9) becomes

$$-\frac{\Delta E}{\Delta x} \sim amv - \tfrac{1}{2}a^2m\Delta x$$

or $$-\frac{\Delta E}{\Delta x} = \alpha_1 v - \alpha_2 \Delta x, \quad \ldots\ldots\ldots \quad (10)$$

where $\alpha_1 v = -\frac{dE}{dx}$, and α_1 and α_2 are constants.

Equation (10) may be seen at once to express the results of both equation (3) and equation (5*b*)—to the former when v is fixed and Δx varies, to the latter when Δx is fixed and v varies.

The following table sets out some values of $\alpha_1 v (= -dE/dx)$, $\alpha_1 v/E^{1/2}$ and α_2 as we have calculated them by a least-squares analysis of the experimental data of Eckardt and Reusse:

TABLE II.

E keV.	$\alpha_1 v$ keV/$m\mu$ of celluloid	$\alpha_1 v/E^{1/2}$	α_2
5·8	0·0395 ± 0·0062	0·0164 ± 0·0026	0·00018 ± 0·00008
10·2	0·0621 ± 0·0040	0·0195 ± 0·0013	0·00019 ± 0·00003
31	0·0890 ± 0·0059	0·0160 ± 0·0011	0·00009 ± 0·00001
44	0·1313 ± 0·0061	0·0198 ± 0·0009	0·00017 ± 0·00001

The fact that α_1 and α_2 are essentially independent of velocity may readily been seen. However, the value of $(\alpha_1^2 v^2)/(\alpha_2 E)$, which should be 4 (*cf.* equations (10)), is found from Table II. to be 2·4 ± 0·6 (approx.).

In comparing equation (8) with equation (4) we see that they are in agreement only if v_0 is set equal to zero. The discrepancy probably arises because we have made a more careful analysis of the data, using least-squares solutions throughout, than did Eckardt and Reusse. In this analysis the parameter v_0 appeared, but it is doubtful that the experiments in themselves are accurate enough to give v_0 any significance. In any case it is clear that the energy loss cannot cease at and below v_0, as equation (4) would demand (v_0 corresponds to about 0·2 keV. proton energy).

The result of the experiments of Eckardt and Reusse is, therefore, that for protons traversing celluloid the rate of energy loss, $-dE/dx$, is a linear function of velocity. The quantitative expression of this relation is

$$-\left(\frac{dE}{dx}\right)_{\text{celluloid}} = (4{\cdot}45 \pm 0{\cdot}11) \times 10^{-2}(v \times 10^{-8} - 0{\cdot}18) \text{ keV. per m}\mu \text{ with } v \text{ in cm./sec.}$$

The result is of use to our problem only if we can derive from it the absolute value of the rate of energy loss in air or in hydrogen, and thus, using our initial assumptions, find the energy loss in a layer of ice. It is important to attempt this conversion, since the celluloid measurements extend to much lower energies (4 keV.) than do the measurements on air and H_2. We will therefore consider this matter in the next section.

§ 5. Conversion of Celluloid Data to Air.

To convert $(dE/dx)_{\text{celluloid}}$ into $(dE/dx)_{\text{air}}$ two alternative methods are possible. The first method is briefly as follows: over the small range of velocities covered by Gerthsen, the plot of (dE/dx) vs. v (fig. 2) does not depart by more than about ± 10 per cent from the linear relation expressed by equation (4). If, therefore, one draws a straight line through these points, with an intercept at v_0 on the v axis, its slope is not likely to be in error by more than about ± 10 per cent. By comparing this slope with the slope of the corresponding line for the energy loss in celluloid (*cf.* fig. 4), one finds the number of cms. of air at 1 mm. pressure which are equivalent to 1 mμ of celluloid. The result of this comparison is

$$-\left(\frac{dE}{dx}\right)_{\text{air}} = (0{\cdot}40 \pm 0{\cdot}04)(v \times 10^{-8} - 0{\cdot}18), \quad . \; . \; . \quad (11)$$

where v is in cm./sec. and (dE/dx) air is in keV. per cm. of air at 1 mm. pressure.

The second method is to assume, with Gerthsen, that celluloid may be considered as a combination of air and hydrogen. That is

$$\left(\frac{dE}{dx}\right)_{\text{celluloid}} = A\left(\frac{dE}{dx}\right)_{\text{air}} + B\left(\frac{dE}{dx}\right)_{H_2}$$

$$= (A + 0{\cdot}4B) \cdot \left(\frac{dE}{dx}\right)_{\text{air}}.$$

The constants A and B may be evaluated from the composition and density of celluloid. For the density, which is not stated by Eckardt and Reusse, we have assumed a value of 1·48 gm./cm.^{3}, which lies midway between the accepted limits of 1·35 and 1·60. We thus subject ourselves to a possible error of ± 10 per cent. Our estimate of $(dE/dx)_{air}$ by this means is

$$-\left(\frac{dE}{dx}\right)_{air} = (0{\cdot}37 \pm 0{\cdot}04)(v \times 10^{-8} - 0{\cdot}18). \quad . \quad . \quad . \quad (12)$$

The striking agreement between (11) and (12) is heartening but probably fortuitous. We shall average them and so obtain, as the final outcome of the experiments of Eckardt and Reusse, the following relation for energy losses of protons in air between 4 and 50 keV. :

$$-\left(\frac{dE}{dx}\right)_{air} = (0{\cdot}385 \pm 0{\cdot}04)(v \times 10^{-8} - 0{\cdot}18) \text{ keV. per cm. at 1 mm.}$$

We have now arrived at two expressions for the energy loss of protons in air, one from Gerthsen's experiments (formula in § 3) and the other from Eckardt and Reusse, above. Before converting these into energy losses in D_2O, we will discuss Crenshaw's work, on which the conversion will largely depend.

§ 6. The Experiments of Crenshaw.

We have already made several references to Crenshaw's paper, which describes a very useful study of the energy losses of hydrogen ions in air, H_2 and D_2, He and water vapour.

A resolved beam from a Cockcroft–Walton accelerator was passed through a series of small diaphragms into a chamber which could be filled to a few mm. pressure with a gas without impairing the vacuum in the acceleration tube. After traversing the chamber the beam passed once more into high vacuum through a second series of diaphragms. It was then bent by a magnet, and fell upon a fluorescent screen. The shift of the beam spot caused by the admission of gas to the retarding chamber was compensated by altering the magnetic field. Pairs of values of magnetic field with and without gas in the chamber were obtained for numerous values of initial beam energy, mostly between 60 and 340 keV. The initial energy was measured with a carefully calibrated resistance voltmeter. The energy loss was found from the change of magnetic field, this latter being itself calibrated in terms of the resistance voltmeter. The experiment was performed for several values of pressure in the retarding chamber, and was thus precisely analogous to the differential measurements on celluloid. The initial slope of a curve of ΔE vs. Δp led to the value of (dE/dx). End effects in the retarding chamber, due to pressure gradients in the diaphragm systems, were eliminated by changing the distance between the entrance and exit systems.

The point most carefully studied in these experiments was the identity of energy losses by protons and deuterons in H_2 and D_2. Some earlier work by Crenshaw and others (1942) had indicated a difference of energy losses in H_2 and D_2, but this was not substantiated. Within the spread of the measurements (about ± 10 per cent at the highest energies and ± 5 per cent at the lowest) all four rates of energy loss were found to be equal for a given proton or deuteron velocity. After this had been established, further measurements on the energy losses of protons in

Fig. 5.

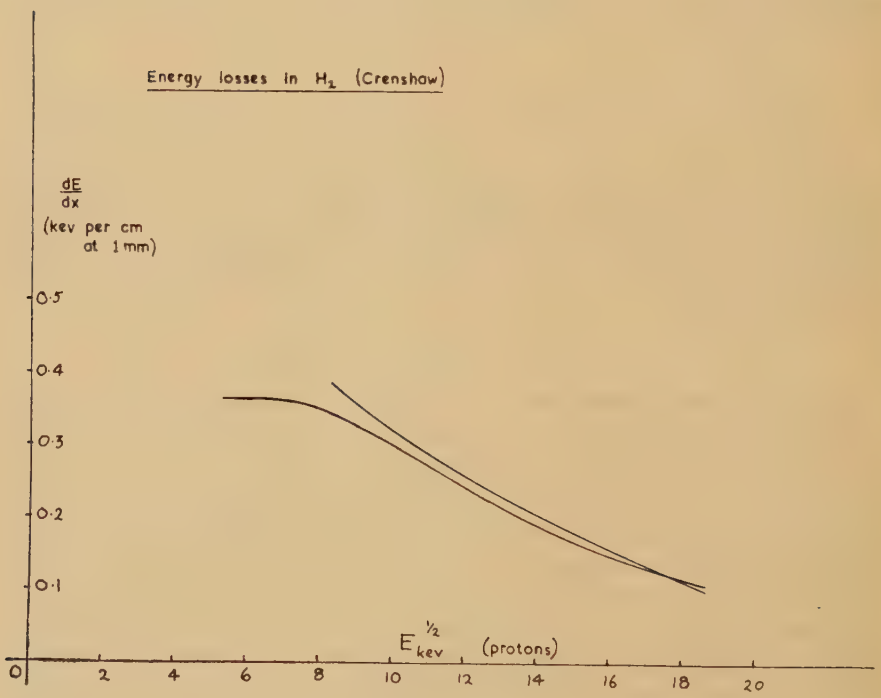

H_2 and D_2 were carried out. The results of these two investigations are shown graphically in fig. 5. For convenience, $\sqrt{E}$ is used as abscissa, and (dE/dx) is given in keV. per cm. at 1 mm. pressure.

The other aspect of Crenshaw's work which interests us here is his study of the stopping powers of hydrogen and water vapour relative to air. In fig. 6 we have plotted the stopping power of hydrogen relative to air over the range 40 keV. to 5 MeV. proton energy. In this graph the results of Gerthsen, Crenshaw and Bethe* are combined. It may be seen that a good smooth curve can be drawn through them, so that the ratio S.P.(H_2)/S.P.(air) is well defined at all energies. We propose to

* Livingston and Bethe, 1937, *Rev. Mod. Phys.*, **9**, 272.

use this curve to obtain S.P.(D_2O)/S.P.(H_2), and hence the energy loss in ice, in the following manner :

(1) We read off values of S.P.(H_2)/S.P. (air) for various energies.

(2) We compute S.P.(H_2O)/S.P. (air) from the relation

$$\frac{\text{S.P.}(H_2O)}{\text{S.P. (air)}} = \frac{\text{S.P. }(H_2)}{\text{S.P. (air)}} + \frac{1}{2}\frac{\text{S.P. }(O_2)}{\text{S.P. (air)}}$$

$$= \frac{\text{S.P. }(H_2)}{\text{S.P. (air)}} + 0{\cdot}535.$$

Fig. 6.

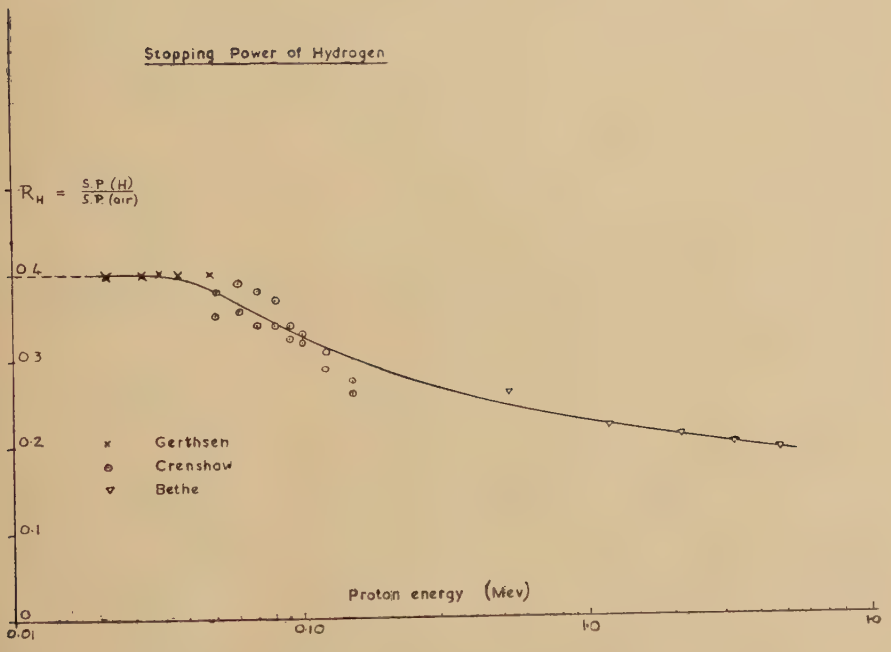

The figure 0·535 for oxygen is valid for alpha-particles near the end of their range *, and cannot be very seriously in error at lower energies. The smooth curve resulting from this is shown as A in fig. 7.

(3) We plot Crenshaw's own values of S.P.(H_2O)/S.P.(air) also in fig. 7, and draw through them a line (B) parallel to the curve A of (2) above. This we take to be the true representation of S.P.(D_2O)/S.P.(air). We consider this procedure is preferable to using Crenshaw's individual values of S.P.(H_2O)/S.P.(air) as they stand, because it takes into account the probable trend of the stopping power with energy. With this curve we can now convert the results of Gerthsen, Eckardt and Reusse into energy losses in D_2O. (We may comment, parenthetically, that Crenshaw's

* Rutherford, Chadwick and Ellis, 1930, *Radiations from Radioactive Substances* (Cambridge: University Press), p. 97.

Fig. 7.

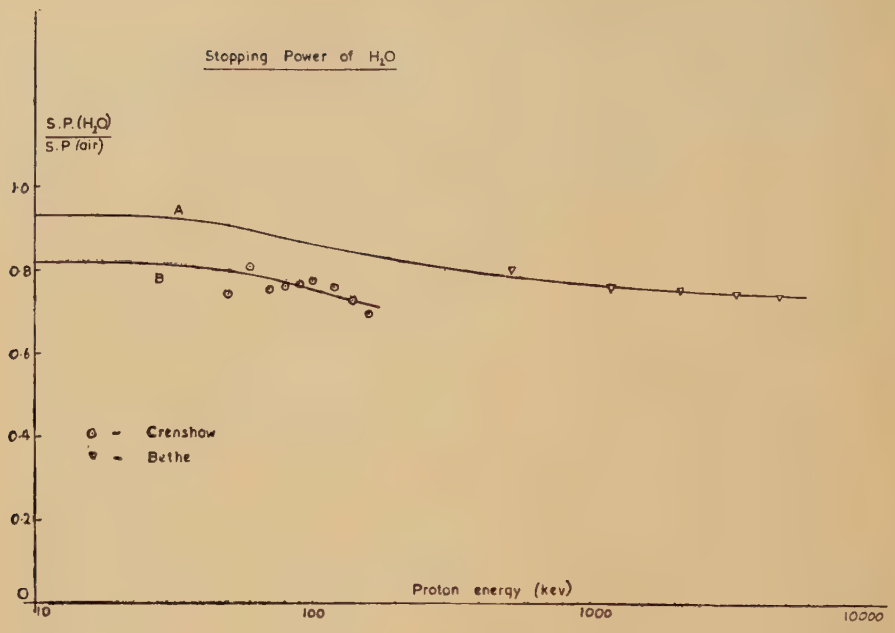
Stopping Power of H_2O
$\frac{S.P.(H_2O)}{S.P.(air)}$
1·0
0·8
0·6
0·4
0·2
0
A
B
o - Crenshow
▽ - Bethe
Proton energy (kev)
10
100
1000
10000

Fig. 8.

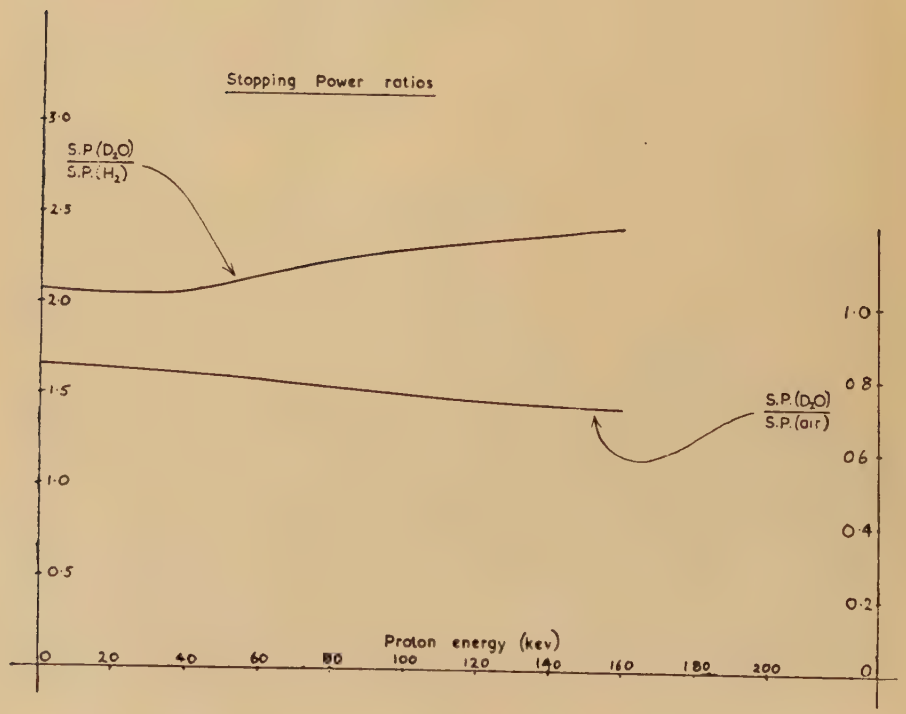
Stopping Power ratios
3·0
$\frac{S.P.(D_2O)}{S.P.(H_2)}$
2·5
2·0
1·5
1·0
0·5
$\frac{S.P.(D_2O)}{S.P.(air)}$
1·0
0·8
0·6
0·4
0·2
0
Proton energy (kev)
0
20
40
60
80
100
120
140
160
180
200

values of the stopping power of D_2O do seem surprisingly low, and cannot readily be joined to the computed curve at high energies. This, however, does not entitle us to ignore his results.)

(4) Using the curve of fig. 6 and curve B of fig. 7, we find the ratio

$$\frac{\text{S.P.}(D_2O)/\text{S.P.(air)}}{\text{S.P.}(H_2)/\text{S.P.(air)}} = \text{S.P.}(D_2O)/\text{S.P.}(H_2).$$

The resulting curve is shown in fig. 8. For completeness our final curve of S.P.(D_2O)/S.P.(air) is also shown on this same graph.

(5) With the aid of our curve from (4), we can now convert Crenshaw's values (fig. 5) of energy losses in hydrogen into energy losses in D_2O.

The above procedure may seem unduly elaborate, but we consider that it extracts a maximum of significant data from Crenshaw's results. To use the measurements on water vapour alone would be to discard the largest and most carefully conducted section of his work.

§7. The Energy Loss in Ice.

We now have five sets of measurements which we can adapt to our needs in obtaining a final version of the energy loss curve. They are :

1. Gerthsen	Protons in air. 20 to 60 keV.
2. Eckardt and Reusse	Protons in celluloid. 4 to 50 keV.
3. Crenshaw	Protons and deuterons in H_2 and D_2. (Equivalent proton energy : 30 to 340 keV.)
4. Crenshaw	Protons in H_2 and D_2. 60 to 340 keV.
5. Crenshaw.	Deuterons in H_2O. (Equivalent proton energy : 50 to 170 keV.)

Using the results of the previous section, we have converted the first four into energy losses in D_2O vapour. The fifth is brought into line by plotting the points as though they were obtained for protons of half the energy. Fig. 9 shows the collected values, as usual in keV. per cm. path at 1 mm. pressure. The broken line is our attempt to integrate the various data into a single curve for the energy loss of protons from zero energy up to 340 keV. The maximum deviation from any of the parent curves may be seen to be about 10 per cent, which we regard as tolerably satisfactory in view of the numerous assumptions that have gone into the analysis.

It remains only to make the final conversion into energy losses in ice, on the basis of our initial assumption (*d*) (§ 1). This we have done, with the supposition that both Gerthsen and Crenshaw conducted their experiments at a laboratory temperature of about 15° C. Under these conditions, one cm.^{3} of D_2O vapour weighs 1·11 micrograms. Table III. below lists the values of (dE/dm) in keV. per microgram at representative points over the whole range of energies covered in this review. Fig. 10 presents the results as a smooth curve over the limited range 10–120 keV. deuteron energy. (Note that Table III. goes up to 700 keV. equivalent deuteron energy.)

Fig. 9.

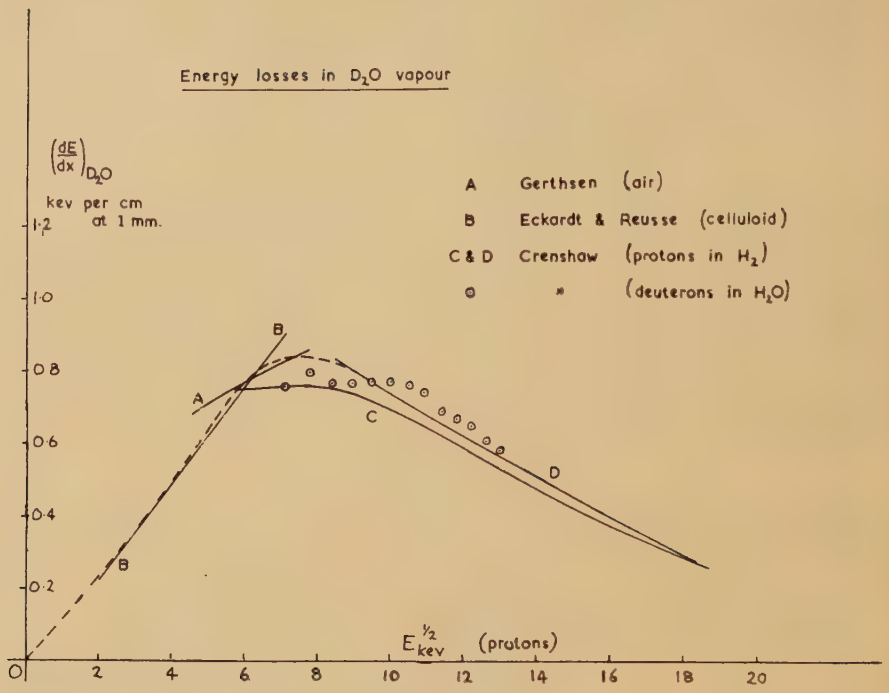
Energy losses in D_2O vapour
$\left(\frac{dE}{dx}\right)_{D_2O}$
kev per cm at 1 mm.
A Gerthsen (air)
B Eckardt & Reusse (celluloid)
C & D Crenshaw (protons in H_2)
o " (deuterons in H_2O)
1·2
1·0
0·8
0·6
0·4
0·2
O
2
4
6
8
10
12
14
16
18
20
$E^{1/2}_{kev}$ (protons)

Fig. 10.

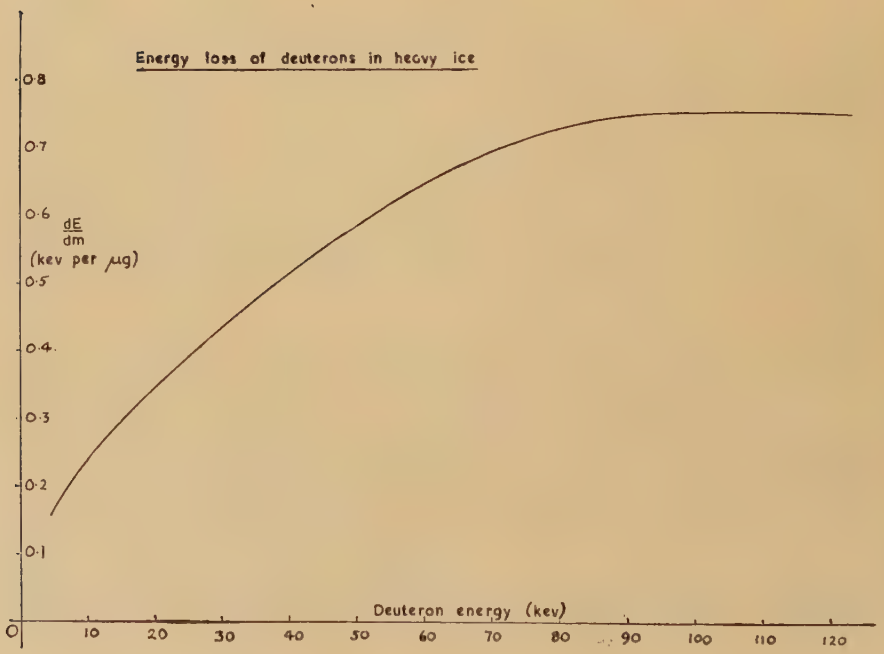
Energy loss of deuterons in heavy ice
$\frac{dE}{dm}$ (kev per μg)
0·8
0·7
0·6
0·5
0·4
0·3
0·2
0·1
O
10
20
30
40
50
60
70
80
90
100
110
120
Deuteron energy (kev)

§8. Concluding Remarks.

Of the probable accuracy of the results given in Table III. we can say little. One might hope, taking an optimistic view, that they were good to ±10 per cent, but we are after all confronted with complete uncertainty concerning the relative stopping powers of water vapour and ice. It is therefore of interest to mention a somewhat different approach to the problem.

The analysis presented in this paper was undertaken in order to deduce the cross-section of the D(d, p) reaction, as a function of deuteron energy E, from measured values of thick target yields N(E). In the original account (Bretscher and the authors 1948) of the experiments, values of both yields and cross-sections are given. The former are considered to be fairly accurate, but the latter were, by an oversight, obtained without reference to Crenshaw's work on energy losses, and the present analysis should lead to more significant values of cross-sections.

Table III.

$\sqrt{E_p}$	E_p keV.	(dE/dm) keV./μg	$\sqrt{E_p}$	E_p keV.	(dE/dm) keV./μg
2	4	0·211	11	121	0·608
3	9	0·325	12	144	0·556
4	16	0·451	13	169	0·506
5	25	0·580	14	196	0·455
6	36	0·700	15	225	0·407
7	49	0·753	16	256	0·356
8	64	0·748	17	289	0·300
9	81	0·712	18	324	0·262
10	100	0·660	18·7	350	0·230

This view has recently acquired support through the publication of results by Sanders, Moffatt and Roaf (1950). These workers obtained the D+D cross-section at a given energy directly by employing thin targets. Thus one can in fact use their values of cross-section, combined with values of dN/dE from Bretscher, French and Seidl (1948) to *deduce* values of dE/dx. If we do this, we find almost perfect agreement with the curve of fig. 10 at the lowest energy, and a maximum divergence of about 15–20 per cent at the highest energy for which a comparison is possible. (The values of Table III. rise more steeply than they should in this region). Unfortunately the measurements of Sanders *et al.* do not go to a high enough energy to permit a comparison over the whole range of Table III., but the extent of agreement where the comparison is possible conforms rather well to the estimated accuracy of our values of dE/dx.

When more complete data on thin target yields are available, these can clearly be used to establish a more reliable energy-loss curve than that of fig. 10. In the meantime, however, it is hoped that our present range-energy relation may be of value. It should also be applicable to tritons in D_2O, subject to our initial assumption (*a*) that hydrogen nuclei with equal velocities lose energy at equal rates.

References.

Bretscher, French and Seidl, 1948, *Phys. Rev.*, **73,** 815.
Crenshaw, 1942, *Phys. Rev.*, **62,** 54.
Crenshaw, Young and Manning, 1942, *Phys. Rev.*, **61,** 388.
Eckardt, 1930, *Ann. d. Phys., Lpz.*, **5,** 401.
Gerthsen, 1930 a, *Ann. d. Phys.* (*Lpz.*), **5,** 657 ; 1930 b, *Phys. Zeits.*, **31,** 948.
Gray, 1944, *Proc. Camb. Phil. Soc.*, **40,** 72.
Joos, 1942, *Ann. d. Phys.* (*Lpz.*), **41,** 426.
Jussuf, 1942, *Ann. d. Phys.* (*Lpz.*), **41,** 435.
Koops, 1938, *Ann. d. Phys.* (*Lpz.*), **33,** 57.
Reusse, 1932, *Ann. d. Phys.* (*Lpz.*), **15,** 256.
Sanders, Moffatt and Roaf, 1950 a, *Bull. Am. Phys. Soc.* ; 1950 b, *Phys Rev.*, **77,** 754.

LVIII. *The Photodisintegration of the Deuteron.*

By W. M. Gibson,
H. H. Wills Physical Laboratory, University of Bristol
and
T. Grotdal, J. J. Orlin and B. Trumpy,
Fysisk Institutt, University of Bergen*.

[Received March 16, 1951.]

Summary.

The photodisintegration of the deuteron has been observed in photographic plates exposed, while wet with heavy water, to the γ-rays arising from the bombardment of fluorine with 1·4 MeV. protons. Two groups of protons, produced by the known γ-ray lines at 6·15 MeV. and 7·01 MeV., have been clearly resolved. It is shown that γ-ray energies of this order of magnitude can be measured with a probable error of 0·05 MeV., and γ-ray lines with an energy difference of 0·6 MeV. can be resolved. Suggestions are made for a further improvement of the technique which should increase the resolving power of the method.

The angular distribution of the protons produced by each of the two γ-ray lines has been measured, but statistical uncertainties must be further reduced before any useful comparison with theory can be made.

§1. Introduction.

The photo-disintegration of the deuteron into a neutron and a proton, one of the simplest of nuclear processes, has been the subject of many experimental and theoretical investigations. The importance of the study lies, first, in the fact that any theory must be able to give a detailed account of the cross section and angular distribution of the products of the interaction for photons of different quantum energy, and accurate observations of these characteristics should provide a stringent test of the validity of different theories; and, second, because the process makes it possible to determine γ-ray energies and thus provides a method for the investigation of γ-ray spectra.

At first sight it would appear that the reaction is particularly susceptible to detailed and accurate investigation. The absorption of the γ-ray leads to the production of only two product particles, a neutron and proton, which recoil from one another. Suppose the quantum energy and the direction of motion of the γ-ray to be known: its momentum is then defined, and the observation of the velocity of the recoiling proton is sufficient for the complete solution of the dynamics of the disintegration.

* Communicated by Professor C. F. Powell, F.R.S.

In practice, however, it has proved to be very difficult to make observations of sufficient precision. This is largely due to the very low cross section for the reaction, which is of the order of 10^{-27} cm.^{2} for γ-rays of energy less than 20 MeV. As a result, competing nuclear processes can give rise, in some of the experimental conditions employed, to large numbers of protons which may be confused with those due to the disintegration of the deuteron ; and in other experiments the proton tracks have to be distinguished against a dense background of electrons produced by Compton recoil or pair production.

In spite of these difficulties, the cross-section has been recently measured with a sufficient accuracy to provide a test of the validity of the various theories. Measurements have been made at quantum energies up to 2·76 MeV. by Bishop, Collie *et al.* (1950), and at a series of energies, ranging from 4·45 MeV. to 17·6 MeV. (2·2 MeV. to 15·4 MeV. above the threshold), by Wilkinson (1950). Theoretical calculations for these and higher eneriges have been made by Hansson and Hulthen (1949) and by Marshall and Guth (1949).

Information about the angular distribution of the emitted protons is, however, very limited. Rough determinations, at a number of energies, have shown that there are no serious divergences from the predictions of the various theories, but the observations are not sufficiently precise to provide a crucial test. For such experiments Phillips, Lawson and Kruger (1950) have employed a Wilson chamber containing heavy methane, CD_4, whilst other observers have detected the disintegration protons, emitted from solid or gaseous targets containing deuterium, by observing their tracks in neighbouring photographic plates. Most observations, however, have been made with the "target" deuterium atoms incorporated in sensitive photographic emulsions, a method first suggested by Powell (1940).

The use of emulsions "loaded" with deuterium has the advantage that, as in similar experiments with a Wilson chamber, the point of origin of a proton track can usually be accurately determined. Its length can therefore be measured with precision, and the inaccuracies which arise in experiments where the protons originate in a separate target of finite thickness can be eliminated. Further, the photographic method has an advantage over the expansion chamber, for these particular experiments, in being continuously sensitive. Whilst there are difficulties in applying the method to determinations of the absolute values of the cross-section for the reaction, it is well suited for making studies of the angular distributions.

In applying the photographic method to the present problem, the most important technical difficulty to be overcome is that of incorporating the deuterium in the plates in sufficient concentration and in the form of a suitable chemical compound. The maximum γ-ray flux which can be allowed to pass through the plate is limited by the maximum background fog, due to secondary electrons, which can be tolerated if the proton

tracks are to be distinguished. With this flux, and if the deuterium content of the plate is low, the number of disintegration protons per unit area is small and the work of searching the plate arduous. On the other hand, if the amount of loading material is large, there is a reduction in the quality of the proton tracks which leads to a reduction in the precision of the measurements of range ; and the inaccuracies are accentuated by the increase in the shrinkage factor of the emulsion, which leads to larger errors in the determination of the angles of dip of tracks.

Several methods of "loading" an emulsion with deuterium have been employed : Gibson, Green and Livesey (1947) described experiments in which calcium nitrate, with about 6 per cent by weight of heavy water of crystallization, was incorporated in the emulsion, but this method has various disadvantages ; the most important of these are that the calcium nitrate adversely effects the recording properties of the emulsion, and that the plates must be kept in hermetically sealed boxes to prevent water from the atmosphere taking the place of the heavy water in the emulsion.

Tests have been made with emulsions containing about 50 per cent by volume of hexa-deutero-diacetin, but although these appeared promising, their properties do not yet appear to have been described in the literature.

The method of loading most frequently employed has been to soak the emulsions in heavy water and to expose them to the γ-radiation while wet (Goldhaber 1948, Waffler and Yoanis 1949, Hough 1950). The most important advantage of this procedure is that it gives a plate containing a large and reproducible concentration of deuterium, so that the number of proton tracks per unit area is relatively large for a given amount of γ-ray blackening ; but there are the corresponding disadvantages, mentioned above, associated with the greatly increased volume of the emulsion during exposure and its large shrinkage when processed. The effect on the quality of the tracks can now be overcome, at least in part, by the use of more sensitive emulsions, but the difficulty of the inaccuracies introduced in the measurements of the angles of dip remains.

In the present paper it is shown that modern emulsions soaked in heavy water can be successfully employed for the measurement of γ-ray energies in the region of 6 MeV. with an accuracy of 0·05 MeV., and allow γ-ray lines with a separation of $\sim 0{\cdot}5$ MeV. to be resolved. Secondly, results are described of experiments on the angular distribution of the protons produced in the disintegration of deuterons by 6·15 MeV. and 7·01 MeV. γ-rays, and methods for the further improvement of the measurements are discussed.

§ 2. Irradiation of Plates.

The γ-rays employed for the irradiation of the plates were produced by bombarding a thick target of calcium fluoride with 1·4 MeV. protons. The latter were accelerated by the 1·7 MeV. Van der Graaf generator, built for the University of Bergen from designs by O. Dahl and B. Trumpy, which came into operation in March 1950. The target was 5 mm. in

diameter, and eight plates were located with their centres 10 cm. from it and in a plane perpendicular to the proton beam. Four plates were orientated (see fig. 1) so that the γ-rays entered their surfaces at, or near, normal incidence, and the other four so that the mean angle of incidence was 15°. This disposition of the plates was based on the following considerations :—

The most accurate measurements of range are those made on tracks with small angles of dip. Further, for determining γ-ray energies, the most accurate results are obtained from the measurements on protons ejected at nearly 90° to the line of motion of the parent photon: for in such cases the momentum of the photon has little influence on the calculated energy of the neutron, which is nearly equal to that of the proton. For a given exposure the plates placed with their surfaces normal to the γ-ray flux yield the greatest number of tracks fulfilling these conditions, and they are therefore most suitable for the determination of the energy of the γ-radiation.

Fig. 1.

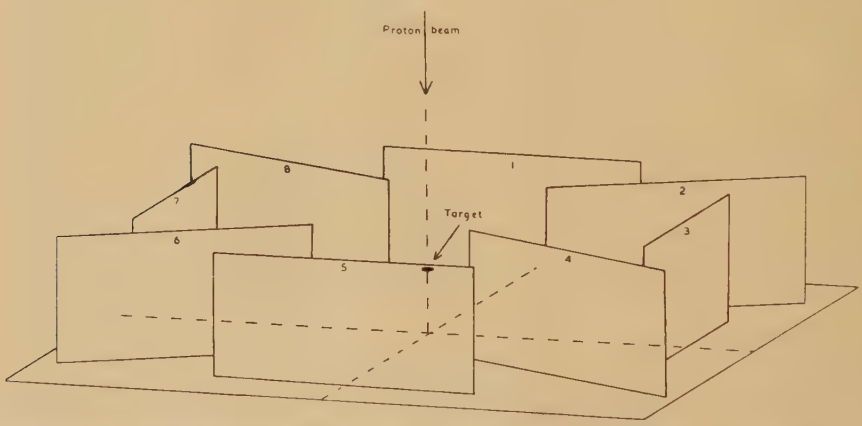

Arrangement of plates around target : plates 1, 3, 5, 7 received γ-rays approximately perpendicularly, plates 2, 4, 6, 8 obliquely ; plates 1, 2, 3, 4, were soaked in D_2O, 5, 6, 7, 8 in H_2O.

On the other hand, the best conditions for the investigation of the angular distribution of the protons are provided by plates in which all angles of emission are observed with equal probability. If observations are confined to tracks with small angles of dip, these conditions are provided by allowing the γ-rays to pass nearly tangentially through the emulsion. For such experiments an angle of approach of 15° has been chosen to avoid appreciable reduction of the intensity of the radiation in passing obliquely through the walls of the containers and through the emulsions.

The plates were contained in boxes of thin brass securely bolted to a base-plate which was attached to the target-holder, so that the geometry

was well defined; there were no unnecessarily large masses of metal present, and the γ-rays before reaching the emulsion had to traverse not more than a few millimetres of brass.

An hour before the exposure, an Ilford C2 plate, 4 in. $\times$ 2 in., with emulsion 200 μ thick, was placed in each box, and half the boxes were filled with D_2O and half with H_2O. After exposure, during which the total flux of protons to the target corresponded to the passage of 18 millicoulombs, the plates were dried to prevent fading of the latent image, and later processed by the " temperature development " method. This procedure was found to be more convenient than one in which processing commenced immediately after exposure.

Direct measurements with a micrometer showed that the ratio of the thicknesses of the emulsion during exposure and after processing and drying was $8{\cdot}5 \pm 0{\cdot}5$.

§ 3. Examination of Plates.

A total of 943 tracks has been measured in one of the plates soaked in D_2O and exposed with the γ-rays entering at 15°. With some tracks it was impossible to be certain of the direction of motion of the proton, and these were rejected. It was confirmed that these tracks constituted a random sample, exceptional only because they were nearly rectilinear, the increased scattering commonly observed at the end of the range being not apparent. Their rejection therefore produced no effect on the measured distributions in energy or angle of the protons. For each of the 943 tracks the following quantities were measured :—

(i.) the coordinates, x and y, of the point of origin of the proton in the plate ;

(ii.) the length, a, of its projection on a plane parallel to the surface of the emulsion, in units of length 0·85 μ ;

(iii.) the difference in depth, h, in microns, of the beginning and end points of the track: this quantity, multiplied by 10, gives, in units of 0·85 μ, the original difference in depth of these points at the time the track was formed, since the shrinkage factor is equal to 8·5 ;

(iv.) the angle α (see fig. 2) between the direction of the projection of the track on the surface of the emulsion and a standard direction OX, usually chosen to correspond to one of the edges of the plate.

From these observations it is possible to calculate

(v.) the angle of dip, δ, at the time of formation of the track: this angle is the mean inclination of the track, at the time of its formation, to the surface of the emulsion;

(vi.) the true range of the proton in the wet emulsion, in units of 0·85 μ ;

(vii.) two angles η and ϵ (see fig. 2) defining the direction of motion of the parent γ-ray and analogous to α and δ: η and ϵ are functions of x and y ;

(viii.) the angle θ between the direction of motion of the incident γ-ray and the projected proton. θ was directly determined from α, δ, η, and ϵ by a method of stereographic projection.

Fig. 2.

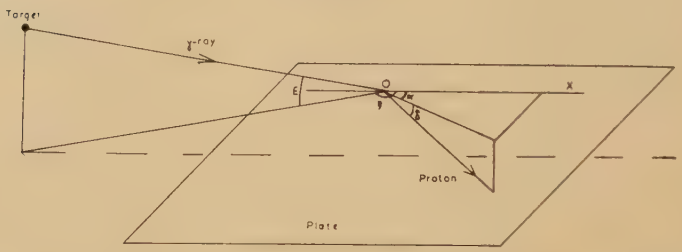

Diagram to show how α, δ, η, ϵ define the proton and γ-ray directions.

Fig. 3.

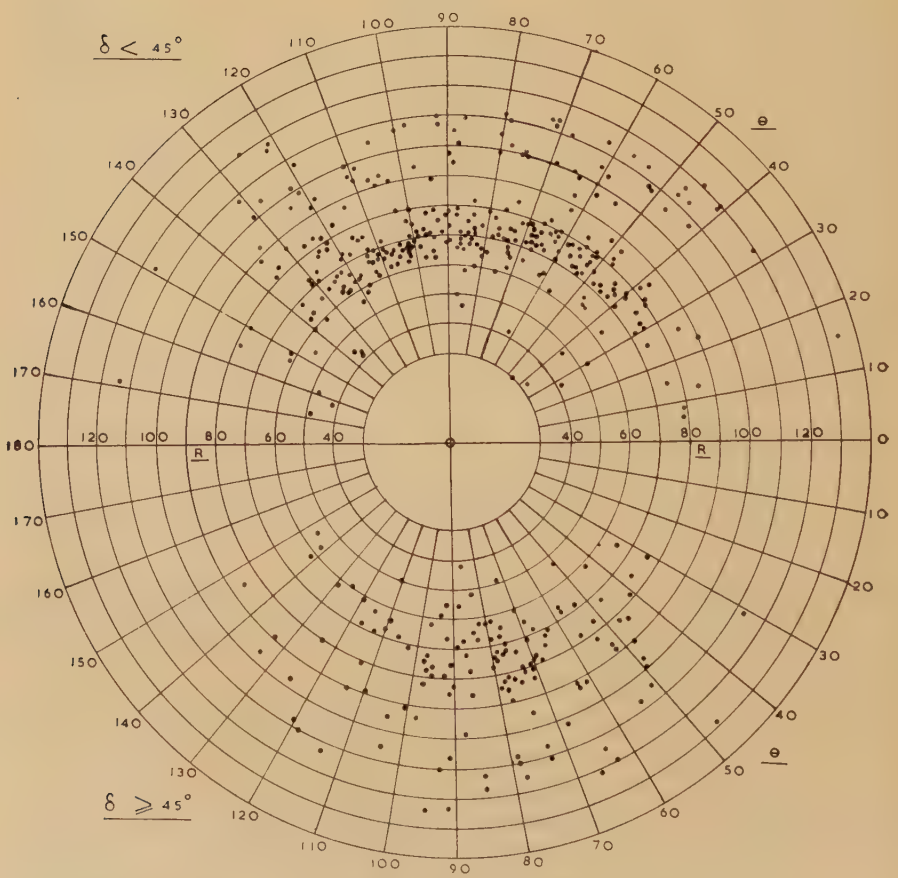

Plot of range R (one div.$=0{\cdot}85\,\mu$) against laboratory angle θ. 425 tracks.

The results of the measurements for each track were plotted in a polar diagram showing R as a function of θ, those for which $\delta \geqslant 45°$ being plotted separately from those for $\delta < 45°$. In the most unfavourable conditions, corresponding to large values of δ, the errors in θ were sometimes as great as 5°, and in R five divisions. For $\delta < 45°$ the probable errors in θ and R were 1·5° and one division respectively. A typical result for 425 tracks is shown in fig. 3.

§ 4. Calculations.

The distribution in energy of the γ-rays, and the angular distribution of the disintegration protons in a coordinate system—the C-system or centre of mass system—moving with the deuteron after the absorption of the γ-ray, were determined from the observed values of R and θ by the following method :

(*a*) Calculations of the stopping power to be expected for an emulsion saturated with D_2O, based on the range-energy relation for a normal emulsion (Rotblat 1951) ,and the data of Livingston and Bethe (1937), give, for the range-energy relation between 1·5 MeV. and 3 MeV.,

$$\left.\begin{aligned} &R = 19{\cdot}3\, E^{1{\cdot}65} \text{ (in microns)}, \\ \text{or} \quad &R = 22{\cdot}7\, E^{1{\cdot}65} \text{ (in units of } 0{\cdot}85\,\mu), \end{aligned}\right\} \quad . \quad . \quad . \quad . \quad (1)$$

where the energy E is measured in MeV.

(*b*) The dynamics of the photodisintegration of the deuteron give, for the energy, E_c, of the proton in the centre of mass system—to a very close approximation—the relation

$$E_c = E_L\,(1 - 0{\cdot}102 \cos\theta) \quad . \quad . \quad . \quad . \quad . \quad . \quad (2)$$

where E_L is the observed energy of a proton emitted at an angle θ in the laboratory system of coordinates, the L-system.

Equations (1) and (2) together give for the range R_C, of a proton of energy E_C

$$R_C = R\,(1 - 0{\cdot}168 \cos\theta),$$

where R is the observed range. R_C is also the expected observed range of a proton emitted at right angles to the direction of motion of the parent photon.

Now, to a close approximation, E_C is related to the γ-ray energy E_γ by the relation

$$E_C = \tfrac{1}{2}\,(E_\gamma - 2{\cdot}202), \quad . \quad . \quad . \quad . \quad . \quad . \quad . \quad (4)$$

all energies being measured in MeV. It follows that, for any particular γ-ray energy, E_C and the corresponding range R_C may be calculated.

By means of the above relations a map was constructed on tracing paper showing lines corresponding to given values of E_γ on the polar diagram R, θ. These lines are defined by the relation

$$R\,(1 - 0{\cdot}168 \cos\theta) = \text{constant},$$

and with a very small (calculable) error they are circles, of radius R_C, with centre at a distance of 0·168 R_C from the origin. They were drawn at intervals of 0·2 MeV. in the values of E_γ.

The mechanics of the reaction give, to an adequate approximation, $\tan\theta = \sin\phi/(\cos\phi + 0{\cdot}051,)$ where ϕ is the angle of emission of the proton in the C-system. From this relation lines of constant ϕ were drawn on the map at 10° intervals.

It may be noted that this map, reproduced in fig. 4, is completely independent of the measurements; it is based on theoretical calculation and well-established experimental facts, and no arbitrary parameters are involved.

§ 5. Energy Distributions.

When the map was superimposed on the plots of the results, it was seen that the points were distributed in two clearly marked bands, corresponding to two photon energies very close to the accepted values for the γ-rays arising from the bombardment of fluorine with protons. The fact that in each plot the mean line through the points forming the more abundant band is so nearly parallel to the line for $E_\gamma = 6{\cdot}15$ MeV. gives a

Fig. 4.

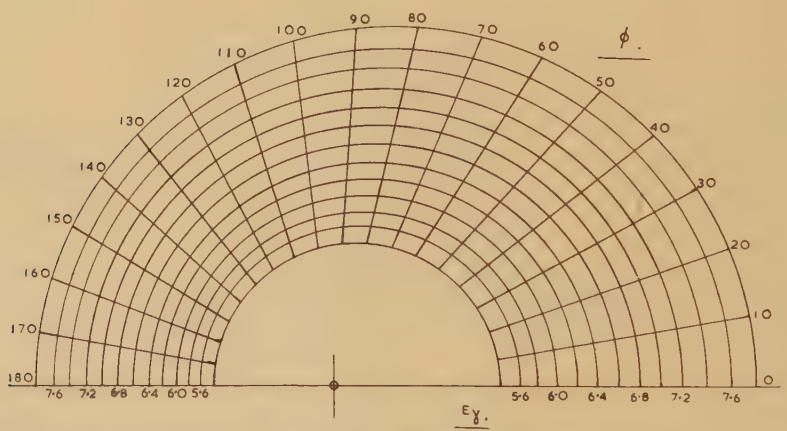

Map for obtaining γ-ray energy E_γ and centre of mass angle ϕ from R and θ.

very satisfactory check of the correctness of the calculations. The marked departure of the distribution of the experimental points in fig. 3 from circular symmetry is a direct demonstration of the momentum of the photon, and the agreement of the experimental distribution with that anticipated is a confirmation of the generally accepted relationship between momentum and energy for a particle of zero rest-mass.

Fig. 5 shows three plots of the distribution of the values of the energy of the γ-rays as deduced from the observations. They were obtained, for 0·2 MeV. intervals in the value of E_γ, by counting the numbers of experimental points between successive lines of constant E_γ. Fig. 5(*a*) is based on tracks with $\delta \geqslant 45°$, and shows poor resolution because of the inaccuracies, resulting from the large shrinkage factor, in the determinations of the range of these tracks. Fig. 5(*b*) is based on tracks with $\delta < 45°$, and gives clear evidence for the presence of two unresolved groups of different intensity. Fig. 5(*c*), which shows two completely separated

groups with mean energies $6{\cdot}15 \pm 0{\cdot}05$ MeV. and $7{\cdot}06 \pm 0{\cdot}07$ MeV., has been deduced from the tracks for which $\delta < 45°$ and $60° < \phi < 120°$. Curves (*b*) and (*c*) presumably differ because the direction of motion of a small

Fig. 5.

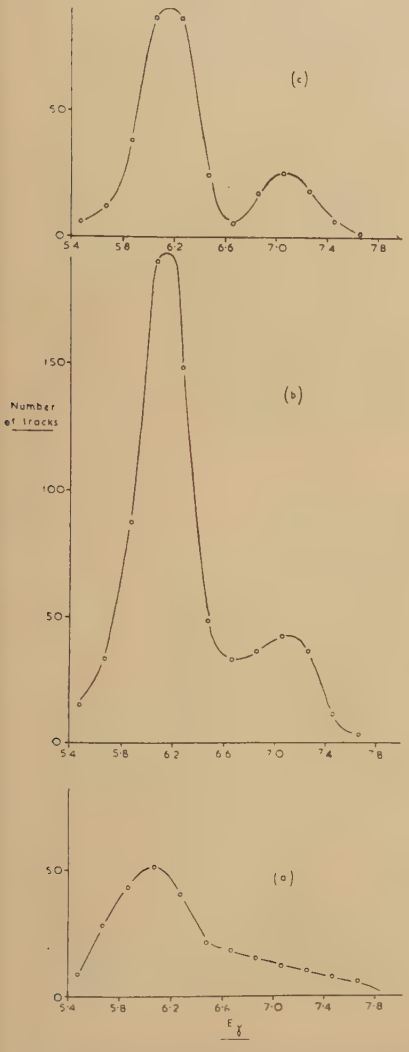

Numbers of tracks within 0·2 MeV. intervals of E_γ, plotted against E_γ; (*a*) is based on tracks with angle of dip $\delta \geqslant 45°$, (*b*) on tracks with $\delta < 45°$, and (*c*) on tracks with $\delta < 45°$ and $60° < \phi < 120°$.

Fig. 6.

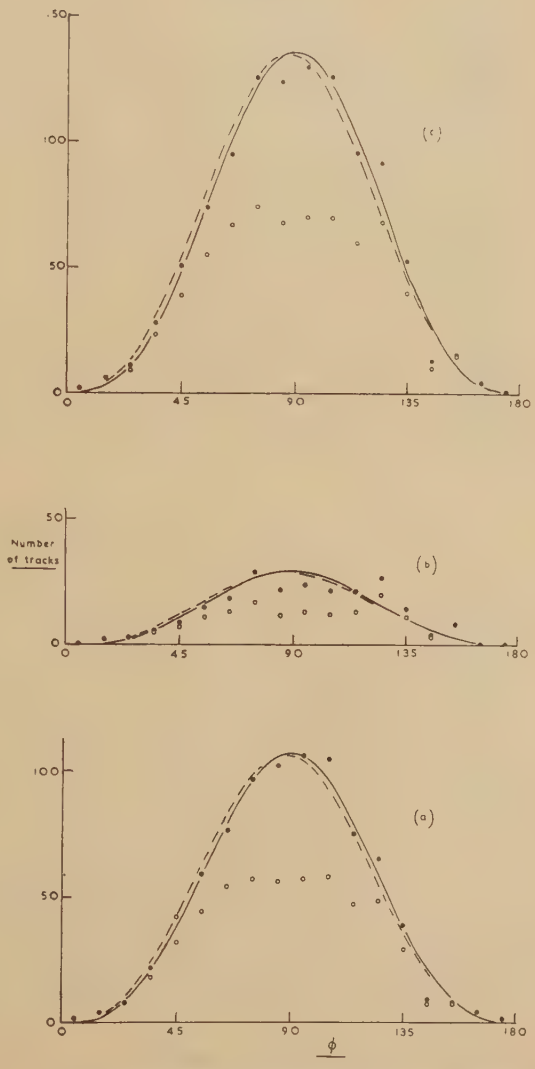

Centre of mass angular distributions: circles represent observed numbers of tracks with $\delta < 45°$, dots the numbers corrected for the effect of the limitation on the dip, full lines the distributions predicted by the simple theory, and broken lines the distributions predicted by the theory of Marshall and Guth. (*a*) is for the 6·15 MeV. group, (*b*) for the 7·01 MeV. group, and (*c*) for the two groups together.

proportion of the protons has been wrongly identified; for values of ϕ near to 90° such an error makes little difference to the calculated value of E_γ, but the resulting error is much greater if the value of ϕ is near 0° or 180°.

The γ-ray energies $6{\cdot}15 \pm 0{\cdot}05$ MeV. and $7{\cdot}06 \pm 0{\cdot}07$ MeV. are in good agreement with the values 6·15 MeV. and 7·01 MeV. which the energies measured by Rasmussen, Hornyak and Lauritsen (1950), together with the relative yields obtained by Bennett, Bonner, Mandeville and Watt (1946) for the various resonances in the disintegration of fluorine by protons, give for the mean energies of the γ-rays produced when 1·4 MeV. protons fall on a thick target containing fluorine. The close agreement for the 6·15 MeV. line shows that systematic errors are slight, and that the uncertainty arising from "straggling" of the proton ranges, and from inaccuracies of measurement and geometry, is not greater than our estimate of 0·05 MeV. Less accuracy is claimed for the figure 7·06 MeV., since it is based on relatively few tracks.

The degree of resolution of the two groups shown in fig. 5 (*c*) indicates that it would be possible to observe as separate peaks two γ-ray lines of which the energies differed by as little as 0·6 MeV., and to infer the existence of a doublet even if the separation were considerably less than this value.

§ 6. Angular Distributions.

The lines of constant ϕ in the map shown in fig. 4 are used to obtain distributions of the observed tracks, corresponding to each of the two γ-ray lines, according to the angle of emission of the proton in the centre of mass system. The observed distribution with $\delta < 45°$ is shown in fig. 6, together with the corrected results when account is taken of geometrical factors involved in limiting the tracks to those with angles of dip less than 45°. The total number after correction is slightly greater than the total number of tracks observed with all values of δ, a result which is to be expected in view of the difficulty of observing very steeply dipping tracks, and of their greater chance of escaping from the emulsion. It was calculated that the effect of escape on the angular distribution obtained from tracks with $\delta < 45°$ would be negligible in comparison with the statistical uncertainties, so no correction has been applied for it.

Fig. 6 shows the expected angular distributions in the centre of mass system if the number of protons emitted per unit solid angle, at angle ϕ, were proportional to

(*a*) $\sin^2 \phi$;

(*b*) $a + \sin^2 \phi\,(1 + 2\beta \cos \phi)$, where β is the ratio of the velocity of the proton to that of light. (*a*) would result from a simple electric dipole interaction of the photon with the deuteron, and (*b*) if there were interference between electric dipole and quadrupole terms (Marshall and Guth 1949). The constant "a" is related to the nature of the neutron-proton interaction, but it has a magnitude of only about 0·02 at this γ-ray energy, and makes very little difference to the shape of the curve.

It will be seen that our observed angular distributions are consistent with both (*a*) and (*b*) ; detailed examination of the results suggests that an increase of about a factor 4 in the number of measured tracks might reduce the statistical errors sufficiently to allow it to be shown whether or not this interference effect takes place.

Conclusion.

The results given above show that photographic plates soaked in heavy water are capable of giving useful information when used for measuring both γ-rays energies and the angular distributions of protons from the photodisintegration of deuterons. It would therefore be valuable to increase the ease and accuracy with which the measurements can be made, and to this end we are studying the use of plates exposed at right angles to the incident γ-rays and of more sensitive emulsions ; the former would make it possible to observe a given number of tracks suitable for the accurate determination of γ-ray energy with less effort and calculation, and the latter would make the tracks themselves easier to find and would give more reliable measurements. This would probably more than offset any increase in the background due to electrons. Meanwhile, the statistical accuracy of the determinations of the angular distributions is being increased by the measurement of more tracks in plates exposed with the γ-rays entering obliquely.

Acknowledgments.

Finally, we should like to express our thanks to all those who helped to make the exposures successful, to Miss J. A. Burnell and Miss M. J. Chapple for their valuable work at the microscope, to Dr. E. J. Burge for assistance with some of the calculations, and to Prof. C. F. Powell for his advice and encouragement.

We also wish to acknowledge the financial support of Norges Teknisk-Naturvitenskapelig Forskningsräd in the construction of the 1·7 MV. generator, and one of us (W.M.G.) is glad of this opportunity to record his sincere thanks for the hospitality which he received in Bergen.

References.

Bennett, Bonner, Mandeville and Watt, 1946, *Phys. Rev.*, **70,** 882.
Bishop, Collie, Halban *et al.*, 1950, *Phys. Rev.*, **80,** 211.
Fuller, 1950, *Phys. Rev.*, **79,** 303.
Gibson, Green, and Livesey, 1947, *Nature, Lond.*, **160,** 534.
Goldhaber, 1948, *Phys. Rev.*, 74, 1725.
Hansson, and Hulthen, 1949, *Phys. Rev.*, **76,** 1163.
Hough, 1950, *Phys. Rev.*, **80,** 1069.
Livingston and Bethe, 1937, *Rev. Mod. Phys.*, **9,** 245.
Marshall, and Guth, 1949, *Phys. Rev.*, **76,** 1879, 1880 ; 1950, *Ibid.*, **78,** 738.
Phillips, Lawson, and Kruger, 1950, *Phys. Rev.*, **80,** 326.
Powell, 1940, *Nature, Lond.*, **145,** 155.
Rasmussen, Hornyak, and Lauritsen, 1950, *Phys. Rev.*, **77,** 617.
Rotblat, 1951, *Nature, Lond.*, **167,** 550.
Waffler, and Younis, 1949, *Helv. Phys. Acta*, **22,** 414.
Wilkinson, 1950, *Harwell Conference Report.*

LIX. CORRESPONDENCE.

Alpha-particles from the Proton Bombardment of Oxygen-18.

By J. SEED,
Cavendish Laboratory, Cambridge*.

[Received February 28, 1951.]

THE yield of alpha-particles from the reaction $^{18}O(p\alpha)^{15}N$ has been studied using protons of energies 490 to 960 keV. having an energy homogeneity of 0·5 per cent.

The alpha-particles emitted at an angle of 120° with the incident proton beam were analysed magnetically, and were detected by a thin zinc sulphide screen and E.M.I. photomultiplier.

The oxygen targets were in the form of thin layers of oxide on copper discs, and were prepared as follows: a polished copper target button was heated to redness *in vacuo* by means of an induction heater, and about 0·2 c.c. (at N.T.P.) of oxygen gas enriched about 30 times in ^{18}O was allowed to enter, so that the surface of the disc was thinly oxidized. The oxide film was hardly visible, and from the observed width of the $(p\alpha)$ group and known analyser resolution (4 per cent in energy), the target thickness was estimated to be about 5 keV. for 600 keV. protons.

The yield of alpha-particles from these copper oxide targets was studied as a function of incident proton energy by observing the maximum intensity of the alpha-particle group obtained in the analyser: this is justified because the resolution width of the analyser was greater than the natural width of the alpha-particle group, calculated from target thickness and beam homogeneity.

The excitation function, given in the figure, shows resonances at 640 and 850 keV. The former resonance is close to that found at 680 keV. by Mileikowsky and Pauli (1950), who studied the alpha-particles from the $^{18}O(p\alpha)$ reaction at an angle of 90° with the incident protons. The difference is larger than can be accounted for by error in the proton energy in the present experiment, for which the voltage scale of the high tension equipment was calibrated directly at 441·4 and 873·5 keV. by observation of the thick target γ-ray excitation functions of the reactions $^{7}Li(p\gamma)^{8}Be$ (Fowler and Lauritsen 1949), and $^{19}F(p, \alpha\gamma)^{16}O$ (Chao *et al.* 1950).

The magnetic analyser used in the present experiment was calibrated by observations on the alpha-particle and proton groups from the reactions $^{9}Be(d\alpha)^{7}Li$, $^{9}Be(d\alpha)^{7}Li^*$ ($Q = 7{\cdot}150 \pm 0{\cdot}008$ MeV. and $Q = 6{\cdot}668 \pm 0{\cdot}009$ MeV. respectively, Buechner and Strait 1949 and 1950 a) and $^{12}C(dp)^{13}C$

* Communicated by the Author.

($Q=2{\cdot}716\pm0{\cdot}005$), Buechner and Strait 1950 b). From measurement of the energy of the alpha-particle group from $^{18}O(p\alpha)$ at the 850 keV. resonance, a Q value of $3{\cdot}96\pm0{\cdot}04$ MeV. was obtained for the transition to the ^{15}N ground state, in confirmation of the values reported in the literature (Burcham and Smith 1939, Freeman 1950).

Taking this value for the energy release, the resonances at proton energies of 640 and 850 keV. would correspond to levels at 8·59 and 8·80 MeV. in the ^{19}F nucleus. No other reaction has yet given evidence of levels in ^{19}F in this region, though the reaction $^{18}O(pn)$ shows closely spaced levels at about 10 MeV. excitation: by analogy with similar nuclei (^{11}B, ^{15}N) having one particle less than an alpha-particle core, one would expect the ^{19}F nucleus to have a fairly large number of low-lying excited states.

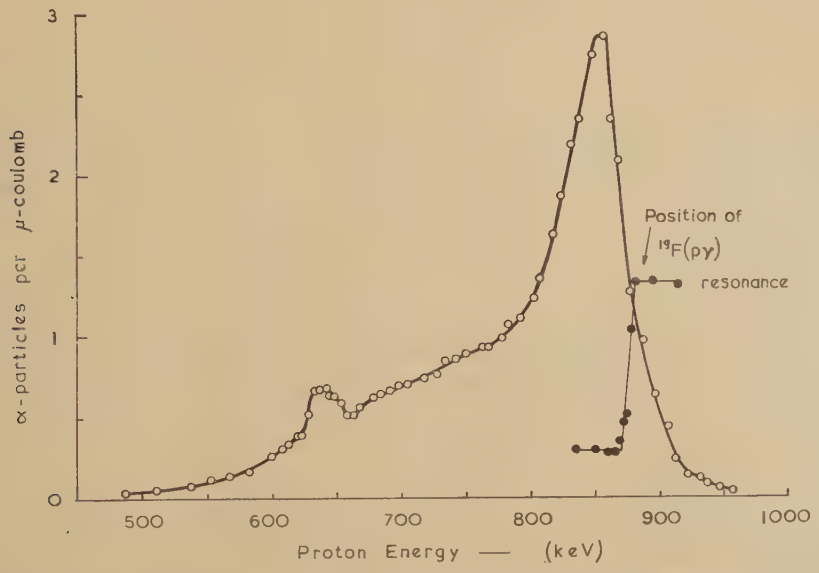

Excitation function for the reaction $^{18}O(p\alpha)^{15}N$ taken at 120°, and showing the position of the 873·5 keV. resonance in the reaction $^{19}F(p\gamma)$.

A search for an alpha-particle group corresponding to transitions to excited states of ^{15}N was made using protons of energy 685, 837, and 957 keV. and of homogeneity 30 keV. No group of intensity greater than one-tenth of the main group at alpha-energies greater than 1·2 MeV. was found.

I wish to express my thanks to Dr. A. S. Baxter and Dr. A. P. French for help and advice during the experiment, and to Sir John Cockcroft and his staff at the Atomic Energy Research Establishment, Harwell, for the gift of the enriched oxygen used in this work, also to the Department of Scientific and Industrial Research for a grant.

REFERENCES.

BUECHNER, W. W., and STRAIT, E. N., 1949, *Phys. Rev.*, **76**, 1547; 1950 a, *Rev. Mod. Phys.*, **22**, 306; 1950 b, *Ibid.*, **22**, 331.
BURCHAM, W. E., and SMITH, C. L., 1939, *Nature, Lond.*, **143**, 795.
CHAO, C. V., TOLLESTRUP, A. V., FOWLER, W. A., and LAURITSEN, C. C., 1950. *Phys. Rev.*, **79**, 108.
FOWLER, W. A., and LAURITSEN, C. C., 1949, *Phys. Rev.*, **76**. 314.
FREEMAN, J. M., 1950, *Proc. Phys. Soc.* A, **63**, 668.
MILEIKOWSKY, C., and PAULI, R. T., 1950, *Nature, Lond.*, **166**, 602.

The Isomeric State of RaE.

By N. FEATHER, F.R.S.,
The University, Edinburgh†.

[Received March 16, 1951.]

THE published results of Neumann, Howland and Perlman (1950) already make it very probable that $^{210}_{83}$RaE possesses an isomeric state which decays predominantly by α-disintegration, with disintegration energy $5{\cdot}12 \pm 0{\cdot}05$ MeV., to produce $^{206}_{81}$Tl (4·2 m.). These authors concluded that the lifetime for α-emission from the isomeric state is greater than 25 years. They also indicated some of the difficulties in accounting for the facts, which they established, that RaF is not produced to the extent of more than 1 in 2000 disintegrations of RaE* (either directly by β-disintegration or indirectly through isomeric transition to RaE followed by β-disintegration), and that RaD is not produced to the extent of more than about 1 in 200 disintegrations (by electron capture). On the assumption that the α-disintegration of RaE* is to the ground state of $^{206}_{81}$Tl—which leads to the smallest permissible value for the excitation energy of the isomeric state—they suggested that the chief difficulty lies in explaining the slowness of the isomeric transition RaE* → RaE. Even if this transition is of the fifth order they concluded that the excitation energy must lie very close to the lower limit of the experimentally deduced value of $0{\cdot}18 \pm 0{\cdot}11$ MeV. Moreover, in this connection it should not be forgotten that the nucleus $^{210}_{83}$RaE is already known to possess at least three non-isomeric states in the range of excitation energies from 0 to 0·05 MeV. (Feather 1949).

Accepting a lifetime of the order of 100 years for α-emission, it is clear that the difficulty in explaining the slowness of the isomeric transition RaE* → RaE is more acute than that regarding the competing β-disintegration RaE* → RaF. It being generally accepted that the normal β-disintegration of RaE is characterized by the spin change 2 → 0, reference to the revised Sargent diagram of Feather and Richardson (1948) indicates

† Communicated by the Author.

that β-disintegration from the isomeric state need not be characterized by a spin change of more than $5 \rightarrow 0$ in order to explain its non-observation. This would only require the change $5 \rightarrow 2$ (with or without change of parity) for the isomeric transition.

There are, however, some difficulties regarding the important assumption that the α-disintegration of RaE* is to the ground state of $^{206}_{81}$Tl. The spin of this β-active state is likely to be 0 or 1, for the β-disintegration of $^{206}_{81}$Tl is clearly allowed (Feather and Richardson 1948) and $^{206}_{82}$Pb is generally regarded as having spin 0. On the above assumption, then, and accepting the conclusions which follow from it, we should expect the α-disintegration $^{210}_{83}\mathrm{RaE}^* \rightarrow {}^{206}_{81}$Tl to be considerably less favoured than the parallel disintegration from the ground state RaE. The latter disintegration would be characterized by the spin change $2 \rightarrow 0(1)$, the former by the change $\geqslant 6 \rightarrow 0(1)$. Plainly contrary to this conclusion is the evidence from the Geiger–Nuttall diagram for $Z=83$ (Broda and Feather 1947). On the basis of this diagram the α-disintegration of RaE* ($\tau \sim 100$ y.) appears more favoured, by a factor possibly as great as 10 (rather than less favoured by a factor of the order of 10^3) than the α-disintegration of RaE, due allowance being made for the difference in energy. It would appear that there are three possibilities of resolving this seeming contradiction :

(i) the lifetime of RaE* for α-emission may in fact be of the order of 10^5 to 10^6 y.;

(ii) the β-disintegration of RaE* may be to an isomeric state of $^{206}_{81}$Tl;

(iii) the α-disintegration of RaE* may be abnormal in the sense that it violates the general regularities exhibited in the Geiger–Nuttall diagram.

No doubt direct evidence concerning (i) will not long continue lacking, but, judging the present position it would appear surprising that the activity of RaE* has been detected at all, if its lifetime is really as long as 10^5 y. Also, the longer the lifetime for α-emission, the smaller the experimental upper limit to the transition probability for the isomeric transition $\mathrm{RaE}^* \rightarrow \mathrm{RaE}$ and the larger the spin which has to be assigned to the isomeric state in order to explain its properties. Possibility (i), in fact, does not alone provide a satisfactory basis of resolution.

Possibility (ii) introduces similar difficulties. Since its acceptance leads inevitably to the conclusion that the excitation energy of the isomeric state RaE* is greater than previously supposed, it likewise makes more difficult the problem of explaining the relative slowness of all processes, except α-disintegration, which lead to the de-excitation of this state. Again, an isomeric state of $^{206}_{81}$Tl is hardly likely to have escaped detection in the experiments of Fajans and Voigt (1940) and Neumann *et al.* (1950).

Concerning possibility (iii), this would be realized formally if the effective nuclear radius of the isomeric state RaE* were greater than that of the ground state RaE. Physically, however, the smallness of the

α-disintegration constants which characterize all ground-state nuclei having $Z = 83$ (when these are compared with the α-disintegration constants of nuclei for which $Z \geqslant 84$) is most probably connected not so much with a real decrease in nuclear radius as Z decreases from 84 to 83 as with the difficulty of formation of the nascent α-particle when only one of its constituent protons is available in a loosely bound state ("outside" the closed shell of 82 protons). If possibility (iii) were to be interpreted in this way it would obviously imply that one of the properties of RaE*, the isomeric state of the nucleus containing (126+1) neutrons and (82+1) protons, is that the intranuclear formation of an α-particle is less difficult in this state than it is in the ground state of the same system—or in any of the known non-isomeric states of any nucleus of proton number 83 and neutron number 128 or greater. This is a possibility of a type not hitherto considered in theories of α-disintegratiou.

References.

Broda, E., and Feather, N., 1947, *Proc. Roy. Soc.* A, **190,** 20.
Fajans, K., and Voigt, A. F., 1940, *Phys. Rev.*, **58,** 177.
Feather, N., 1949, *Nucleonics*, **5,** 22.
Feather, N., and Richardson, H. O. W., 1948, *Proc. Phys. Soc.*, **61,** 452.
Neumann, H. M., *et al.*, 1950, *Phys. Rev.*, **77,** 720.

An Example of the $(n, p ; \pi^-)$ Reaction in the Photographic Emulsion.

By S. J. Goldsack and N. Page,
University, Manchester*.

[Received March 9, 1951.]

[Plate XX.]

We have recently found the event shown in Pl. XX. in a 400 micron thick Ilford G5 Nuclear Research Emulsion, exposed vertically for 21 days at an altitude of 2860 m. in a magnetic field of 34,000 gauss (Dilworth *et al.* 1950). The event is interpreted as the production of a π^--meson (track A) in the collision of a high-energy, cosmic-ray neutron with a proton in the emulsion, according to the following scheme :

$$n + p \rightarrow p + p + \pi \quad . \quad . \quad . \quad . \quad . \quad . \quad . \quad . \quad (1)$$

The technical details of the event are as follows. Track A is almost continuous throughout its length and shows marked scattering especially towards the right-hand end of the track where there are two sharp deflections. The grain density of the track increases noticeably from the

---

* Communicated by G. D. Rochester.

Observer: Mrs. J. Cunliffe.

FIG. 1.

Vertical

centre of the star up to the second sharp deflection, but at this point there is a decrease in grain density and the track becomes quite straight (D). The grain density and scattering of track A are consistent with its having been produced by a slow meson (presumably a π^--meson) moving to the right and producing a single-prong star (D) at the end of its range. The small scattering and high grain density of track D exclude the possibility of its being a μ^+-meson arising from the decay of a positive π-meson. The range of the meson is 370 μ corresponding to a kinetic energy of 3·6 MeV.

The meson is created in a star which has two lightly-ionizing particles (B and C) but no evaporation or recoil particles. The track B is only 180 μ long and is therefore too short to be identified, but its grain density is near minimum. Minimum ionization in this plate corresponds to $34{\cdot}2 \pm 0{\cdot}8$ grains/100 μ : track B has $37{\cdot}0 \pm 6{\cdot}0$ grains/100 μ. Track C, which is 1·1 cm. long, has a grain density of $46{\cdot}8 \pm 0{\cdot}7$ grains/100 μ and is therefore slightly above minimum. The small angle multiple scattering of this track has been measured by the method of Fowler (1950), and the arithmetic mean angle of scattering is $0{\cdot}048 \pm 0{\cdot}006°/100\ \mu$ corresponding to a value of $p\beta = 700 \pm 85$ MeV./c.

The grain density of a proton showing this scattering should be $1{\cdot}5 \pm 0{\cdot}15$ times minimum. The particle is therefore identified as a proton, the kinetic energy being 400 ± 50 MeV., and the momentum 990 ± 120 MeV./c. This identification is confirmed by the sign of the magnetic deflection. The total deviation between the ends of the track is 1·23°. To this must be added a small correction for the distortion of the emulsion : measured by the method of Cosyns and Vanderhaeghe (1950), this proves to be +0·05°. Assuming that the particle is moving downwards from the star, it is positive with a probability of 97 per cent.

It is clear that the equation (1) is the simplest interpretation of the event which is consistent with conservation of charge, the third particle being a knock-on proton, initially at rest in the emulsion.

If the particle B is a proton, its energy must be at least 650 MeV. and hence the kinetic energy of the incident neutron which produced the star must have been at least 1200 MeV.

Finally it is of interest to review the evidence for possible simple schemes for single meson production in nucleon–nucleon interactions. These are collected in Table I.

It is seen from the Table that at least six such reactions are possible all of which might be observed in the Ilford G5 emulsion. Events 1 and 2 can occur in collisions with hydrogen nuclei in the emulsion which, it is estimated, account for 4 per cent of the total geometrical cross section of the emulsion. All six events could occur in collisions with nucleons in the nuclei of heavier atoms in the emulsion, but in such cases an evaporation star or a nuclear recoil fragment would usually be observed. It is possible, however, that the two interacting nucleons might leave the nucleus without imparting an appreciable amount of energy to it.

Event 2 has been observed in the cloud chamber (Armenteros *et al.* 1951 a); two examples of type 3 occurring in Ilford G5 emulsion have been reported by Cosyns *et al.* (1949), and a similar event was produced in Ilford C2 emulsion using artificially produced neutrons from the Berkeley cyclotron (Smith *et al.* 1950). Armenteros *et al.* (1951 b) have pointed out that the event described by Hopper and Biswas (1950) and interpreted by them as an example of the decay of a neutral V particle similar to those found by Rochester and Butler (1947) and by Seriff *et al.* (1950) may be another example of this process.

At present it appears impossible to distinguish, in the emulsion, between high energy events of the types 3 and 4 b and the decay of V particles.

TABLE I.

Types of simple star involving the production of one meson.

Type	Incident Particle	Target Particle	Products	No. of prongs per star	References
1 (*a*)	Neutron	Proton	$p+p+\pi^-$	3	Present letter
(*b*)	Neutron	Proton	$n+n+\pi^+$	1	
2	Proton	Proton	$n+p+\pi^+$	3	Armenteros *et al.* 1951 a
3	Neutron	Neutron	$n+p+\pi^-$	2	Cosyns, *et al* .1949 Smith, *et al.* 1950
4 (*a*)	Proton	Neutron	$p+p+\pi^-$	4	
(*b*)	Proton	Neutron	$n+n+\pi^+$	2	

REFERENCES.

ARMENTEROS, R., BARKER, K. H., BUTLER, C. C., CACHON, A., and CHAPMAN, A. H., 1951 a, (private communication); 1951 b, *Nature, Lond.*, **167,** 501.

COSYNS, M., DILWORTH, C. C., OCCHIALINI, G. P. S., and SCHÖNBERG, M., 1949, *Nature, Lond.*, **164,** 129.

COSYNS, M., and VANDERHAEGHE, G., 1950, *Note No.* 15. *Bull. Cen. Phys. Nuc. de L'Université Libre de Bruxelles.*

DILWORTH, C. C., GOLDSACK, S. J., GOLDSMIDT-CLERMONT, Y., and LEVY, F., 1950, *Phil. Mag.*, **41,** 1032.

FOWLER, P. H., 1950, *Phil. Mag.*, **41,** 169.

HOPPER, V. D., and BISWAS, S., 1950, *Phys. Rev.*, **80,** 1099.

ROCHESTER, G. D., and BUTLER, C. C., 1947, *Nature, Lond.*, **160,** 855.

SERIFF, A. J., LEIGHTON, R. B., HSIO, C., COWAN, E. W., and ANDERSON, C. D., 1950, *Phys. Rev.*, **78,** 290.

SMITH, F. M., GARDNER, E., and BRADNER, H., 1950, *Phys. Rev.*, **77,** 562.
